THESIS APPROVAL

GRADUATE SCHOOL, KASETSART UNIVERSITY

Master of Engineering (Chemical Engineering)
DEGREE

Chemical Engineering
FIELD

Chemical Engineering
DEPARTMENT

TITLE: Selective Production of Higher Hydrocarbons over Cobalt Support SBA-15 Mesoporous Silica Catalysts

NAME: Miss Sinee Kraokaw

THIS THESIS HAS BEEN ACCEPTED BY

THESIS ADVISOR
(Associate Professor Metta Chareonpanich, D.Eng)

THESIS CO-ADVISOR
(Assistant Professor Paisan Kongkachuichay, Ph.D..)

DEPARTMENT HEAD
(Assistant Professor Paisan Kongkachuichay, Ph.D..)

APPROVED BY THE GRADUATE SCHOOL ON

DEAN
(Associate Professor Gunjana Theeragool, D.Agr.)

THESIS

SELECTIVE PRODUCTION OF HIGHER HYDROCARBONS OVER COBALT SUPPORT SBA-15 MESOPOROUS SILICA CATALYSTS

SINEE KRAOKAW

A Thesis Submitted in Partial Fulfillment of
the Requirements for the Degree of
Master of Engineering (Chemical Engineering)
Graduate School, Kasetsart University
2009

Sinee Kraokaw 2009: Selective Production of Higher Hydrocarbons over Cobalt Support SBA-15 Mesoporous Silica Catalysts. Master of Engineering (Chemical Engineering), Major Field: Chemical Engineering, Department of Chemical Engineering. Thesis Advisor: Associate Professor Metta Chareonpanich, D. Eng. 121 pages.

Fischer-Tropsch synthesis (FTS) is one of the most promising ways for the conversion of syngas to hydrocarbon products. Supported cobalt is the preferred catalyst for FTS due to its high selectivity to heavy hydrocarbons, low activity for water-gas-shift reaction and comparatively low price. Cobalt loaded SBA-15 catalysts were prepared by two different metal loading techniques including post-synthesis and direct-synthesis methods. For the post-synthesis method, the conventional wetness impregnation and solvothermal technique were applied. In order to prepared uniform dispersion of cobalt catalyst on silica support, the direct-synthesis method was applied by using pH-adjusting approach. Also, the FTS catalytic performances of Co/SBA-15 catalysts prepared by different metal loading techniques were comparatively investigated. It was clearly observed that the pH value of synthesis solution affected the structural order of direct-synthesis catalysts. The degree of cobalt incorporation was increased when pH value of synthesis mixture was increased. The optimum cobalt loading (ca. 10 wt. %) with well-ordered mesostructure of SBA-15 silca was obtained at pH of 7.5. Direct-synthesis catalysts with highly distributed cobalt particles significantly promoted the selectivity towards long-chain hydrocarbons, especially the diesel-range products (C_{12}-C_{20}). The undesired methane product, normally occurred over cobalt catalysts prepared by the conventional impregnation method, was distinguishly reduced. Nonetheless, the reactivity of direct-synthesis catalysts were noticeably decreased due to the lower accessibility of reactants to cobalt active sites, resulting in the decrease of reduction degree of cobalt species.

____________________________ ____________________________ ___ / ___ / ___

Student's signature Thesis Advisor's signature

ACKNOWLEDGEMENTS

I would like to express my sincere gratitude to my advisor, Associate Professor Metta Chareonpanich, for her guidance, invaluable suggestion and support throughout this research. I am very thankful to Associate Professor Paisan Kongkachuichay for his kindly giving the time to revise and approve my thesis.

I am grateful for the financial support from the Kasetsart University Research and Development Institute (KURDI), the Thailand Research Fund (TRF) and National Center of Exellence for Petroleum, Petrochemicals and Advanced Materials (PPAM). The Graduate School of Kasetsart University is also acknowledged.

I would like to thank for the help of my senior research colleagues and for the assistance and valuable suggestion from administrative staffs and technical staffs at Department of Chemical Engineering, Kasetsart University. The kind assistance of characterization and measurement from the staffs at National Metal and Materials Technology Center (MTEC), Office of Atoms for Peace (OAP) and Scientific and Technological Research Equipment Center of Chulalongkorn University (STREC) are admirably acknowledged.

Finally, I have a lot to be thankful to my family and for their adoration, support, encouragement, and their understanding during the whole period of my education.

Sinee Kraokaw
January 2009

TABLE OF CONTENTS

Page

LIST OF TABLES

Table **Page**

Appendix Table

LIST OF FIGURES

Figure **Page**

LIST OF FIGURES (Continued)

LIST OF FIGURES (Continued)

LIST OF FIGURES (Continued)

Appendix Figure **Page**

LIST OF ABBREVIATIONS

ASF = Anderson-Schultz-Flory
BET = Brunauer-Emmett-Teller
FID = Flame Ionization Detector
FT = Fischer-Tropsch
GC = Gas Chromatograph
FTS = Fischer-Tropsch Synthesis
kPa = Kilo Pascal
M = Molar
mA = Milli Ampare
MCM-41 = Mobil Composition of Matter No. 41
NTP = Normal Temperature and Pressure
nm = Nanometer
P = Pressure
SANS = Small Angle Neutron Scattering
SAXS = Small Angle X-ray Scattering
SBA-15 = Santa Barbara Amorphous Silica No. 15
T = Temperature
TCD = Thermal Conductivity Detector
TEM = Transmission Electron Microscopy
TGA = Thermogravimetric Analysis
WGS = Water Gas Shift
wt. % = Percent by weight

SELECTIVE PRODUCTION OF HIGHER HYDROCARBONS OVER COBALT SUPPORT SBA-15 MESOPOROUS SILICA CATALYSTS

INTRODUCTION

Recently, the intensive concerns of fossil energy depletion, air pollution and global climate have encouraged many researchers to produce alternative energy. In order to deal with the continually massive fuel consumption (as shown in Figure 1) and the restriction of the emitted pollutants, high quality of transportation fuels are also needed. One of the promising alternative energy is synthetic fuels produced by the Fischer-Tropsch (FT) process, which have received increasing attention worldwide due to the compatibility with existing petroleum infrastructure and vehicles (Takeshita and Yamaji, 2008).

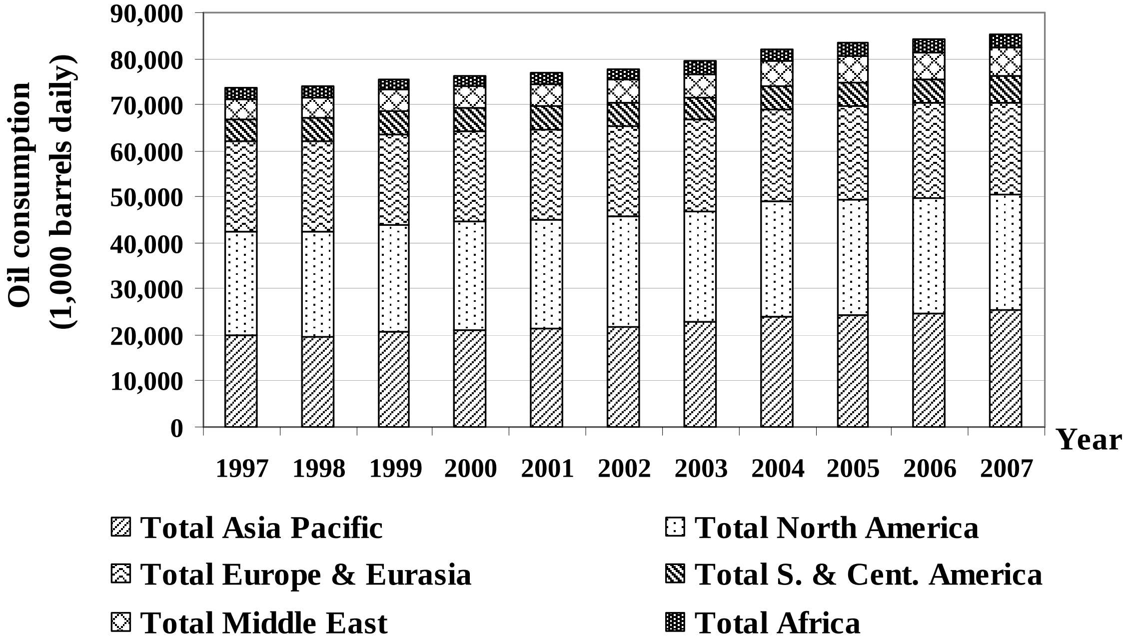

Figure 1 World petroleum consumption (1,000 barrels per day).

Source: Anonymous (2008)

Fischer-Tropsch (FT) synthesis is a well-known catalytic process that very clean alternative fuels can be produced from the conversion of synthesis gas (a mixture of carbon monoxide and hydrogen) which can be generated from natural gas, coal and biomass. FT fuels are of high quality and cetane number, being free of sulfur, nitrogen, aromatics, and other contaminants typically found in petroleum products, which are friendly to environment (Van der Laan *et al.,* 1999). Undoubtedly, FT synthesis has become a promising way to produce petroleum substitutes for renewable transportation fuels (Knottenbelt, 2002). Moreover, the synthesis gas which is used as reactant gas in FT synthesis can be produced from the reaction of carbon dioxide reforming of methane in present of catalyst, so called dry reforming reaction (Kodama *et al.,* 2001). By this process carbon dioxide and methane which are greenhouse gases can be reduced and converted into reactant gases in FT process in the same time.

According to the catalytic reaction of FT synthesis, most of VIII group metals have measurable activity in carbon monoxide hydrogenation but yield different products, including hydrocarbons, acids, alcohols and esters. Generally, iron and cobalt metals are widely used as FT catalysts for larger hydrocarbon production (Iglesia, 1997; Ernst, 1999). However, the supported cobalt catalysts are particularly suited for the FT synthesis since they give high yield of long chain hydrocarbons, low activity for the water-gas-shift reaction and have long active life time (Jacob *et al.,* 2002; Soled *et al.,* 2003; Davis, 2005).

The discovery of mesoporous silica opened up new possibilities in many areas of chemistry and material sciences (Kresge *et al.,* 1992; Zhao *et al.,* 1998; Imperor-Clerc *et al.,* 2000). These materials have high specific surface areas, high pore volumes, and well-ordered pore structures with uniform mesopores, adjustable from about 2 to 10 nm. In the family of mesoporous materials, SBA-15 synthesized with triblock copolymer as a structure-directing agent under strong acidic conditions is formed as a hexagonal array of uniform tubular channels and exhibits large pore size, thick pore wall, high thermal and hydrothermal stabilities (Zhao *et al.,* 1998). Therefore, SBA-15 material is a good choice to use as a catalyst support in larger hydrocarbon synthesis.

The performances of cobalt catalysts for the FT synthesis mainly depend on the overall amount of exposed metallic cobalt atoms. Thus, a highly active cobalt catalyst requires high dispersion of cobalt metal. Post-synthesis methods such as impregnation and grafting have been widely used for preparing metal supported catalysts. However, this metal loading technique exhibits the disadvantage upon the catalytic performances because it often leads to the loss of specific surface areas and the blockage of pores by large cobalt oxide particles which could play negative roles on catalytic behaviors (Lira *et al.,* 2008). Such that, many researchers have been working on the modification of catalyst preparation to synthesize FT catalysts with high activity and selectivity.

Preparing the highly dispersed metallic nanoclusters with SBA-15 as a catalyst support is a great challenge to obtain high performance FT catalysts and only a few reports were presented to demonstrate the direct incorporation of cobalt species into the SBA-15 silica framework. The alternative way to introduce cobalt species into the mesoporous silica support is adding the cobalt precursor directly into the synthesis mixture of silica, structure directing agent, hydrochloric acid and distilled water, followed by hydrothermal treatment; so called the direct synthesis method. However, the incorporation of metal ions into the framework of SBA-15 by means of condensation process is very difficult because of the strongly acidic synthesis conditions (Melero *et al.,* 2005).

The aim of this research is to increase the performance of cobalt catalyst in FT synthesis in order to obtain higher hydrocarbon selectivity in the range of diesel (C_{10} – C_{20}). By this reason, a simple sol-gel method is modified to directly incorporate cobalt atoms into SBA-15 support by pH adjusting approach and the obtained catalysts are characterized by various instruments such as N_2 sorption analysis, Transmission Electron Microscopy (TEM), and Thermogravimetric Analysis (TGA). In addition, the effect of different techniques of metal loading on cobalt dispersion in silica-supported catalysts and the catalytic performance of FT synthesis is also investigated. Cobalt-containing SBA-15 materials are prepared by two different techniques including the direct thermal synthesis and the conventional impregnation method, and characteristics and performances of the obtained catalysts were studied comparatively.

OBJECTIVES

1. To study the effect of metal loading techniques on carbon monoxide conversion and hydrocarbon selectivity in Fischer-Tropsch synthesis reaction.

2. To directly synthesize cobalt-containing SBA-15 catalyst with well-ordered mesoporous structure by a simple modification of a sol-gel process.

3. To investigate the role of cobalt dispersion on Fischer-Tropsch synthesis performances.

Benefits

1. Highly dispersed cobalt support SBA-15 mesoporous silica catalysts can be successfully synthesized via the direct synthesis method by using simple adjustment of sol-gel process.

2. High selectivity of long chain hydrocarbon products in the range of diesel in Fischer-Tropsch synthesis can be achieved over the catalysts prepared by direct synthesis method.

3. The influence of metal loading technique and metal dispersion on FT catalytic behavior is clearly discussed.

LITERATURE REVIEW

Ficher-Tropsch (FT) synthesis is one of the major routes for converting coal-based and/or natural gas-derived syngas into high quality chemicals and fuels. The main goal of FT synthesis research is to develop FT catalysts with high activity and selectivity by improving the selectivity of C_{5+} hydrocarbons while decreasing the selectivity of methane. In particular, liquid fuels in the range of diesel fuels produced by Fischer-Tropsch process (synthesis of hydrocarbons from CO and H_2) exhibit attractive potential as very clean alternative energy, relative to the conventional fossil petroleum. The products generated from FT synthesis are mainly composed of linear paraffins with high cetane number and are free of sulfur and aromatic pollutants (Van der Laan and Beenacker, 1999). In order to improve the performances of FT catalysts and increase the selectivity of the desired hydrocarbon products (C_{10}-C_{20}), informative research understanding is reviewed as the following description.

Fischer-Tropsch Synthesis

In the last decades, the interest in Fischer-Tropsch (FT) synthesis has been increased as a result of change in fossil energy reserves, environmental demands and technological developments FT synfuels have become a key alternative fuel regardless of CO_2 policy because of their low transportation cost and compatibility with existing petroleum infrastructure and vehicles (Takeshita and Yamaji, 2008). In addition, FT synfuels are virtually interchangeable with conventional diesel fuels and can be blended with diesel at any ratio without or with little modification. Concerning carbon monoxide and particulate matter, FT fuels offer important emission benefits compared with diesel.

1. The Fischer-Tropsch Process

Fischer-Tropsch (FT) process is a method for the synthesis of hydrocarbons and other aliphatic compounds principally for producing synthetic petroleum substitutes. FT process was discovered by Franz Fischer and Hans Tropsch, the German coal researchers, in 1923. This process was invented in petroleum-poor but coal-rich Germany to produce alternative fuels during the World War II. The original Fischer-Tropsch synthesis was described by the following chemical equations:

$$CH_4 + 1/2O_2 \longrightarrow 2H_2 + CO \qquad (1)$$

$$(2n+1)H_2 + nCO \longrightarrow C_nH_{2n+2} + nH_2O \qquad (2)$$

FT synthesis reaction is regarded as a surface catalyzed polymerization process and a lot of heat is involved during reaction. The adsorbed CH_x monomers, formed by hydrogenation of adsorbed CO, react with the surface H atoms and hydrocarbon fragments to produce hydrocarbons with a broad range of chain lengths due to the limitation of the typical Anderson-Schultz-Flory (ASF) distribution (Iglesia, 1997). In this process, synthesis gas (a mixture of hydrogen and carbon monoxide) can be converted to large ranges of petroleum products such as methane, synthetic gasoline, waxes, alcohols, and water over heterogeneous catalysts (Van Der Laan *et al.*, 1999; Davis, 2001; Saib *et al.*, 2002). The mechanism of FT synthesis reaction is quite complex because there are many reactions occurred during the reaction (as shown in Table 1) and the product selectivity typically follows the Anderson-Schultz-Flory (ASF) distribution (Iglesia, 1997; Burton, 2001).

Table 1 Major overall reactions in the Fischer-Tropsch synthesis

Main reactions	Chemical equations
1) Paraffins	$(2n + 1)H_2 + nCO \rightarrow C_nH2_{n+2} + nH_2O$
2) Olefins	$2_nH_2 + nCO \rightarrow C_nH_{2n} + nH_2O$
3) Water gas shift reaction	$CO + H_2O \leftrightarrow CO_2 + H_2$
Side reactions	
4) Alcohols	$2nH_2 + nCO \rightarrow C_nH_{2n+2}O + (n - 1)H_2O$
5) Boudouard reaction	$2CO \rightarrow C + CO_2$

Table 1 (Continued)

Catalyst modifications	Chemical equations
6) Catalyst oxidation/reduction	$M_xO_y + yH_2 \leftrightarrow yH_2O + xM$
	$M_xO_y + yCO \leftrightarrow yCO_2 + xM$
7) Bulk carbide formation	$yC + xM \leftrightarrow M_xC_y$
Overall reactions	$nCO + (n + 0.5m)H_2 \rightarrow C_nH_m + nH_2O$
	$CO + 2H_2 \rightarrow -CH_2- + H_2O$ ($\Delta H° = -165$ kJ/mol)

Source: Henricus (2001)

2. Mechanism of the Fischer-Tropsch Synthesis

Although studies over 70 years concerned the mechanism of the Fischer-Tropsch synthesis, there still was a controversy over the reaction pathway. A mechanism for Fischer-Tropsch synthesis was quite complex and difficult to propose the existent procedures. Unlike many reactions, Fischer-Tropsch synthesis converts two of the simplest compounds, H_2 and CO, into a complex array of products, consisting predominantly of alkenes and alkanes but also varieties of minor compounds including the range of oxygenate compounds. The major mechanisms and modified forms were reported as follows.

In the 1950s, the oxygenate (enol) mechanism was achieved widely acceptance. This mechanism involved the chemisorption of CO which reacted with adsorbed hydrogen to form a unit species such as:

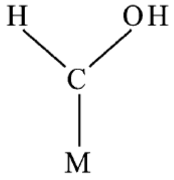

where M is metal active site.

A combination of condensation and water elimination steps by using adjacent groups on the site of active metal resulted in structural growth (Davis, 2001). The enol groups were condensed as depicted in Figure 2.

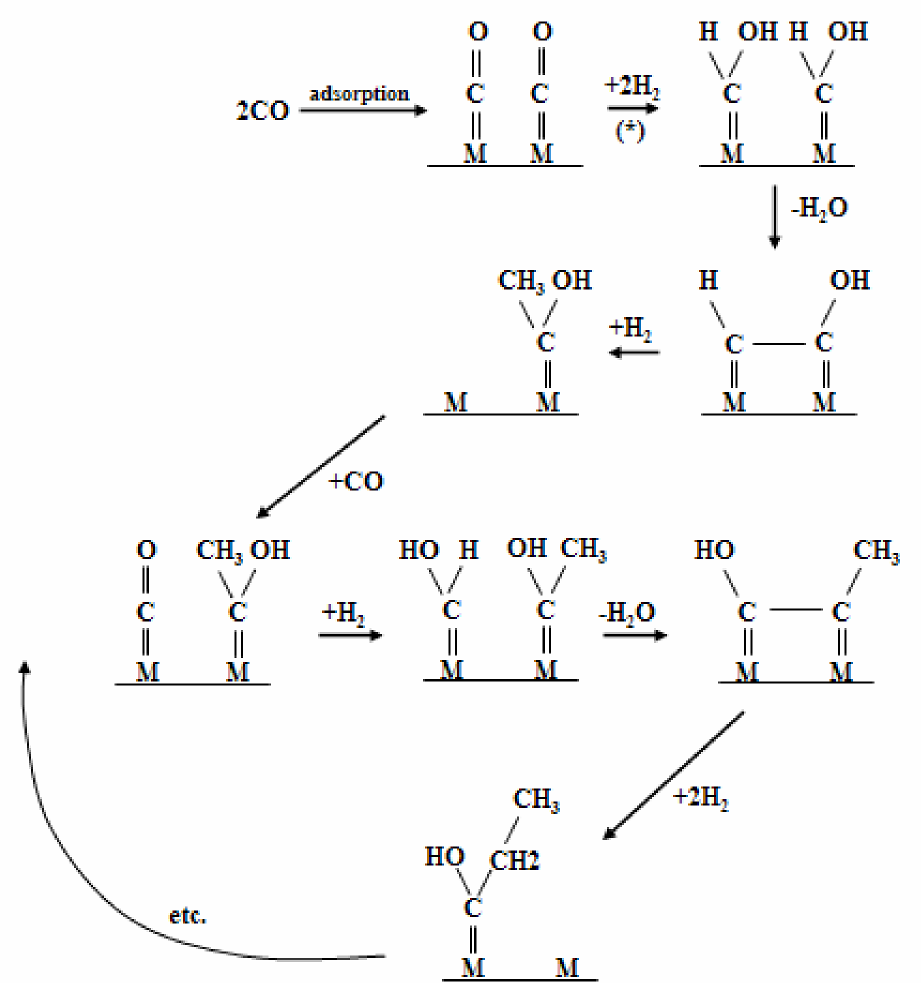

(* rate controlling)

Figure 2 Scheme of the oxygenate (enol) mechanism.

Source: Dry (1993)

Furthermore, the oxygenate mechanism that involved the reaction between CO and adsorbed hydrogen was proposed. Besides, an insertion mechanism composed of the insertion of CO into a metal-methyl or metal-methylene carbon bond was also proposed. The inserted metal-methyl or metal-methylene was then hydrogenated to produce an alcohol or alkene; oxygen in the alcohol or alcohol precursor can also be eliminated to produce an alkene product. The scheme of this mechanism was shown in Figure 3.

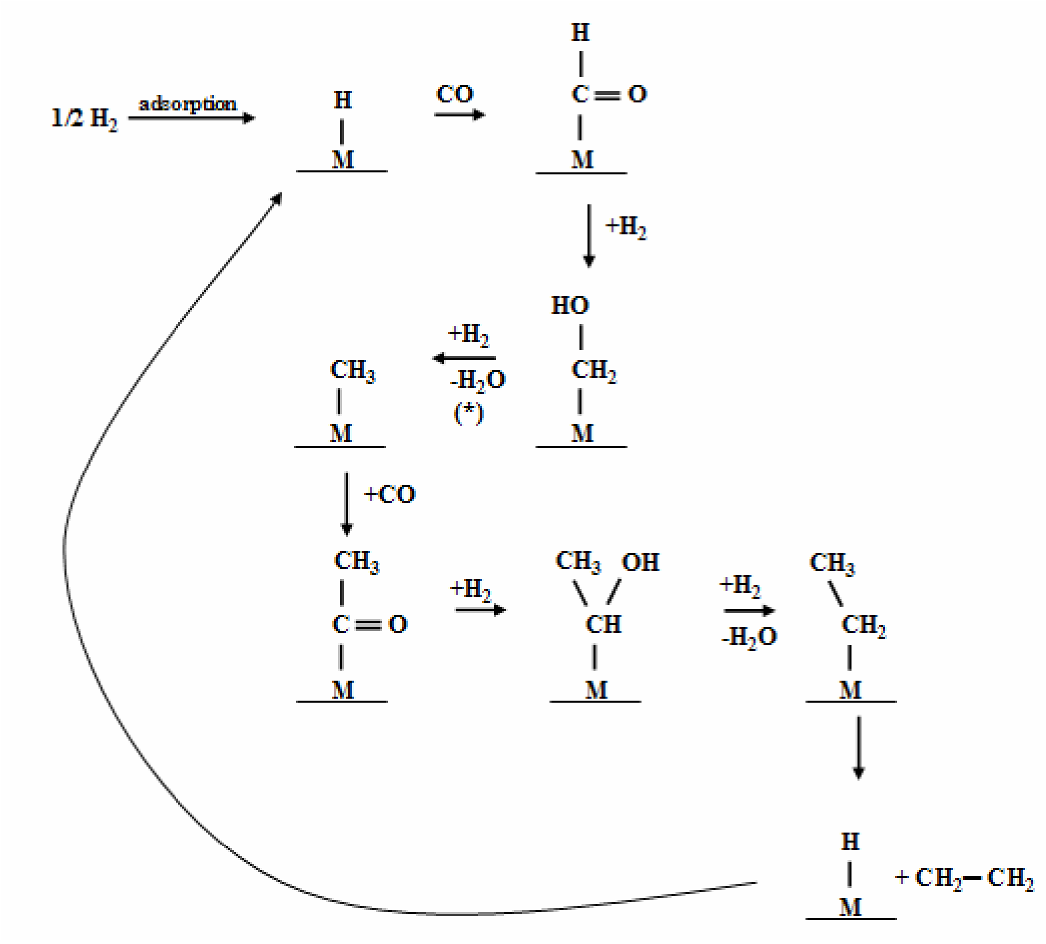

(* rate controlling)

Figure 3 The insertion of CO into a metal-methyl or metal-methylene carbon bond.
Source: Wender *et al.* (1958)

Davis (2001) also reported the original carbide mechanism for the formation of hydrocarbon and oxygenate products in Fischer-Trpsch synthesis (FTS). The carbide mechanism included the formation of metal carbide followed by the hydrogenation of metal carbide to produce various hydrocarbon products.

With the general availability of surface science instruments, it was found that CO adsorbed on active metal surfaces to produce the surface covered with carbon, and some of oxygen. This phenomenon led to the conclusion that CO was chemisorbed and dissociated to form adsorbed C and adsorbed O. This step was followed by the rapid hydrogenation of adsorbed O to produce water. The hydrogenation of adsorbed carbon to form CH_2 is much slower. This mechanism was proposed by Maitlis (1989) as shown in Figure 4.

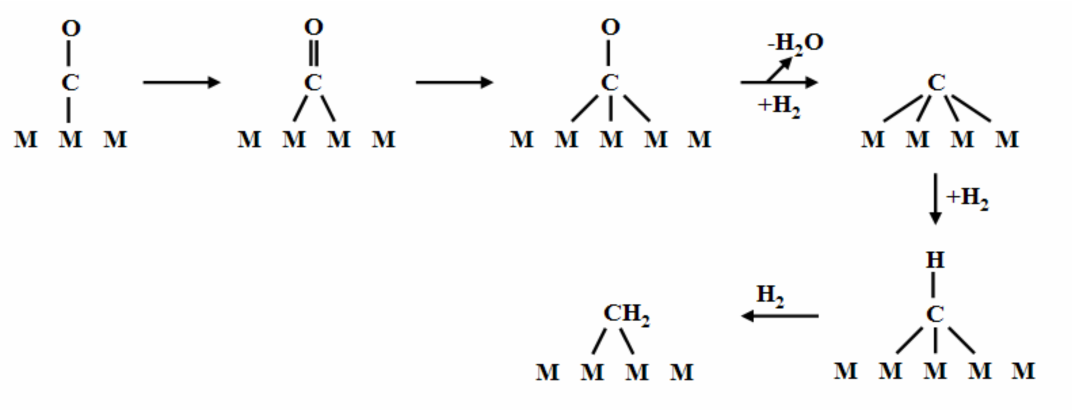

Figure 4 A mechanism for the insertion of CO into a metal-methyl or metal methylene carbon bond.

Source: Maitlis (1989)

Fischer-Tropsch synthesis (FTS) had been typically characterized as a surface polymerization since the monomer units were produced from the syngas (hydrogen and carbon monoxide) on the surface of catalyst. In 1999, Steen and Schulz reported the developed equations describing the rate of CO consumption in FT synthesis. As the FTS reaction yielded aliphatic organic compounds and the by-products water and/or carbon dioxide. Carbon monoxide was consumed for the formation of organic compounds or carbon dioxide. Therefore, the rate of CO consumption equaled the rate of organic compound formation on carbon basis and could be written as:

$$-r_{CO} = r_{C,\,org} + r_{CO_2} \tag{3}$$

where $r_{C,\ org}$ is the rate of consumption of CO for the formation of organic compounds in FT synthesis.

According to polymerization reaction, the formation of organic compounds in FTS was featured as three classes of reaction including initiation, propagation, and termination. The initiation step could be defined as the formation of a chain starter from CO and H_2. The propagation step was the incorporation of monomer units into growing chain (the chain growth step); the monomer was produced in situ on the catalyst surface during FTS reaction. Finally the termination step was the desorption of growing chains from the catalyst surface. Such that the rate of carbon monoxide for the formation of organic compounds thus equaled the sum of the rate of carbon monoxide consumption in the initiation, propagation and termination steps.

Steen and Schultz also developed the polymerization kinetics of Fischer-Tropsch CO hydrogenation based on an assumption that the rate of reaction in the FTS was controlled by the rate of hydrogenation of surface carbon which was formed through CO dissociation. Surface carbon was hydrogenated and CH_x-surface species was obtained, this reaction was regarded as a chain starter. Figure 5 presents a simplified scheme for the formation of chain starters and incorporation into growing alkyl chains using the polymerization principle.

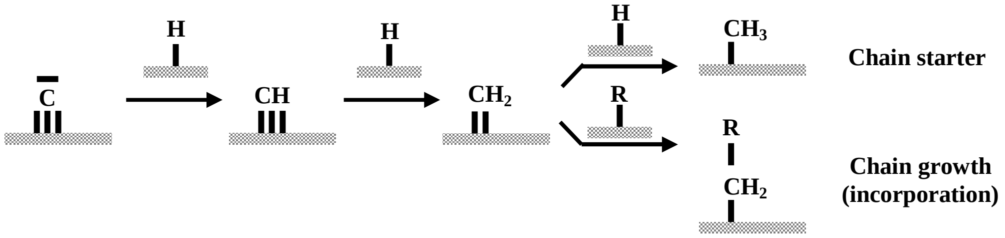

Figure 5 Simplified kinetic scheme of the successive hydrogenation of surface carbon yielding chain starters and incorporation into growing chains.

Source: Steen and Schulz (1999)

The FT synthesis produced different olefins and paraffins of different chain lengths. This process was basically a chain-building mechanism, where the chain either gained length by adsorbing another CO group, or terminated and left the catalyst as either paraffin or olefin. This was graphically shown in Figure 6.

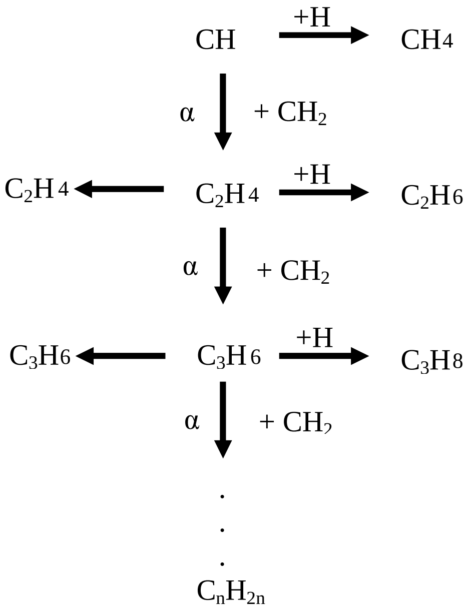

Where α is a chain growth probability

Figure 6 Two possibilities of termination; to a paraffin (right side) or a olefin (arrow to the left), or to grow further with the absorption of CO and H_2 as CH_2.

Source: Iglesia (1997)

Recently, many researchers specified the CH_2 insertion as dominant mechanism for the FTS. However, the formation of oxygenate compounds were hardly possible via the CH_2 insertion mechanism so that oxygenate compounds were assumed to be formed via the CO insertion mechanism. In order to explain both of the formation of hydrocarbons and oxygenates, the formation of CH_2 monomers was proposed and carbide mechanism involving C-O bond dissociation was firstly introduced to react with H_2 to form methylene (CH_2). In 2008, Gaube and Klein proposed a new mechanism of the FTS on iron and cobalt catalysts based on the hypothesis that two incompatible mechanisms were involved on CH_2 insertion and on CO insertion, respectively. The development of the novel mechanism was based on experimental studies of many researchers who employed various types of iron and cobalt catalysts.

3. Fischer-Tropsch Catalysts

Fischer-Tropsch synthesis (FTS) process was shown to be catalyzed by certain transition metal, with cobalt (Co), iron (Fe) and ruthenium (Ru) presenting the noticeably high activity (Vannice, 1977). Cobalt and iron based catalysts were typically applied to FTS process. Moreover, ruthenium and nickel based catalysts also had good activity for FTS, however the availability of ruthenium was limited, thus it was not economically possible. The nickel based catalyst had high activity but methane selectivity was very high, and additionally the performance at high pressure was poor, due to production of volatile carbonyls. Consequently, the FTS reaction was catalyzed focusing on cobalt (Iglesia, 1997 and schultz, 1999) and iron (Luo and Davis, 2003 and Zhang *et al.,* 2006) as practical catalysts.

Nevertheless, the supported Co-based catalysts have been widely used for the synthesis of long chain paraffins (Dry, 1990; Chanenchuk *et al.,* 1991; Iglesia,1997) according to their high activity for syngas conversion and high yields of linear hydrocarbons in FTS reaction at medium reaction temperature and pressure (Iglesia, 1997; Ernst *et al,* 1999). Moreover, Co-based catalysts were more stable toward deactivation by water (by-product of the FTS reaction), less active for the competing water-gas-shift (WGS) reaction and produced less oxygenates than the Fe-based systems. In order to achieve high amount of surface-active sites (Co^0), cobalt precursors were dispersed on porous carriers such as SiO_2, Al_3O_4 and TiO_2.

In order to increase the conversion and product selectivity of cobalt catalyst, Martinez *et al.* (2003) studied the performance of FTS by investigating the influence of cobalt loading (10–40 wt. % Co) and type of cobalt precursor on catalytic properties of cobalt support SBA-15 mesoporous silica catalysts (Co/SBA-15). The performance of Co/SBA-15 catalysts were tested in a fixed-bed stainless-steel reactor at the reaction temperature of 220 °C (P = 20 bar, $H_2/CO = 2$). From the result, a maximum CO conversion of 33.1 % was obtained from the cobalt loading amount of 30 wt. % of which the highest amount of Co active sites were obtained. Moreover, the selectivity of hydrocarbon products was found influenced by the amount of cobalt loading attributed to the higher reducibility of metals with high degree of metal content.

Cobalt catalyst had been widely applied together with another metal. A lot of researchers worked on adding the promoters to enhance the performance of FTS reaction. In order to obtain higher selectivity of heavy hydrocarbons, FTS catalysts were modified to increase catalytic activity and FTS performances. Ruthenium and cobalt can also be applied as catalysts for FT synthesis. Dunn *et al.* (2004) prepared cobalt and ruthenium loaded on a silica aerogel support. Rhutenium catalysts were considerably more active than cobalt catalysts at the same metal loading amount where the product distributions were similar. Hydrocarbon products from C_1 through C_{15} were detected with the product distribution centered around C_9-C_{10} at 265 °C and C_{13} at 225 °C.

In 2008, Wan *et al.* investigated the effects of copper (Cu) and potassium (K) promoters on precipitated iron-based catalysts for FTS. The incorporation of Cu and K promoters to precipitated Fe catalyst was found to have significant role on the adsorption, reduction behaviors and catalytic performances of FTS. The addition of Cu metal promoted high dispersion of cobalt metal on SBA-15 support and the application of using both of Cu and K as promoters exhibited excellent stability and significantly improved the FTS and water-gas shift (WGS) activities as well as the chain growth reaction.

Form the previous information, it is clearly seen that the performances of FTS reaction can be strongly promoted by selection of catalysts, mostly iron or cobalt catalyst where the reaction takes place.

Preparation of Metal Supported Mesoporous Silica Catalysts

Mesoporous silica with unique structural properties have demonstrated a considerable potential for the development of processes and materials designed to meet a range of environmental and technological challenges. The discovery of ordered mesoporous materials with well-defined pore sizes within the range of 2-50 nm, regular channel systems, high thermal stability and the potential for the isomorphous substitution rises up the new opportunities in material chemistry and catalysis (Kresge *et al.,* 1992; Beck *et al.,* 1992; Inagaki *et al.,* 1993; Zhao *et al.,* 1998).

1. Mesoporous Silica Support

Periodic mesoporous silicas have attracted great attention to many researchers to use as catalyst support materials. Narrow pore-size distribution, high surface area and pore volume make them suitable as the excellent supports for metal and metal oxide catalysts (Zhao *et al.*, 1998; Zholobenko *et al.*, 2001). Two most common types of periodic mesoporous silica are MCM-41 and SBA-15. MCM-41 materials were usually synthesized in basic mediums, while SBA-15 materials were typically prepared in acidic conditions. SBA-15 materials had larger pore than MCM-41 and the pore size can be adjusted from 2 to 30 nm at the stage of synthesis by using various surfactants and different reaction conditions (Coma, 1997; Zhao *et al.* 1998; Zholobenlo *et al.* 2001). In addition, SBA-15 material with high specific surface area and pore wall thickness, 2D hexagonal pore-arrangement, and controllable uniform mesopore diameters has attracted great attention for large number of applications in catalysis and separation (Guari *et al.,* 2001; Konya *et al.,* 2002; Mirji *et al.,* 2007). Recently, SBA-15 material was used commercially as a catalyst support and represented good properties for catalytic reaction according to their large internal surface area (~1,000 m^2/g) and narrow pore size distribution.

During the last several years, SBA-15, which is the polymer-templated silica with hexagonally ordered mesopores, has been extensively studied and evaluated for numerous applications in the field of catalysis and separations (Zhao *et al.,* 1998; Selvaraj *et al.,* 2002; Jana *et al.,* 2003; Tuel *et al.,* 2004; Grieken *et al.,* 2006). In 2004, Ohtsuka *et al*. prepared mesoporous molecular sieves (MCM-41 and SBA-15) with different pore diameters and used as high loading supports of cobalt catalysts. The performances of the cobalt catalysts in FT synthesis were comparatively studied. Template ion exchange method and conventional impregnation method were used to incorporate cobalt into the support framework. SBA-15 mesoporous silica with larger pore diameter compared with MCM-41 material exhibited higher CO conversion in FT synthesis. The catalyst with pore diameter of 8.2 nm showed the highest CO conversion of 72 %. In addition, Saib *et al.* (2002) reported that MCM-41 support with smaller pore size compared to that of SBA-15, could lead to the formation of smaller cobalt oxide particles, where were more difficult than the larger particles to reduce to metal because of the stronger interaction between metals and support.

In addition, the thicker pore wall of SBA-15 compared to that of MCM-41 exhibited the different behavior of mesoporous silicas. SBA-15 has higher thermal stability compared to MCM-41, as a result, SBA-15 structure was not destroyed during the preparation process, i.e., drying, calcination and impregnation (Khodakov *et al.,* 2005). Another feature of SBA-15 was the existence of micropores interconnecting hexagonally ordered mesopores, which makes it more suitable for catalysis because the interconnection facilitates diffusion inside the entire porous structure (Shah *et al.,* 2007).

In 2005, Nanta-ngern *et al.* successfully synthesized SBA-15 mesoporous silica with average pore diameter of 9 nm from rice husk ash under strong acidic condition using Pluronic P123 as the structure-directing agent. The molar ratio of SiO_2 : Pluronic P123 : H_2O : HCl of 1: 0.0875 : 200 : 4 was used. The highly ordered pore structure of SBA-15 (as shown in Figure 7) was obtained at the hydrolysis-condensation temperature of 40 °C for 24 h and hydrothermal aging temperature of 100 °C for 24 h.

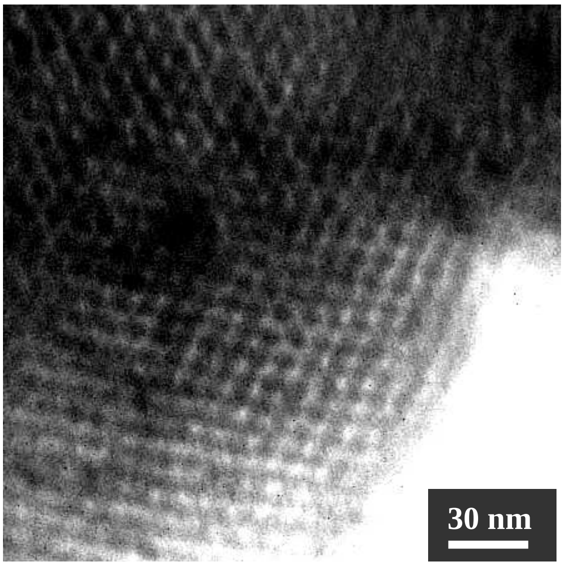

Figure 7 TEM image of SBA-15 synthesized at the molar ratio of 1 SiO_2 : 0.00875 Pluronic P123 : 200 H_2O : 4 HCl.

Source: Nanta-ngern *et al.* (2005)

Chareonpanich *et al.* (2007) also applied an ultrasonic technique for the synthesis of SBA-15 mesoporous silica with highly ordered hexagonal pore-arrangement and narrow pore size distribution within much shorter hydrolysis–condensation time. In their work, SBA-15 mesoporous silica was synthesized from rice husk ash using the ultrasonic technique at the stage of hydrolysis–condensation. The hydrolysis–condensation time was reduced from 24 h to 3 h compared with the conventional method (Nanta-ngern *et al.*, 2005).

In this present work, so as to incorporate metal ions directly into SBA-15 structure by modification of sol-gel process, the understanding of the stage during the synthesis procedure of SBA-15 mesoporous silica is also needed. In 2008, Zholobenko *et al.* reported the valuable structural information of SBA-15 synthesis. In order to obtain structural data, Synchrotron based Small Angle X-ray Scattering (SAXS) and Small Angle Neutron Scattering (SANS) techniques were applied to clarify the formation mechanism of SBA-15 mesoporous silica; the synthesis mixture was characterized during the reaction of SBA-15 synthesis. The investigation of the kinetics of the initial stage for SBA-15 synthesis under the reaction condition was also focused. The evolution of the ordered mesoporous silica during SBA-15 synthesis was monitored and the results confirmed that the formation of SBA-15 proceeded according to the cooperative self-assembly mechanism. Through the hydrolysis and condensation reaction, three major stages in the synthesis of SBA-15 were identified (Figure 8).

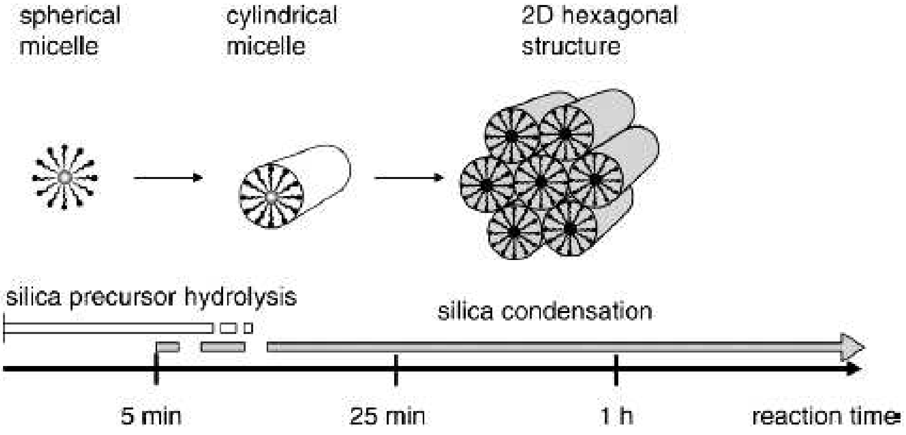

Figure 8 Three initial stages of the evolution of the ordered mesoporous silica during SBA-15 synthesis.

Source: Zholobenko *et al.* 2008

During the first stage, only spherical micelles of poly(ethylene oxide)-poly(propylene oxide)-poly(ethylene oxide) block copolymer (PEO-PPO-PEO) were presented in the synthesis mixture, within the first 5 minutes of the reaction. The PPO (polypropylene oxide units) hydrophobic blocks made up the inner micelle core and the PEO (polyethylene oxide units) hydrophilic blocks interacting with water molecules and silicate species represented the micelle corona; in the synthesis mixture, these micelles were surrounded by an aqueous solution of hydrochloric acid. In the second stage, between 5 and 20 minutes of the reaction period, the formation of hybrid organic-inorganic micelles was observed accompanied with the transformation from spherical to cylindrical micelles. The precipitation of the ordered SBA-15 was taken place during the third stage. These micelles began to aggregate into a two-dimensional hexagonal structure confirming that the precipitation occurred as the result of self-assembly of hybrid cylindrical micelles into the structure of SBA-15 mesoporous silica.

In the hexagonal matrix, the cylinders were weakly linked initially by the corona. As the synthesis proceeded, the voids between the cylinders were filled with silica species and further condensation reaction resulted in cross-linking and covalent bonding between coronas of the cylindrical micelles. Then, the condensation of silica species continued for the reaction duration of about 20 h, at 40 °C. In this stage, the diameter of the inner core of the obtained SBA-15 structure remained equal to the diameter of the PPO core in the surfactant-silicate cylindrical micelles. Subsequently, the synthesis mixture exposed to the higher temperature typically 80-100 °C under hydrothermal condition and about 500 °C during calcination. It led to further condensation and densification of the structure with an increase of pore size, resulting in the formation of highly ordered and thermally stable SBA-15 mesoporous phase.

2. Effect of Catalyst Preparation on FTS Performances

The selectivity towards the desired products is the main subject in FT synthesis. One of the most important product selectivity is the selectivity of C_{5+} hydrocarbon products. Because the ultra clean liquid fuels are of industrial interest, it is significant to improve the performances of FT synthesis by increasing the C_{5+} selectivity and suppress the formation of undesired metane in FT products. Either the properties of synthesized catalyst support or the methods or chemicals used in catalyst preparation have direct influence on FTS catalytic performance. The regarding information is presented as follows.

2.1 Effect of Catalyst Support on FTS Performance

In fact, it was well-known that the catalytic conversion of carbon monoxide occurred on the surface of porous catalyst. For this reason, the structure of catalyst support greatly affected the orientation of metal particles locating on the surface of catalyst support. Many studies have been carried out on Fischer-Tropsch synthesis using different supports for cobalt loading, including alumina (Bechara *et al.*, 2001 and Hosseini *et al*., 2004), titania (Zennaro *et al.*, 2000), silica (Khodakov *et al.*, 1997; Sun *et al.*, 2000; Tsubaki *et al.*, 2001), and etc.

In 2002, the study of the influence of average pore diameter of silica support on the physical and chemical properties of supported cobalt catalysts and their performances in FT synthesis were carried out by Saib *et al.* As an average pore diameter larger or equal to 4 nm, the metal crystallite size and degree of reduction were higher with increasing pore diameter of the support. For the impregnated catalysts, the metal crystallites seemed to appear in clusters on the surface of catalyst support and when the average pore diameter increased, the size of cobalt clusters also increased.

SBA-15 mesoporous silicas were good catalyst supports to synthesize long chain hydrocarbons according to their large pore diameters. Khodakov *et al.* (2002) determined the pore size effects on the FTS reaction rate and selectivity over cobalt catalysts using SBA-15 and MCM-41 mesoporous silicas as catalytic supports. As a result, the cobalt catalysts with pore diameter exceeded 3 nm provided much higher reaction rate and C_{5+} selectivities. Furthermore, the size of cobalt particles and the degree of reducibility in wide pores (SBA-15) and narrow pore (MCM-41) were different. The larger pore diameter lead the size of supported cobalt species to increase. The supported catalyst with pore diameter of 10 nm was found to be the most active and selective catalyst for hydrocarbon formation in FT synthesis (Khodakov *et al.*, 2003). Similarily, Ohtsuka *et al.* (2004) also reported that the performance of Co support SBA-15 catalyst in the FT synthesis was higher than that of MCM-41 supported catalyst. The Co/SBA-15 catalyst with the pore diameter of 8.3 nm gave highest conversion (72 %) and efficient production of C_{10}-C_{20} fraction as the main component of diesel fuel.

2.2 Effect of metal dispersion on catalytic performance

The dispersion of metal species on catalyst support have significant role on catalytic FTS performance. Higher concentration of cobalt metal sites favors higher rate of FTS reaction. So, cobalt dispersion and reducibility seem to be important parameters affecting the number of cobalt surface sites and thus the overall catalytic performance (Iglesia, 1997).

Catalytic activity and selectivity are also strongly influenced by the surface properties of the support because they can change the interaction between cobalt and the support, resulting in different dispersion and reducibility of the supported cobalt. In 2003, Khodakov *et al.* reported the effect of support structure on the cobalt dispersion. Two types of silicas were used as catalytic support including including the SBA-15 mesoporous silica with pore diameter of 9.1 nm and narrow pore size distribution and the commercial mesoporous silica (Cab-osil M5) with pore diameter of 33 nm and broad pore size distribution. The results showed that metal dispersion was better when SBA-15 material was applied; this was because SBA-15 led to higher cobalt dispersion and also prevented cobalt particles from sintering.

In addition, metal precursors and pretreatment conditions mainly influenced on the structure and catalytic performance of Co/SiO_2. Although silica support promoted high reducibility according to weak interaction between metal and silica support, they favored the agglomeration of supported cobalt particles. A solid-state reaction of silica and cobalt oxides also resulted in cobalt silicate (mixed oxide) which played negative role on the catalytic performance (Coulter and Sault, 1995).

In 2005, Giradon *et al.* prepared the FTS catalysts via aqueous impregnation of silica using cobalt nitrate and cobalt acetate as metal precursors. Significantly, they reported that higher dispersion was found with the catalyst prepared from cobalt nitrate, whereas the catalyst prepared from cobalt acetate generated cobalt silicate as a dominant phase which caused more difficult reducibility and larger agglomeration of cobalt clusters. The low cobalt dispersion was attributed to the sintering of Co_3O_4 crystallites at high temperature. From this research, it can be concluded that types of metal precursors strongly affect the dispersion of cobalt species on silica support.

The impregnation solvents also have effects on the activity of cobalt catalysts. Zhang *et al.* (2007) prepared silica-supported cobalt catalysts by incipient wetness impregnation with different cobalt nitrate solutions. The catalyst prepared from dehydration of ethanol solution exhibited stable and higher activity, as well as low methane selectivity from that of aqueous solution. Cobalt crystalline size obtained from dehydrated ethanol was more uniform and smaller than that of aqueous solution. The cobalt ions dissolved in dehydrated ethanol favored the distribution of cobalt over entire silica surface, resulting in high dispersion of supported cobalt but only larger clusters existed by using water as a impregnation solvent. According to the decreasing of cobalt crystalline size, the amount of metal active sites and reactive adsorbed CO on the catalyst surface was increased.

Interestingly, Reubroycharoen *et al.* (2006) reported that the drying process also played an important role on the dispersion of active metal sites. The conventional heating method, which drying oven was applied, caused gas flowing inside out from the support. When volatile matters within the catalyst support were not completely removed, the flowing gas resulted in an accumulation of the active species on the outer surface of support and low dispersion. Instead of preparing catalysts by conventional drying and calcination, they used a commercial microwave oven in drying and calcination process of impregnated catalysts to overcome this undesired phenomenon. It can be seen that the cobalt species prepared by microwave irradiation were more uniform and better dispersion within catalyst pellets compared to that prepared by the conventional heating method. The rapid drying of microwave irradiation caused uniform particle size and distribution of Co/SiO_2 (as shown in Figure 9) while the conventional method displayed the partly agglomeration of cobalt particles on the surface.

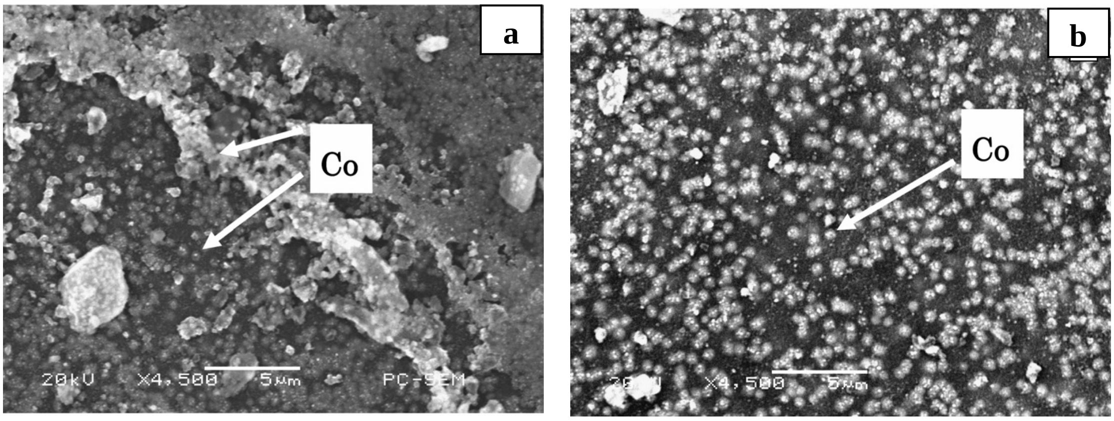

Figure 9 SEM images of Co/SiO_2 catalysts: (a) conventional heating catalyst and (b) microwave irradiation catalyst.

Source: Reubroycharoen *et al.* (2006)

Metal Loading Techniques

SBA-15 mesoporous silica itself is not a suitable catalyst for FTS reaction since it has less activity. However, due to its unique characteristics, it can be applied as a catalyst support material especially cobalt metal for FTS reaction or a catalytic site by partial substituting Si^{4+} by another cations (Lou *et al*., 2008). Therefore, it is a great importance to introduce metal atoms with good distribution into the mesoporous silica framework. A simple way to fuctionalize SBA-15 mesoporous silica is to introduce active metal ions into the silica metrix either during the synthesis (direct synthesis) or by post-synthesis modification of SBA-15. The details of metal loading techniques are described as follows.

1. Post Synthesis Method

As far as we know, most of research works reported the metal containing SBA-15 materials prepared by post-synthesis method. Different strategies of synthesis may lead to major changes in bonding and environment of metal species within SBA-15 mesoporous silica (Li *et al.*, 2005). Generally, impregnation is the most common method for cobalt-containing mesoporous silica synthesis. By using this method, mesoporous catalyst supports are impregnated by various types of cobalt salt solutions, for example cobalt acetate, cobalt nitrate (Bhoware *et al.,* 2006; Mochizuki *et al.,* 2006) and cobalt sulphate (Lou *et al*., 2008).

Co-based catalysts were widely prepared by an impregnation method followed by drying, calcinations and H_2 reduction (Reuel and Bartholomew, 1984). Cobalt nitrate, a conventional Co precursor, was considered to decompose to Co_3O_4 species by drying and calcination process (Earnst *et al.,* 1984; Bian *et al.,* 2003). During H_2 reduction, the Co_3O_4 species were reduced to CoO species and then consecutively reduced to metallic Co or Co-SiO_2 interaction species (Ming and Baker, 1995 and Khodakov *et al.,* 1997).

Martinez *et al.* (2003) prepared mesoporous Co/SBA-15 catalysts for the Fischer-Tropsch synthesis by using impregnation method. The influence of cobalt loading, cobalt precursor, and promoter were investigated. For Co/SBA-15 catalysts prepared from cobalt(II) nitrate, the dispersion of cobalt species was increased and the extent of cobalt reduction was increased with the amount cobalt loading. A maximum CO conversion was found for the catalyst with approximately 30 wt. % Co loading. The addition of 1 wt. % Rhenium enhanced the reducibility of cobalt oxides and increased the catalyst activity. Rhenium could promote the formation of long chain hydrocarbons (C_{10+}) while decreasing methane selectivity. Cobalt dispersion was also improved by the promotion of Mn but the degree of reducibility was decreased, producing catalysts with less active than the unpromoted catalyst.

In 2007, Zhang *et al.* prepared silica-supported cobalt (20 wt. %) catalysts by incipient-wetness impregnation. In order to study the effects of impregnation solvent on Co/SiO_2 catalysts, different cobalt nitrate solutions including ethanol and aqueous solutions were used to prepare the cobalt catalysts. They found that the catalyst activity greatly depended on the type of impregnation solvent. The size of cobalt particles prepared from ethanol dehydration was smaller and more uniform than that of the aqueous solution at the same amount of cobalt loading. However, its reducibility was slightly poorer than that of cobalt catalyst impregnated by aqueous solution. The lower reduction degree of cobalt supported catalyst impregnated by ethanol solution could be ascribed to the decreased polarity of the solvent, which increased the interaction between cobalt complex and silica surface. Using ethanol as impregnation solvent promoted the distribution of Co over the silica surface, resulting in higher dispersion of supported cobalt. Moreover, the catalyst prepared from dehydrated ethanol solution was considered to increase amount of active sites and more reactive adsorbed CO on the surface in liquid-phase FTS reaction, showing high catalyst activity and low methane selectivity.

The cobalt catalysts prepared by post synthesis method somehow play negative role on catalytic performances. In 2006, Bhoware *et al.* studied the performances of cobalt containing MCM-41 catalysts prepared by three different methods including grafting, direct hydrothermal and immobilization methods. The experimental results showed that the BET surface area of cobalt supported catalysts prepared by grafting and immobilization methods (post-synthesis method) were sharply decreased from 1,010 to 820, and 700 m^2/g, respectively. In contrast to the cobalt catalysts prepared by direct hydrothermal method, the substitution of cobalt species into silica framework slightly increased the specific surface area from 1,010 m^2/g to 1,050 m^2/g. As a result, cobalt supported catalyst prepared by direct hydrothermal technique exhibited higher conversion than that of grafted and immobilized catalysts in catalytic reaction.

As mentioned above, it could be concluded that post synthesis methods are not suitable to prepare catalysts with highly isolated active sites. The impregnation method has the disadvantage upon high loadings of metallic cobalt. During the preparation of metal incorporated SBA-15 via post-synthetic methods, metal oxide often formed in the mesopore channels and/or on the external surfaces, resulting in pore blockage and reducing the surface area and pore volume, or played a negative role in catalysis which lower the FTS reaction performances (Chen *et al.,* 2004; Kustrowski *et al.,* 2005). Consequently, many researchers had worked on the modification of metal loading techniques to enhance the dispersion of metal active sites for improving catalytic performances.

2. Direct Synthesis Method

Post-synthesis methods have the disadvantage of uncontrolled growth of metal particles on the surface of catalyst support since no preventive measures are taken to ensure the metal precursors isolation within the channels. So, the preparation of metal supported catalysts with high degree of metal dispersion is one of the major challenges in the design of silica-based FT catalysts. It would be very useful to explore better and simpler methodologies for localizing metal nanoparticles within the mesochannels while retaining high surface area and pore volumes which for catalysis instead of post-synthesis methods i.e., impregnation and grafting techniques (Prashar *et al.,* 2008).

The alternative way to introduce cobalt species into the mesoporous silica framework was an addition of cobalt precursor into the synthesis mixture, followed by hydrothermal treatment; so called direct synthesis method (Yang *et al.,* 2007; Lou *et al.,* 2008). The incorporation of transition metals into the framework of SBA-15 silica by direct synthesis had become a very attractive goal for many researchers because the heteroatom incorporation into the silica structure could be carried out in only one step and more stable metal species were obtained (Melero *et al.,* 2005). Furthermore, the preparation of catalysts with well-dispersed isolated metal species was very important to obtain high activity and selectivity for the catalytic reactions (Bharat *et al.,* 2001; Wang *et al., 2005*; Selvaraj and Kawi, 2008; Aguado et al., 2008). It is still a challenge to find a one-step route of metal incorporation into SBA-15 in order to increase the catalytic performance without changing its structural order or the complexity of the synthesis. For this reason, direct synthesis methods is a crucial way to effectively synthesize highly dispersed metal or metal oxide-containing SBA-15 mesoporous silica.

Many efforts have been devoted to the study of incorporating transition metals into SBA-15 framework for a variety of application. Bharat *et al.* (2000) attempted to achieve a high degree of Ti substitution without the loss of textural properties, especially pore size of the SBA-15. The Ti/SBA-15 catalysts were prepared via direct synthesis method under microwave-hydrothermal conditions. In addition, Vinu *et al.* (2005) reported that the main approach used to incorporate iron atoms into SBA-15 silica was a simple adjustment of the pH of gel mixtures above the isoelectric point of silica (pH~2). In this conditions, the negative charge of silica species can easily interact with the positive charge of iron complex, resulting in incorporation of larger quantities of Fe into the SBA-15 mesoporous silica matrix.

Prashar *et al.* (2008) developed the synthesis method for incorporating platinum (Pt) nanoparticles into mesoporous silica SBA-15 while retaining high surface area and pore volume. Pt nanoparticles were encapsulated into SBA-15 silica by adding surfactant (cetyl trimethyl ammonium bromide, CTAB) to modify polymer micelles in the synthesis mixture. This method treated the electrostatic interaction between metal precursor salt and the ionic surfactant head groups which were incorporated into the polymer micelle in a controlled manner. Pt precursor could diffuse well into the micelle structure initiated by the attractive force towards the ionic head groups. The modifying surfactant facilitated metal precursor diffusion by interaction with cationic head groups without changing the structure of micelles, resulting in the formation of well-ordered SBA-15 silica with highly dispersed, uniform Pt particles within mesochannels. Pt incorporation using this method did not have any effect on the formation of SBA-15 silica and could be utilized in nanocatalysis more effectively. The scheme of Pt particles formation is shown in Figure 10.

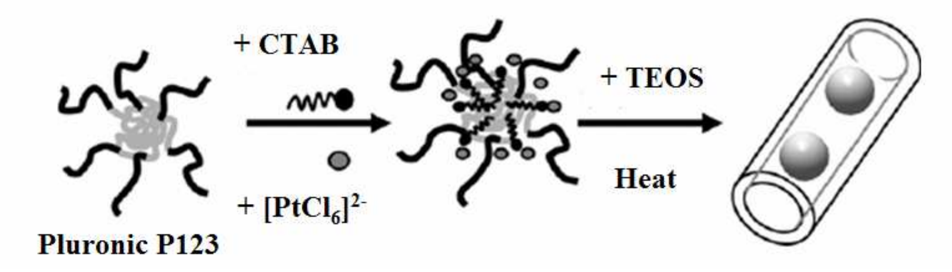

Figure 10 Formation of nanoparticles within the mesochannels by dispersing metal precursors in surfactant-modified polymer micelles.

Source: Prashar *et al.* (2008)

In 2004, Wu *et al.*, firstly reported that Al^{3+} and Ti^{4+} were successfully substituted into SBA-15 mesoporous silica by the so-called pH adjusting approach. Chen *et al.* (2004) synthesized Zr-incorporated SBA-15 and demonstrated that the addition of inorganic salts, e.g., NaCl, could efficiently improve the ordered structure of the mesoporous Zr-SBA-15 silica. A much narrower pore size distribution with the addition of salt was also observed.

Shah *et al.* (2007) prepared Sn/SBA-15 silica via a direct synthetic route under milder acidic conditions than normally employed for the preparation of SBA-15 mesoporous silica. The changes in the pH conditions for the gel were made through the adjustment of the n_{H2O}/n_{HCl} ratio ($1 < pH < 2$) during preparation. As a result, the incorporation of Sn in SBA-15 framework was successfully obtained by adjusting the n_{H2O}/n_{HCl} ratio without affecting the structural order of SBA-15 silica. The pH adjusting approach could also control the amount of Sn incorporation.

The knowhow of incorporation of Co into the SBA-15 framework had been rarely reported. Moreover, it was very difficult to prepare SBA-15 containing heteroatoms in the framework by using condensation process because the metal ions was exist as cations and the formation of metal-O-Si bonds under the strong acidic condition ($pH < 2$) was quite difficult (Baes *et al.*, 1976 and Corma, 1997).

Indeed, the cobalt loading techniques have a great effect on the FTS catalytic behaviors. The cobalt ions incorporated into the framework of molecular sieve materials has attracted considerable attention as a novel catalyst to increase the catalytic FTS performance due to the highly dispersed metal active sites within the catalyst structure. Lou *et al.* (2008) successfully synthesized highly ordered Co-incorporated SBA-15 under mild conditions ($pH>2$) by direct synthesis. They used sodium hydroxide solution to adjust the pH of the synthesis gel. Sodium ion was found to effectively improve the structural order of the mesoporous Co/SBA-15 because the presence of metal salt in the synthesis gel promoted the decrease of the critical micelle concentration and the formation of the mesostructures without affecting structural and textural order. The preparation of Co/SBA-15 catalysts at pH

3 were found to be the optimum condition; the surface area and pore volume were the highest among other pH values. TEM images of Co/SBA-15 sinthesized at pH 3 are shown in Figure 11.

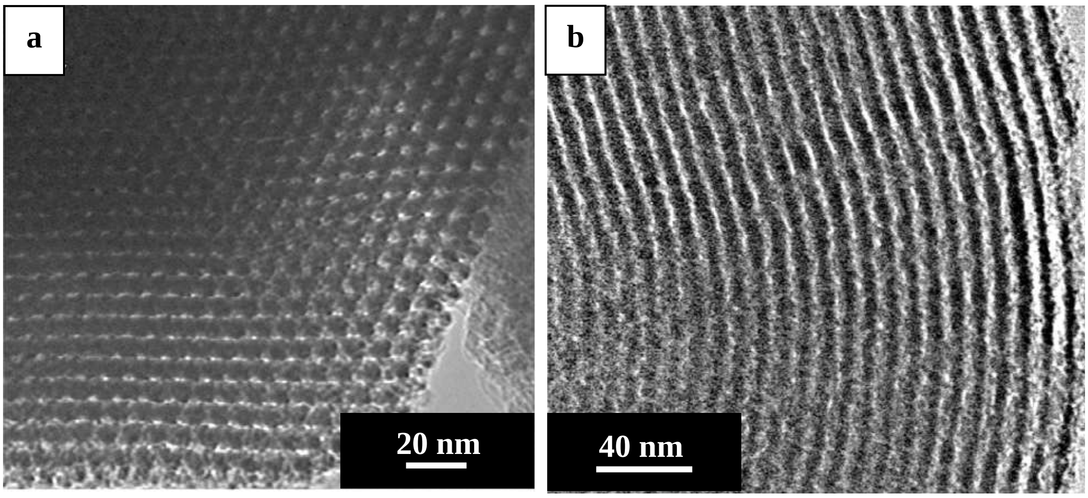

Figure 11 TEM images of calcined Co/SBA-15 catalysts prepared with pH of 3. The pictures of (a) in the direction perpendicular to the pore axis and (b) in the direction parallel to pore axis.

Source: Lou *et al.* (2008)

From the literature reviews, it is clearly seen that methods used for preparing transition metal catalysts play significant role on the catalytic reaction. The catalytic activity and performance of cobalt catalyst in FTS can be improved by preparing the cobalt loaded SBA-15 support with a good metal dispersion. In this research, SBA-15 silica supported cobalt catalysts have been prepared using two different metal loading techniques which were post synthesis method and direct synthesis method. The post synthesis method including the conventional impregnation method and the solvothermal technique were used to prepare 10 wt. % cobalt-containing SBA-15 mesoporous silica. In the direct synthesis method, the sol-gel process was simply modified to synthesize SBA-15 silica containing cobalt metal using pH adjusting approach. Since only a few reports demonstrating the incorporation of Co^{2+} ions into the SBA-15 silica framework were presented, it is still a great challenge in the field of mesoporous silica synthesis and application to prepare cobalt loaded SBA-15 silica with both good metal dispersion and structural regularity of SBA-15 silica support.

The aim of the present study is to synthesize Co-based FTS catalysts with highly order structure by the indirect and direct synthesis methods and to investigate the effect of metal loading techniques on the properties of the Fischer-Tropsch catalysts and their catalytic performances. The influence of cobalt dispersion on the catalytic behavior in FTS reaction have also been extensively investigated.

MATERIALS AND METHODS

In this chapter, the information including the chemicals and instruments, and the experimental preparation and procedures were clarified. In the first part, chemicals and devices used in the preparation of catalysts, testing units of FT synthesis performances, and product analysis unit were explained. The methods of catalyst synthesis and catalyst performance testing were reported in the second part. The preparation of silica support, metal loading techniques and the investigation of FT synthesis reaction were explained in detail.

Chemicals and Equipments

1. Chemicals

The chemicals used for catalyst preparation and Fischer-Tropsch synthesis reaction are listed below:

1.1 Chemicals for Catalyst Preparation

1.1.1 Rice husk ash using as a silica source was refluxed with 1 L of 1 M HCl solution for 2.5 h, washed with distilled water and dried at 120 ^{o}C (Figure 12).

Figure 12 Photo of rice husk.

1.1.2 Pluronic P123 ($PEO_{20}PPO_{70}PEO_{20}$, Aldrich)

1.1.3 Cobalt nitrate ($Co(NO_3)_2·6H_2O$, 99.0% purity, UNIVAR)

1.1.4 Sodium hydroxide ($NaOH$, 99% purity, Merck)

1.1.5 Hydrochloric acid (HCl, 36.5-38.0 wt% purity, J.T. Baker)

1.1.6 Tetrahydrofuran (C_4H_8O, UNILAB)

1.1.7 Distilled water

1.2 Chemicals for Fischer-Tropsch Synthesis Reaction

1.2.1 Reactant gases

- Carbon monoxide (CO, 99.2% purity, TIG)
- Hydrogen (H_2, 99.99% purity, TIG)
- Nitrogen (N_2, 99.99% purity, TIG)
- Oxygen (O_2, 99.5% purity, Linde)

1.2.2 Standard gas

Mixture of 5% carbon monoxide (CO), 5% carbon dioxide (CO_2), 5% methane (CH_4), 5% ethylene (C_2H_4), 5% ethane (C_2H_6), 5% propylene (C_3H_6), 5% propane (C_3H_8), 5% i-butane (C_4H_{10}), 5% n-butane (C_4H_{10}) in helium (He) balance (SOXAL)

1.2.3 Standard liquid hydrocarbons

- n-Pentane (n-C_5H_{12}, 99.64 % purity, Fischer chemicals)
- n-Hexane (n-C_6H_{14}, 99 % purity, Merck)
- n-Heptane (n-C_7H_{16}, 99.5 % purity, Fluka)
- n-Octane (n-C_8H_{18}, 99 % purity, Merck)
- n-Nonane (n-C_9H_{20}, 99 % purity, Merck)
- n-Decane (n-$C_{10}H_{22}$, 99 % purity, Merck)
- n-Undecane (n-$C_{11}H_{24}$, 97 % purity, Fluka)
- n-Dodecane (n-$C_{12}H_{26}$, 99 % purity, Merck)
- n-Tridecane (n-$C_{13}H_{28}$, 99 % purity, Fluka)
- n-Tetradecane (n-$C_{14}H_{30}$, 99 % purity, Fluka)
- n-Pentadecane (n-$C_{15}H_{32}$, 99 % purity, Fluka)
- Toluene (C_7H_8, 99.64 % purity, Fischer chemicals)
- Octanol ($C_8H_{17}OH$, 99.5 % purity, Unilab)

1.2.4 Quartz wool as the catalyst bed support (Alltech)

2. Equipments

The equipments used in this research were classified into 3 major groups including 1) equipments for catalyst preparation, 2) instruments for catalyst characterization, and 3) equipments for Fischer-Tropsch synthesis reaction.

2.1 Equipments for Catalyst Preparation

2.1.1 Digital weighing machine (AT 400, Metler Toledo)
2.1.2 Magnetic hot plate and stirrer (SLR, Schott)
2.1.3 Digital hot plate and stirrer (SLR, Schott)
2.1.4 Furnace (ELF10/6, Carbolite)
2.1.5 Oven (ED53, Binder)
2.1.6 Desicator
2.1.7 pH meter (CG842, Schott)
2.1.8 Autoclave reactor was used in the stage of hydrothermal treatment process in catalyst preparation. The elevated temperature and pressured were used in processing materials (Figure 13).

Figure 13 Teflon-lined pressurized device designed for hydrothermal aging process.

2.2 Instruments for Catalyst Characterization

2.2.1 Surface area and pore size analysis (N_2 adsorption Analysis) (Autosorb-1C, Quantachrome Coorporation)

2.2.2 Transmission Electron Microscopy (TEM) (JEM-2010, JEOL)

2.2.3 Simultaneous Differential Scanning Calorimetry and Thermogravimetric Analysis (DSC-TGA) (SDT 2960 PN 925605.001, Perkin Elmer)

2.2.4 Inductively Coupled Plasma-Atomic Emission Spectrometer (ICP-AES) (PLASMA-1000, Perkin Elmer)

2.2.5 X-Ray Diffraction (XRD) (Phillips XRD X-pert IMS)

2.3 Equipments for Fischer-Tropsch Synthesis Reaction

2.3.1 Catalytic reaction testing unit

- Pressure regulator
- Mass flow controller (GFC117, Aalborg)
- Mass flow controller (8300 Series, KOFLOC)
- Thermocouple (K-type)
- Temperature controller (120-R/E, Shinho)
- Temperature indicator (RI, Shinho)
- Tube furnace (CFW 1300, Carbolite)
- Flexible heating tape (100 Volt)
- Voltage transformer (SB-5, SLIDEUP)
- Bubble flow meter

2.3.2 Gas analysis unit

- Gas chromatograph equipped with thermal conductivity detector (TCD) and chromatopac data processor (GC-2014, Shimadzu)
- Gas chromatograph equipped with flame ionization detector (FID) and chromatopac data processor (GC-8A, Shimadzu)
- Gas syringes (1002LTN Gastight Syringe, Hamilton and A-2 type Gastight Syringe, PS)
- Liquid syringe (80377 Microliter, Hamilton)

Experimental Procedures

In this research, the experiment was devided into three sections: (1) preparation of SBA-15 mesoporous silica, (2) preparation of cobalt support SBA-15 catalysts under different metal loading techniques including post-synthesis method and direct thermal synthesis and (3) testing of Fischer-Tropsch synthesis performance.

1. Methods of SBA-15 Mesoporous Silica Synthesis

In order to synthesize periodic SBA-15 mesoporous silica, sodium silicate was firstly prepared followed by the synthesis of SBA-15 mesoporous silica.

1.1 Preparation of Sodium Silicate from Rice Husk Ash

Sodium silicate solution ($Na_2Si_3O_7$: 4 wt. % NaOH: 27 wt. % SiO_2) was prepared from rice husk ash (RHA). Firstly, 100 g of rice husk was refluxed with 1 L of 1 M HCl for 2.5 h. The treated rice husk was washed with distilled water, dried at 120 ^{o}C and burned in oxygen atmosphere at 700 ^{o}C for 1 h. The residual ash composed of 99.7 wt. % amorphous silica.

Rice husk ash of 1.003 g was ground and dissolved in 7.40 mL of 1 M NaOH solution. The obtained liquid was stirred at 100 ^{o}C. The volume of solution was one half decreased in order to obtain a desired composition of sodium silicate solution ($Na_2Si_3O_7$: 4 wt. % NaOH: 27 wt. % SiO_2).

1.2 Synthesis of SBA-15 Mesoporous Silica

The equipment used in this experiment was set up as shown in Figure 14.

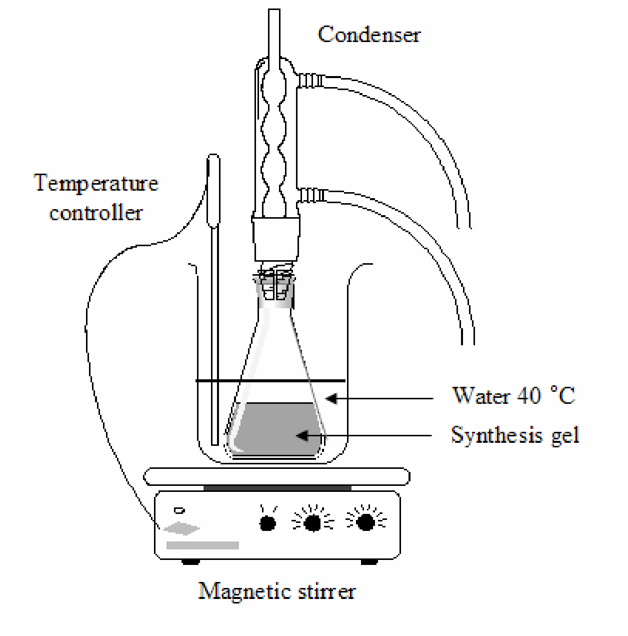

Figure 14 The equipment setup of hydrolysis and condensation process.

1.2.1 A solution of surfactant was prepared by stirring the mixture of 0.00875 mol (0.845g) of Pluronic P123 and 60 mL of distilled water at room temperature until the clear solution was obtained.

1.2.2 Sodium silicate solution (based on one mole of silica) prepared from rice husk ash was added to the Pluronic P123 solution and then mixed properly.

1.2.3 After that, 4 mol of HCl (5.4 mL) was quickly added in the mixture under vigorous stirring at 40^{o}C and the obtained mixture was stirred for 24 h, the sol product was prepared.

1.2.4 The resulting sol was then transferred into a Teflon-lined autoclave and heated statically at 100 ^{o}C under autogeneous pressure for 24 h.

1.2.5 The solid product was washed with large amounts of warm distilled water and separated by filtration.

1.2.6 The solid product was dried at 140 ^{o}C for 3 h and then calcined at 500 ^{o}C for 6 h to remove an organic template and impurity. All of the steps can be summarized as shown in Figure 15.

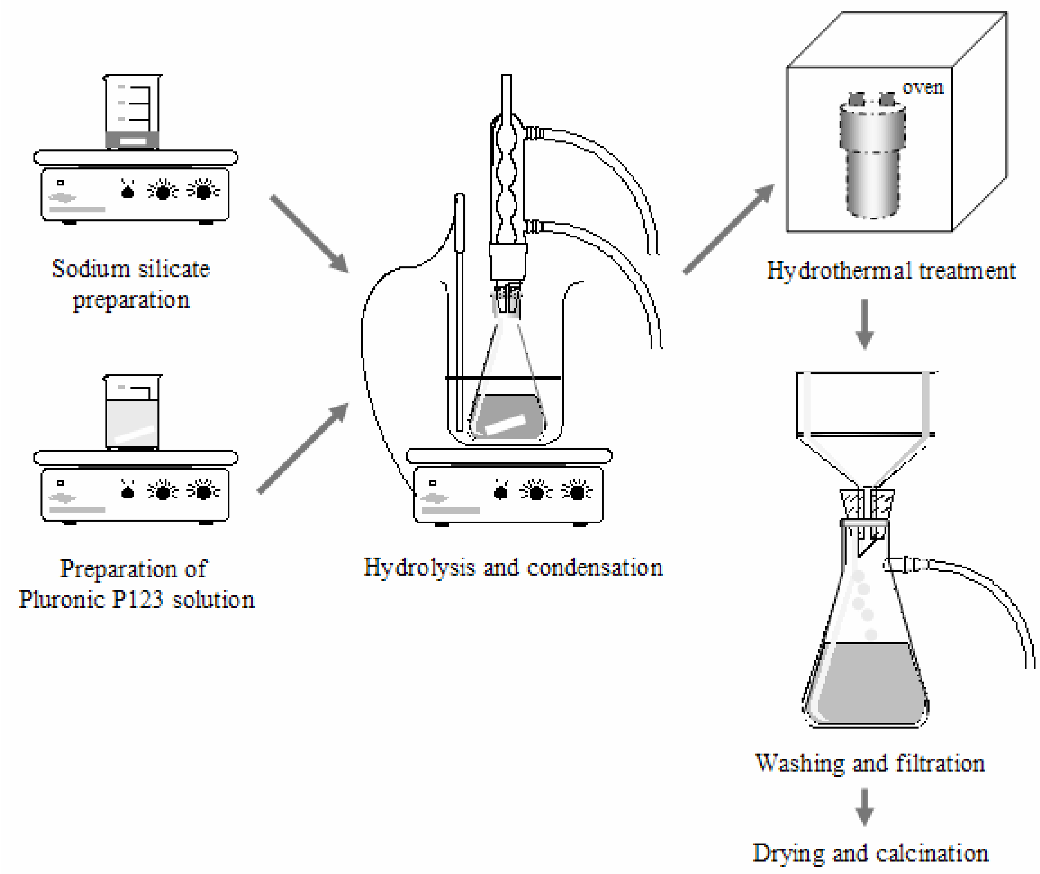

Figure 15 Scheme of SBA-15 mesoporous silica synthesis process.

2. Preparation of Cobalt Support SBA-15 Mesoporous Catalysts

In this research, cobalt loaded SBA-15 catalysts were prepared by two different metal loading techniques including the post-synthesis method and the direct thermal synthesis. Cobalt catalysts were synthesized using rice husk ash and cobalt(II) nitrate ($Co(NO_3)_2{\cdot}6H_2O$) as a silica source and a cobalt precursor, respectively. The obtained catalysts were packed in the stainless steel fixed-bed reactor to test for their FTS performances.

2.1 Post-synthesis Method

Cobalt loaded SBA-15 catalysts (based on 10 wt. % loading) were prepared by wetness impregnation and solvothermal technique. The detail of catalyst preparation was explained as follows:

2.1.1 Wetness impregnation method

Cobalt metal of 10 wt. % were loaded on SAB-15 by using cobalt nitrate salt ($Co (NO_3)_2{\cdot}6H_2O$) as a metal precursor. SBA-15 mesoporous silica used as a catalyst support was prepared by the process mentioned earlier (1.2). By using impregnation method, the procedure of catalyst preparation was explained as follows:

1) The solution of metal precursor was prepared by dissolving certain amount of ($Co (NO_3)_2{\cdot}6H_2O$) in required amount of distilled water under stirring.

2) cobalt solution was slowly added into 1 g of SBA-15 powder (Figure 16) and stirred at room temperature for 1 h.

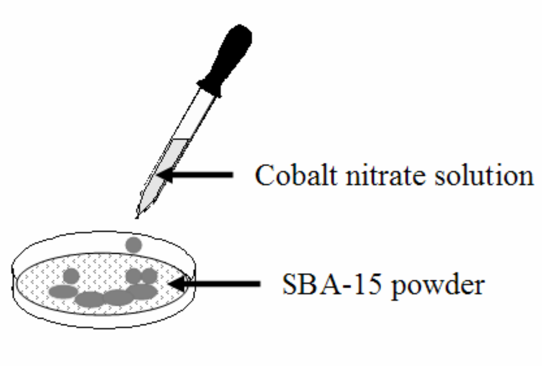

Figure 16 The stage of metal loading in wetness impregnation.

3) The obtained mixture was then dried at 120 °C for 24 h and calcined in air at 550 °C for 4 h, respectively.

4) The obtained catalyst granules were ground and denoted as IMPCo/SBA-15.

2.1.2 Solvothermal technique

In this method, the solvent that used to prepared solution of metal precursor was changed. In order to prepare cobalt particles in smaller sizes, tetrahydrofuran (THF) was applied instead of distilled water. The procedure of this metal loading technique was reported as follows:

1) The solution of metal precursor was prepared by dissolving certain amount of cobalt nitrate (Co $(NO_3)_2\cdot 6H_2O$) in 5 ml of tetrahydrofuran solution (THF) and stirred until a clear solution was obtained.

2) The solution of cobalt salt was slowly added into 1 g of SBA-15 powder and vigorously stirred at room temperature until sample paste was obtained.

3) The obtained sample was then dried at 120 °C for 24 h and calcined in air at 550 °C for 4 h, respectively.

4) The obtained catalyst granules were ground and denoted as SOVCo/SBA-15.

2.2 Direct-synthetis Method

The modification of the sol-gel process was applied to directly incorporate cobalt atoms into the structure of SBA-15 silica. The process of preparing SBA-15 mesoporous silica was simply modified by pH adjusting approach. At the beginning of experiment, same molar composition of the synthesis gel that used for SBA-15 preparation was used (SiO_2: Pluronic P123: HCl: H_2O was 1: 0.00875: 4: 200) (Nantangern, 2005). The synthesis procedure was shown below:

2.2.1 A solution of surfactant was prepared by stirring the mixture of 0.00875 mol of Pluronic P123 and 60 ml of distilled water at room temperature until the clear solution was obtained.

2.2.2 Sodium silicate solution (based on one mole of silica) prepared from rice husk ash was added to the Pluronic P123 solution and then mixed properly.

2.2.3 After that, 4 mol of HCl (5.4 mL) was quickly added in the mixture under vigorous stirring at 40°C and stirred for 24 h.

2.2.4 The aqueous cobalt solution (based on 10 wt. % Co loading) was added into the resulting synthesis gel and then vigorously stirred at room temperature for 15 min. The pink mixture was obtained in this stage.

2.2.5 By using pH adjusting approach, 10 M of NaOH solution was slowly dropped into the synthesis gel under stirring (Figure 17). The pH of the gel which can be observed from pH meter was continually increased through the addition of NaOH solution. Adding of NaOH solution was stopped when the desired pH of the synthesis gel was obtained (pH 3, 6, 7.5, and 9).

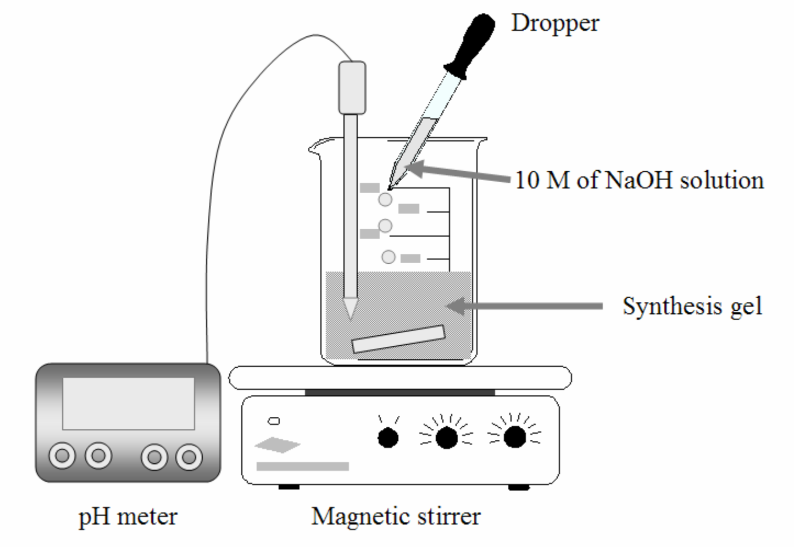

Figure 17 The equipment setup of “pH adjusting” process.

2.2.6 The resulting sol was then transferred into an autoclave and heated statically at 100 °C under autogeneous pressure for 24 h.

2.2.7 The solid sample was obtained by filtration and washing with large amounts of warm distilled water.

2.2.8 The solid product was dried at 140 °C for 3 h and then calcined at 550 °C for 6 h to remove an organic template and impurity.

2.2.9 The obtained catalyst granules were ground and denoted as DSxCo-SBA-15 where x was the pH of synthesis gel.

3. Performance Testing of Fischer-Tropsch Synthesis

The catalytic testing unit for the Fischer-Tropsch synthesis reaction is shown in Figure 18. This experimental unit consists of a feed flow measuring and controlling system, a furnace equipped with stainless steel tube reactor and a sampling system. The catalytic reaction testing unit was designed to operate under high temperature and pressure conditions. The details of particular system are explained below:

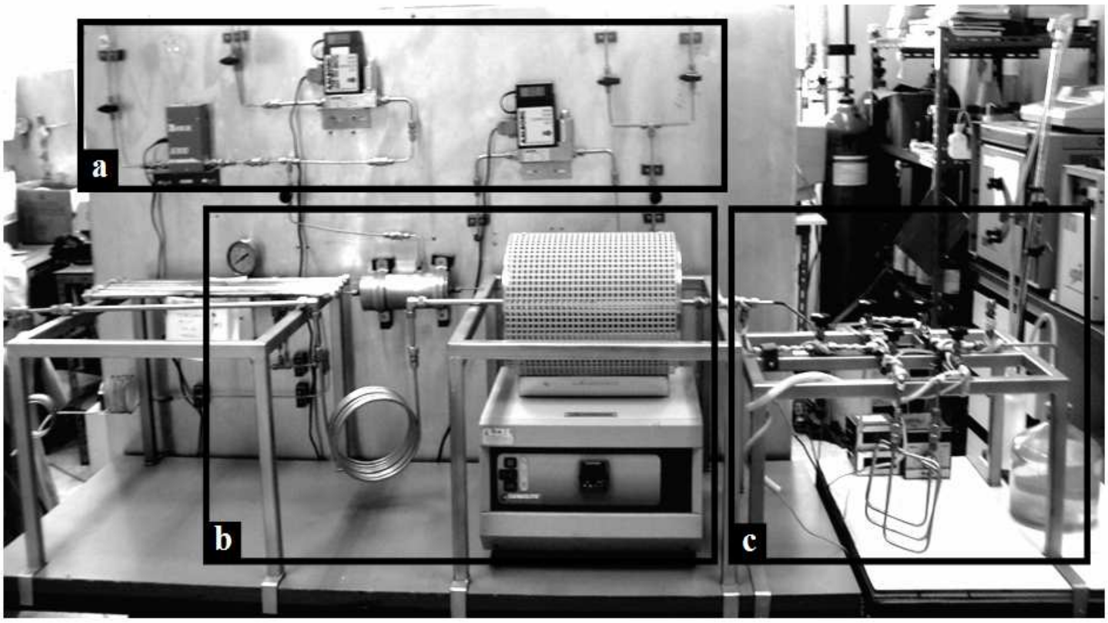

Figure 18 Catalytic reaction testing unit: (a) a feed flow measuring and controlling system, (b) a furnace-equipped stainless steel tube reactor and (c) a sampling system.

3.1 The Feed Flow Measuring and Controlling System

In this system, mass flow controllers were used to indicate and control the flow rate of feed gases including carbon monoxide, hydrogen, oxygen and nitrogen. Carbon monoxide and hydrogen were used as reactant gases, hydrogen was also used for catalyst reduction and oxygen was used for calcinations process. In order to monitor the system leakage, nitrogen gas was applied. Flow rate of hydrogen, oxygen and nitrogen were measured and controlled by Aalborg mass flow controller (Figure 19a) and KOFLOC mass flow controller (Figure 19b) was used to control flow rate of carbon monoxide.

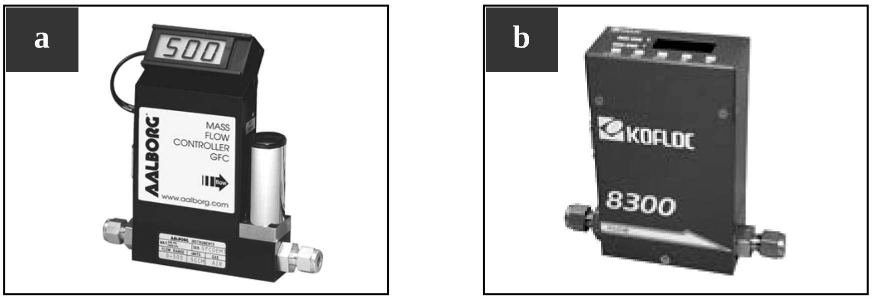

Figure 19 Mass flow controller: (a) Aalborg GFC thermal mass flow controller and (b) KOFLOC mass flow controller and mass flow meter with indicator.

3.2 The Packed-bed Reactor

The stainless steel tube was used as the fixed-bed reactor. At the stage of reaction, the stainless steel tube was heated with an electric heater (Figure 9) controlled by the temperature controller. A K-type thermocouple connected to a temperature controller unit was inserted inside the stainless steel tube in order to measure and control the temperature of the catalyst bed. Catalyst powder was packed in the isothermal zone of tube reactors between quartz wool layers as the scheme shown in Figure 20.

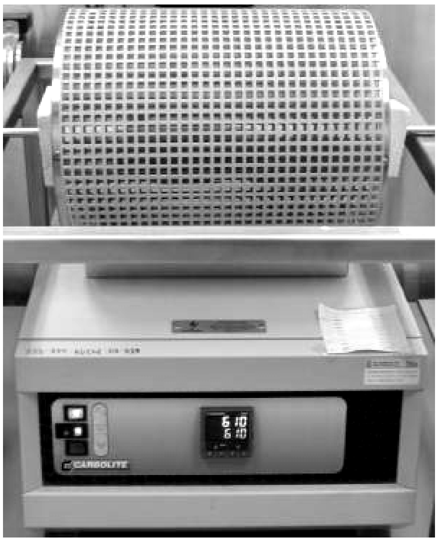

Figure 20 The Fischer-Tropsch synthesis reactor equipped with the electric heater (Carbolite tube furnace).

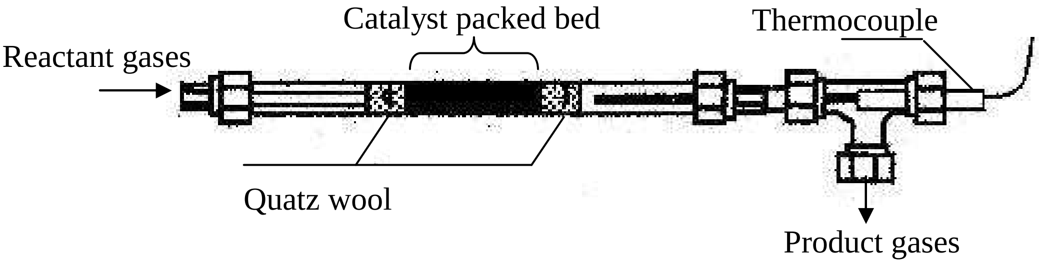

Figure 21 Schematic setup of the stage of Fischer-Tropsch reactor.

3.3 The Sampling System

The product gases were immediately sampled using a gas syringe by taking from a heated sampling port connected to quick release valves as shown Figure 22. Gas samples were analyzed by gas chromatographs. In the sampling unit, the sampling port, tube reactor and metering valves were heated by heating tape to prevent gas condensation. The mixture of tail gas was trapped by water before venting to atmosphere and the exit flow rate was measured by a bubble flow meter.

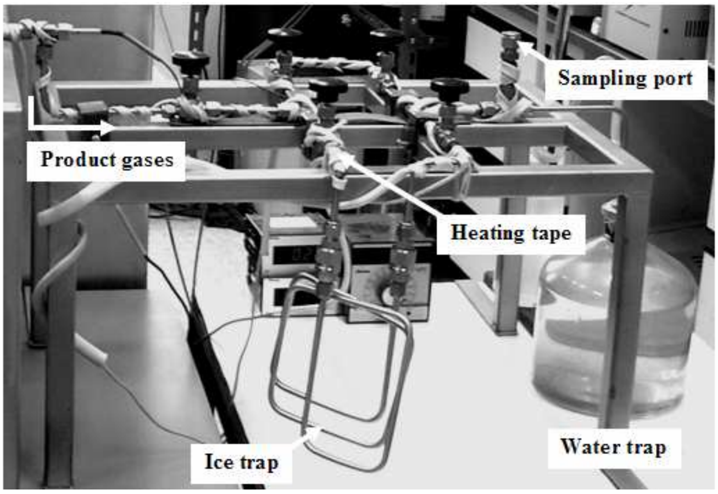

Figure 22 The sampling system consists of release valves, cooling trap, and sampling port heated by heating tapes and connected to bubble flow meter.

3.4 Gas Analysis Unit

Two types of gas chromatographs were applied to analyze product gases. First gas analysis unit (Figure 23) consists of Shimadzu gas chromatograph and chromatopac data processor (GC-2014) equipped with thermal conductivity detector (TCD). The amounts of CO and CO_2 were analyzed using Unibead-C packed column by using helium (99.5 % purity) as carrier gas and internal standard gas for TCD.

Figure 23 Shimadzu gas chromatograph (GC-2014) equipped with thermal conductivity detector (TCD) and chromatopac data processor.

The conditions for analysis of CO and CO_2 were:

- Initial carrier gas (He) flow rate	35	ml/min
- Finall carrier gas (He) flow rate	60	ml/min
- Injector temperature	180	^oC
- Initial column temperature	120	^oC
- Final column temperature	200	^oC
- Detector temperature (Pre)	200	^oC
- Detector temperature	200	^oC
- Current	80	mA

The amount of hydrocarbon products (C_1-C_{15}) were analyzed by gas chromatograph (GC-8A, Shimadzu) with flame ionization detector (FID) as shown in Figure 24. A Porapak-Q packed column (Shimadzu) and an OV-1 Uniport HP packed column (Shimadzu) were used to analyze C_1-C_4 hydrocarbons and C_5-C_{15} hydrocarbon respectively. Helium (99.5 % purity) was used as the carrier gas, while hydrogen and air were used as the combustion gas for flame ionization detection.

Figure 24 Shimadzu gas chromatograph (GC-8A) equipped with flame ionization detector (FID) and chromatopac data processor.

The conditions for analysis of C_1-C_4 hydrocarbons were:

- Primary gas pressure	200	kPa (2 kg/cm^2)
- He carrier gas 1 pressure	50	kPa (1 kg/cm^2)
- H_2 gas 1 pressure	60	kPa (0.6 kg/cm^2)
- Air pressure	50	kPa (0.5 kg/cm^2)
- Injector/Detector temperature	230	^{o}C
- Column temperature	130	^{o}C
- Range	100	
- Attenuation	512	
- Analysis time	15	min

The conditions for analysis of C_5-C_{15} hydrocarbons were:

- Primary gas pressure	200	kPa (2 kg/cm^2)
- He carrier gas 2 pressure	100	kPa (1 kg/cm^2)
- H_2 gas 1 pressure	60	kPa (0.6 kg/cm^2)
- Air pressure	50	kPa (0.5 kg/cm^2)
- Injector/Detector temperature	230	^{o}C
- Initial column temperature	30	^{o}C
- Final column temperature	230	^{o}C
- Temperature program rate	10	^{o}C/min
- Range	100	
- Attenuation	512	
- Holding time	5	min
- Analysis time	50	min

3.5 Catalytic Testing

Before testing the catalytic performance, 1 g of cobalt catalyst was packed in stainless steel tube reactor (7.75 mm inner diameter, 0.89 mm wall thickness). To obtain an active form of catalyst prepared by post-synthesis method, prior to each experiment, the catalyst was activated by reduction in H_2 atmosphere at 400 °C and 12 h. Cobalt catalyst prepared by the direct-synthetic method was activated by reduction in H_2 atmosphere at 650 °C for 12 h at the flow rate of 60 ml/min (NTP) and finally flushed and cooled with nitrogen. After pretreatment procedure, the catalyst was ready for the catalytic performance test.

During the reaction, CO and H_2 were converted to large ranges of hydrocarbon products over cobalt-containing SBA-15 catalyst at a temperature of 230 °C with the CO/H_2 molar ratio of 1/2, total gas pressure of 10 atm and total gas flow rate of 50 ml/min. Light and heavy hydrocarbon products were analyzed by gas chromatographs.

The details of qualitative and quantitative analysis results from gas chromatographs are reported in Appendix A. The data of conversion and selectivity calculated from gas chromatographs results and the detail of calculation are shown in Appendix B.

RESULTS AND DISCUSSION

In this present research, cobalt supported SBA-15 mesoporous silica catalysts were prepared by post-synthesis and direct-synthesis methods to comparatively study the effect of catalyst preparation on the performances of FTS reaction. For the post-synthesis method; the conventional wetness impregnation, and solvothermal technique were applied to incorporate cobalt atoms onto the porous structure of SBA-15 mesoporous silica (Co/SBA-15). The cobalt loading amount was fixed at 10 wt. %. For the direct synthesis method, cobalt-loaded SBA-15 mesoporous catalysts were directly synthesized via the modified sol-gel process under different pH conditions (pH values of 3, 6, 7.5, and 9). In order to adjust the pH value of the synthesis mixture, sodium hydroxide solution was used while the amounts of cobalt in synthesis mixture at the initial stage were based on 10 wt. % cobalt loading. Furthermore, the performances of the obtained catalysts were examined on Fischer-Tropsch synthesis (FTS) reaction at the reaction condition as follows: molar ratio of H_2/CO, 2; temperature, 230 °C; total pressure, 10 atm; and total flow rate, 50 ml/min (NTP).

The experimental results and discussion were reported as characteristics of cobalt support SBA-15 mesoporous silica catalysts and their catalytic performances on FTS reaction. In the first part, chemical and physical properties of catalyst support and cobalt loaded catalysts prepared by both indirect and direct synthesis methods were exhibited. In the second part, the effect of cobalt loading techniques on the catalyst activity and selectivity were discussed.

Characteristics of Cobalt-loaded SBA-15 Catalysts

According to the difference in metal loading techniques, the physical and chemical properties of cobalt loaded catalysts were investigated by using various characterization instruments including Inductively Coupled Plasma-Atomic Emission Spectrometer (ICP-AES), N_2 adsorption analysis and Transmission Electron

Microscopy (TEM). The analytical data and discussion of results were reported as follows.

1. Cobalt-loaded SBA-15 Catalysts Prepared via Post-synthesis Method

Cobalt metal of 10 wt. % were loaded on SBA-15 via wetness impregnation and solvothermal techniques by using cobalt nitrate salt (Co $(NO_3)_2 \cdot 6H_2O$) as a metal precursor. The textural parameters such as specific surface area, pore volume and pore size of SBA-15 silica support and cobalt loaded catalysts were characterized by using N_2 adsorption according to BJH model. Moreover, mesoporous structure of SBA-15 silica support and cobalt-loaded SBA-15 catalysts were studied by transmission electron microscopy (TEM). The characteristics of the cobalt catalysts are reported as follows.

1.1 Physical Properties of SBA-15 and Co/SBA-15

The textural properties of SBA-15 silica support and the cobalt supported SBA-15 catalysts prepared by wetness impregnation and solvothermal techniques are summarized in Table 2. It was clearly found that when SBA-15 silica was impregnated with Co ions by using cobalt (II) nitrate solution as a metal precursor, total surface area and pore volume were sharply decreased from 636 m^2/g to 331 m^2/g for IMPCo/SBA-15 and to 296 m^2/g for SOVCo/SBA-15, respectively. The decreases of specific surface area and pore volume were caused by pore blocking from loaded cobalt species, as were previously found by Marugavel *et al.* (1997), Vinu *et al.* (2005) and Shah *et al.* (2007). By using post-synthesis methods, cobalt oxides often formed in the pore channels and/or on the external surfaces of SBA-15 support. Cobalt oxides formed in the mesopores can partially or fully block the pore channels resulting in pore inaccessible for nitrogen adsorption, thereby reducing the surface area and pore volume.

Table 2 Physicochemical properties of calcined Co loaded SBA-15 catalysts with different cobalt contents and various pH value of synthesis solution

Sample	pH[a]	Co content (wt. %)		Specific surface area (m^2/g)	Pore volume (cm^3/g)	Pore diameter (nm)[c]
		Solution	Product[b]			
SBA-15	< 0[d]	-	-	636	0.86	6.53
IMPCo/SBA-15	-	10	9.91	331	0.82	6.41
SOVCo/SBA-15	-	10	8.92	296	0.69	6.53
DS0Co/SBA-15	< 0[d]	10	-	491	0.83	6.55
DS3Co/SBA-15	3	10	0.01	553	0.84	6.55
DS6Co/SBA-15	6	10	0.17	545	1.37	7.80
DS7.5Co/SBA-15	7.5	10	9.88	466	2.10	7.80
DS9Co/SBA-15	9	10	14.29	297	1.66	3.81

[a] The pH value of synthesis mixture

[b] Calculated by using the data from ICP-AES analysis

[c] Calculated by using the desorption isotherm according to the BJH method

[d] The pH value of synthesis mixture was lower than the measurable pH scale ranging from 0 to 14 of pH meter.

The N_2 adsorption-desorption isotherms at 77 k of the SBA-15 support and cobalt impregnated catalysts are presented in Figure 25. All isotherms are of type IV according to the IUPAC classification and exhibit a H1-type hysteresis loop; it is typical for the mesoporous materials with 2D-hexagonal structure that has large pore size and narrow pore size distribution (Zhao *et al.*, 1998). In this study, the N_2 adsorption-desorption isotherm of SBA-15 support (solid line) presents a sharp inflection at a relative pressure in the range of 0.65-0.75 with a broad hysteresis loop which reflect the long-range mesopores. These properties indicate a highly ordered structure of SBA-15 support with uniform mesopores as were also found by Luan *et al.,* (1999) and Vinu *et al.,* (2005).

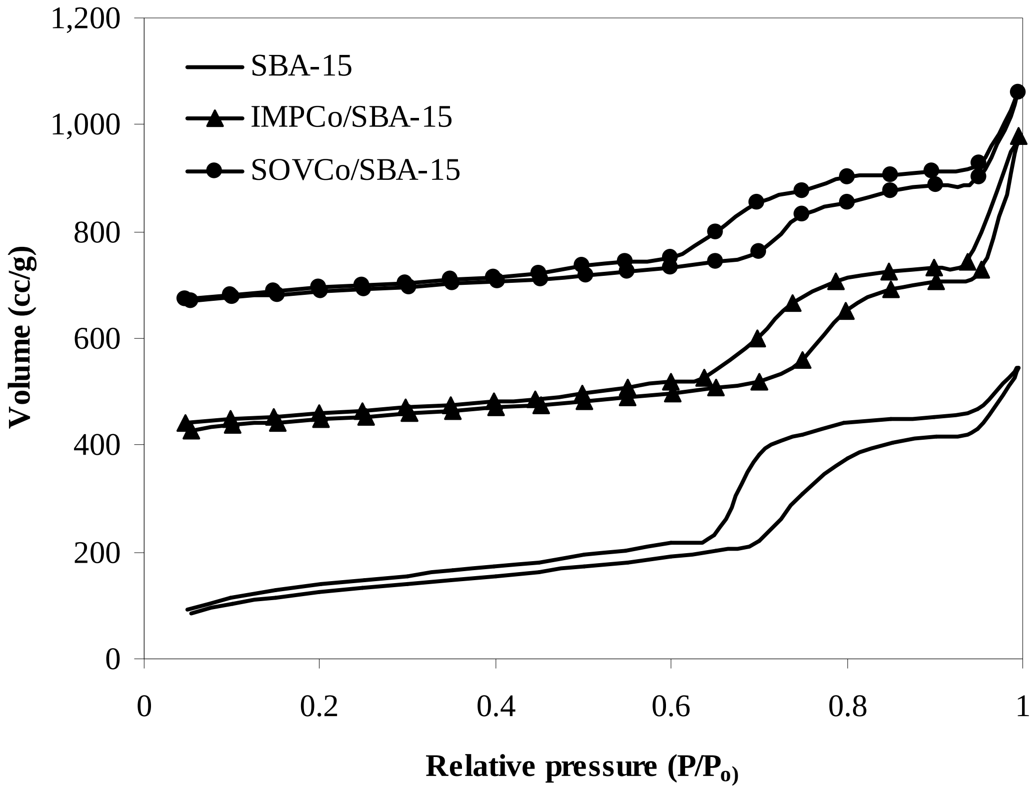

Figure 25 Nitrogen adsorption-desorption isotherms of SBA-15 silica support, calcined IMPCo/SBA-15 and SOVCo/SBA-15 catalysts.

In addition, it was found that the incorporation of Co into the SBA-15 framework had significant effect on the textural properties of catalysts. The N_2 adsorption-desorption isotherms of IMPCo/SBA-15 and SOVCo/SBA-15 catalysts present the decrease in the sharpness of inflection point and the shape of their isotherms are slightly changed compared to that of original SBA-15. The blocking of catalyst pores upon Co impregnation was also confirmed by the decrease of hysteresis loop size and the formation of cobalt oxide cluster destroyed the ordered structure of SBA-15 silica in some extent (Luan *et al.*, 1999). This observation is consistent with the results reported by Khodakov *et al.* (2002) and Martinez *et al.* (2003) that revealed the decrease of pore volume of catalysts after cobalt incorporation.

The BJH pore sizes distribution curves (Figure 26) are broader for the IMPCo/SBA-15 and SOVCo/SBA-15 catalysts and their peak intensities are obviously decreased when compared to those of the pure SBA-15 mesoporous silica. It is an evidence that impregnation of silica with cobalt nitrate was primarily attributed to blogging support pores by cobalt species. It was clearly seen that Co-incorporated SBA-15 prepared by the post-synthesis method destroyed the mesostructure of SBA-15 silica (Cheng *et al.,* 1999 and Sumiya *et al.,* 2001). The cobalt oxide easily deposited in the pore channels or on the surface of SBA-15 and caused the formation of extra framework species with irregular distribution and pore blocking (Murugavel *et al.,* 1997). Such that, the decrease in uniformity of mesopores of SBA-15 structure according to the uncontrollable sizes of cobalt species obtained with IMPCo/SBA-15 and SOVCo/SBA-15 catalysts were clearly observed.

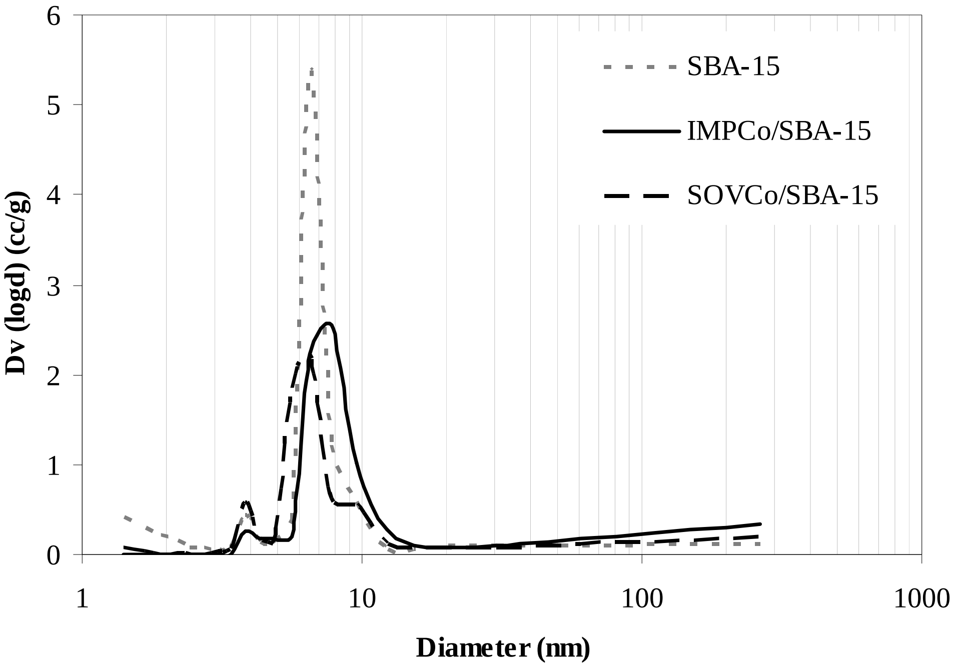

Figure 26 BJH pore size distribution curves from nitrogen desorption isotherms for the SBA-15 silica support, calcined IMPCo/SBA-15 and SOVCo/SBA-15 catalysts.

In addition, the small peaks at the position of around 4 nm are clearly observed in all the calcined SBA-15 silica support, IMPCo/SBA-15 and SOVCo/SBA-15 catalysts (Figure 26); all the mentioned samples exhibited the same behavior. This can be attributed to the formation of silica xerogel from incomplete hydrolysis-condensation reaction during SBA-15 synthesis process. During the sol-gel process, unhydrolyzed silica species could form as small particles of amorphous silica and incorporated with the completely hydrolyzed silica network in the synthesis mixture (Dunn *at al.,* 2004). When the solvent was evaporated during the drying process, unhydrolyzed silica particles could agglomerate (silica xerogel) and retain high porosity with small pore size (smaller than pore size of SBA-15 support) within the entire catalyst structure.

According to the metal incorporation by the post-synthesis method, the obtained silica xerogel also contained dispersed nanoparticles of cobalt within the structure of catalysts. In Figure 26, the slightly reduction of peak intensity of IMPCo/SBA-15 catalyst (black solid line) is clearly observed which could be similarily due to the pore blocking of impregnated cobalt species. Additionally, the black dash line of SOVCo/SBA-15 catalyst shows the peak shoulder on the position of 8-9 nm. It could be explained that the cobalt aggregates obtained from the metal loading process were agglomerated on the silica surface and created the new porosity of cobalt clusters. These cobalt aggregates evidently caused the broadening of pore size distribution curve.

1.2 Textural Properties of SBA-15 and Co/SBA-15

The TEM images of calcined SBA-15 silica support in Figure 27(a) and Figure 27(b) show highly ordered hexagonal arrays of mesopores with dimensional channels along two directions, parallel (Figure 27a) and perpendicular (Figure 27b) to the pore axis of which correlated to a 2-D hexagonal (p6mm) mesopore structure of silica products. The average thickness of the wall is approximately 5 nm and the pore diameter is 7 nm, which is corresponding to the result of mean pore diameter measured by N_2 adsorption analysis (Table 2).

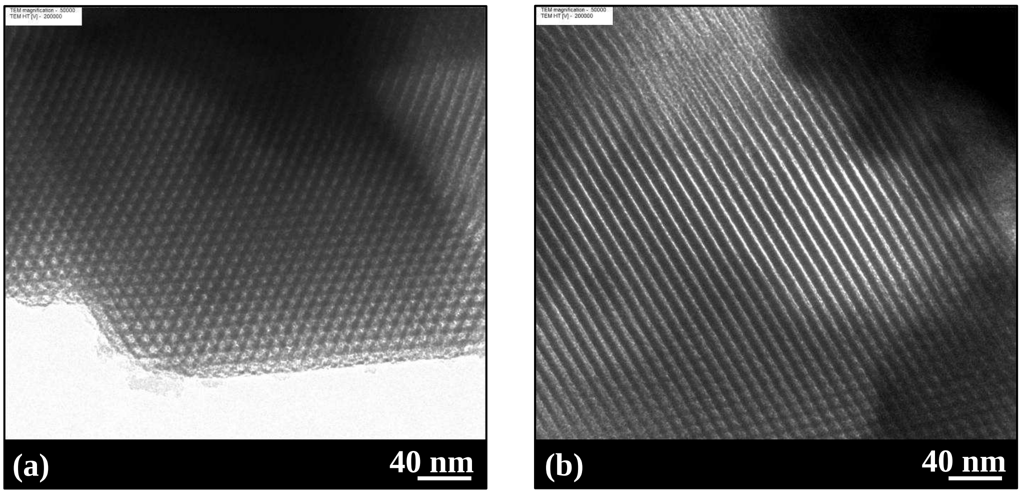

Figure 27 TEM images of calcined SBA-15 mesoporous silica (a) in the direction of pore axis and (b) in the direction perpendicular to pore axis.

The order of hexagonal mesostructure and the homogeneity of the distribution of cobalt species were also determined from TEM images. Figures 28 and 29 show TEM images of IMPCo/SBA-15 catalyst prepared by wetness impregnation method and the images of SOVCo/SBA-15 catalyst prepared by solvothermal technique, respectively. The lighter image corresponding to the SBA-15 silica darker image (dark zone) corresponding to the position of cobalt species were observed. The highly ordered mesostructure with hexagonal pore arrangement of SBA-15 silica after cobalt impregnation and calcination was clearly seen in Figures 28 and 29.

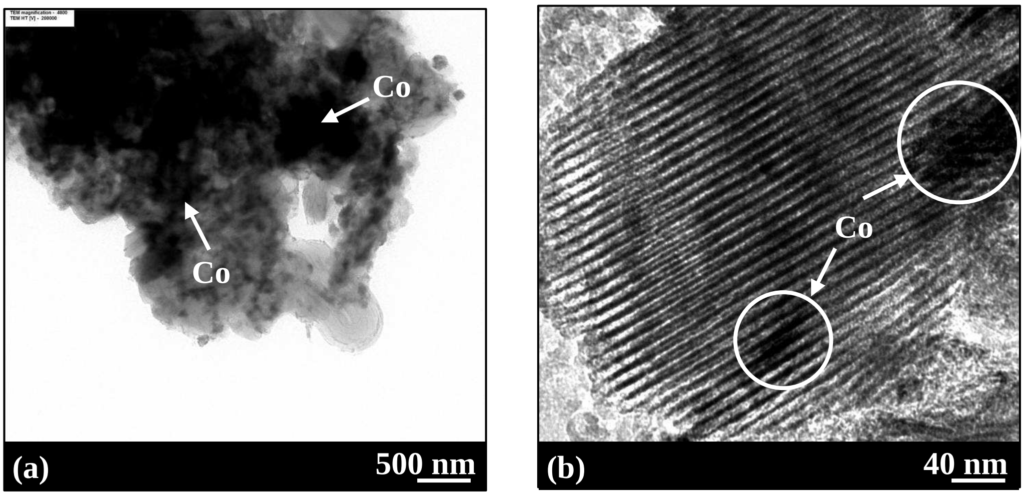

Figure 28 TEM images of calcined IMPCo/SBA-15 with ca. 10 wt. % cobalt loading prepared via wetness impregnation method (a) the overview image of cobalt supported catalyst (b) the direction perpendicular to pore axis.

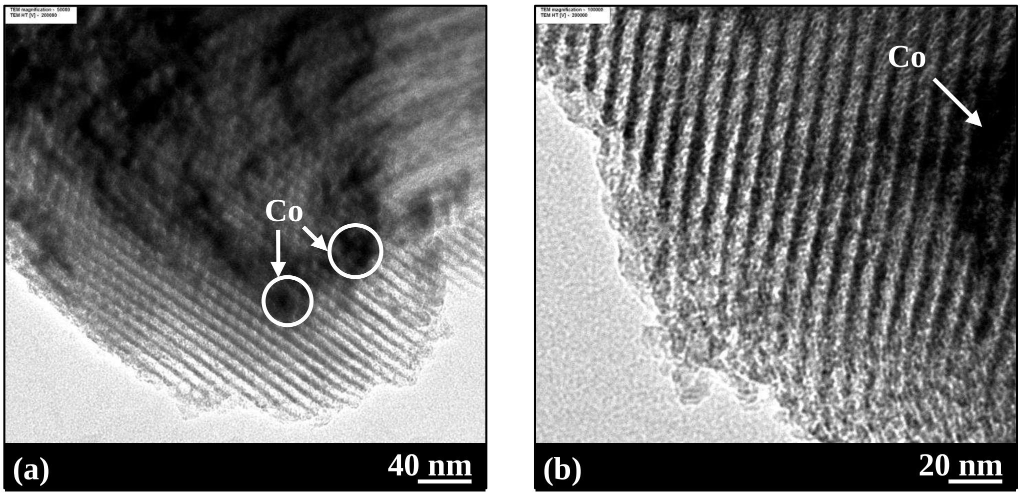

Figure 29 TEM images of calcined SOVCo/SBA-15 catalyst with ca. 10 wt. % cobalt loading prepared via solvothermal technique.

According to Figures 28 and 29, it can be clearly seen that cobalt particles usually formed as large aggregates on the silica surface. It could be observed that cobalt nitrate incorporated by using wetness impregnation and solvothermal techniques were preferentially located inside the pores of SBA-15 silica. A number of studies revealed that, during the catalyst preparation using impregnation method, metal oxides were mostly formed in the SBA-15 porous channels, resulting in large reduction of surface area and pore volume of the catalyst (Bessell, 1993; Dimitrova and Mehandjiev, 1994; Khodakov *et al.,* 2002). These results were in good agreement with our present results obtained from N_2 adsorption data (Table 2). The large decreases in specific surface area and pore volume of IMPCO/SBA-15 and SOVCO/SBA-15 were found when preparing cobalt supported catalyst by the post-synthesis methods.

When SBA-15 silica was impregnated with cobalt nitrate solution, the deposition of cobalt species occurred on the stage of drying by precipitation in the liquid phase inside the SBA-15 silica pores due to the solvent evaporation. This mentioned mechanism indicated that the uncontrolled precipitation of metal phase resulted in the catalysts with large-supported metal particles with low dispersion of supported metal phase (Bourikas *et al.*, 2004), as was clearly observed from Figures 28 and 29. The formation of cobalt species as large aggregates was also affected by the method of drying process. Drying by the conventional heating, applied in this study, led to an outward liquid flowing from the inside of the silica support to the outside surface due to the thermal gradient and heat flow from the heating technique (Reubroychaoen *et al.*, 2007), resulted in an accumulation of cobalt phase on the outer surface of the silica support.

According to the TEM images of IMPCO/SBA-15 and SOVCO/SBA-15 catalysts (Figures 28 and 29), not only the cobalt species were evidenced by the dark area of the pictures but the cobalt phases were also identified by the energy dispersive X-ray spectroscopy (TEM-EDX) analysis where the cobalt peak was easily observed in Figure 30.

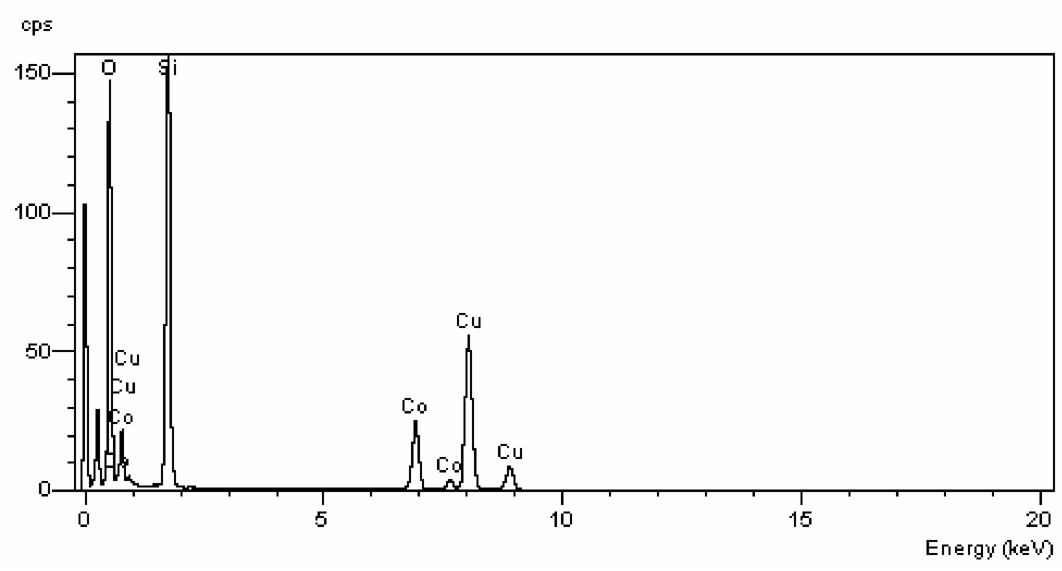

Figure 30 EDX spectra of chemical analysis of IMPCo/SBA-15 catalyst.

2. Co/SBA-15 Catalysts Prepared via Direct-synthesis Method

In order to prepare cobalt loaded catalysts by the direct synthesis method, the modification of sol-gel process was carried out using "pH adjusting" approach. The sol-gel process normally used for SBA-15 silica synthesis was simply modified to improve the incorporation amount of cobalt species under strong acidic solution. In this part, the modification of sol-gel process and effect of pH value on the characteristics of cobalt catalysts were clearly discussed. The degree of metal incorporation was measured by using Inductively Coupled Plasma-Atomic Emission Spectrometer analysis (ICP-AES). N_2-adsorption analysis and Transmission Electron Microscopy (TEM) were applied to characterize their physical properties. The analytical data and discussion of results were reported as follows.

2.1 Modification of Sol-gel Process

SBA-15 mesoporous silica with large pore diameter apparently has advantage in production of heavy hydrocarbons on FTS reaction. Nevertheless, the incorporation of transition metal into the framework structure of silica support by the direct synthesis method is very difficult (Luan *et al.,* 1999; Zhang et al., 2002; Vinu *et al.,* 2003; Wu *et al.,* 2004) because the synthesis of SBA-15 silica requires highly acidic condition. The direct incorporation of cobalt species into high-acidity synthesis solution of SBA-15 silica is almost impossible because the incorporated cobalt atoms are generally less stable and the unavoidable electrostatic repulsion between metal ions and silica species suppresses the contact between them (Srinivasu *et al.,* 2008). In 2005, Wang *et al.* reported that, during hydrolysis-condensation reaction, the pH of synthesis mixture (pH < 0) was lower than isoelectric point of silica (pH ~ 2). In this pH condition, cobalt was primarily found as cations and the silica was also positively charged. For this mentioned reason, almost no cobalt species could be incorporated into the resulting SBA-15 silica. Therefore, the modification of the conventional sol-gel process is undeniably needed in this case.

The order of adding metal precursor into synthesis solution is a particularly important step to be concerned. Typically, the procedure for SBA-15 synthesis includes the preparation of template solution and silica solution, hydrolysis-condensation reaction, hydrothermal aging process, washing and filtration, and calcination, consecutively (Nanta-Ngern, 2005). In this study, cobalt precursor was directly added into the synthesis mixture of Pluronic P123 surfactant and sodium silicate, and the obtained mixture was then carried on the hydrolysis-condensation reaction. The resulting solution was similarly proceeded on hydrothermal aging process, washing and filtration, and calcination, consecutively. As a result, the achieved solid product was obviously found as an amorphous form of silica and the amount of incorporated cobalt species was not detected in this case.

Figure 31 exhibits the morphology of the calcined product obtained from the direct synthesis. From TEM images, the structure of amorphous silica was clearly observed. It implied that the dissolved cobalt precursor in the synthesis solution inhibited the evolution of the ordered mesoporous SBA-15 silica during the stage of hydrolysis-condensation reaction. According to the analysis of literature data, it was shown that, for the first 5-20 minutes of the hydrolysis-condensation reaction period, the formation of hybrid organic-inorganic micelles was occurred corresponding to the transformation from spherical to cylindrical micelles (Zholobenko *et al.,* 2008). It can be explained that the self-assembly mechanism of SBA-15 silica formation was interfered by the existing ions of added metal precursor in the synthesis solution. The transformation of micelles to cylindrical shape was retarded, this was consistent with the observation of TEM images (Figure 31) as the structure of cylindrical-like silica was not shown.

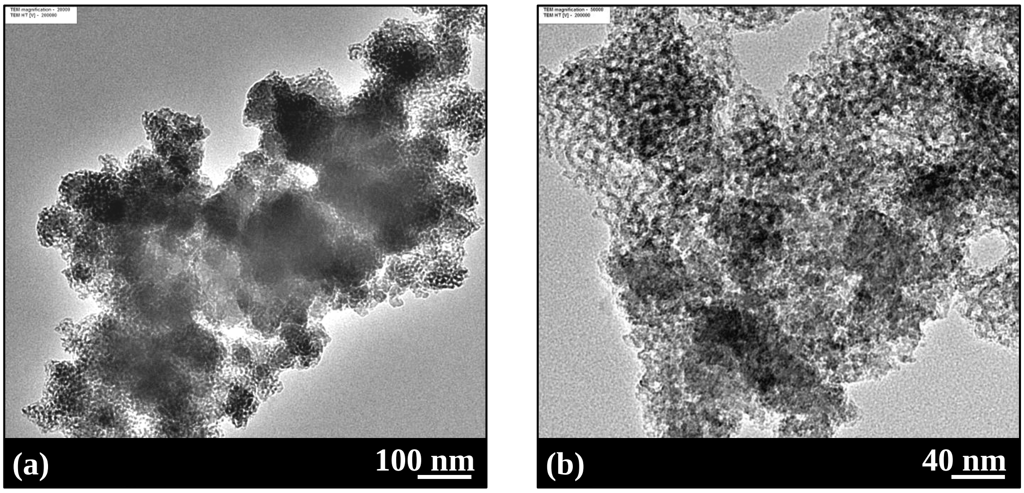

Figure 31 TEM images of calcined cobalt loaded sample prepared by adding cobalt nitrate solution into the synthesis mixture before the stage of hydrolysis-condensation reaction.

Not only the mesostructure of SBA-15 silica was not obtained, but the incorporation of cobalt atoms into the silica framework was also barely possible under high-acidity condition. By these results, the order of adding cobalt precursor was further changed. The stage of adding cobalt solution was performed after the hydrolysis-condensation reaction period, consecutively. In order to prevent metal precursor ions from playing negative role on the formation mechanism of SBA-15 silica, the solution of cobalt nitrate was accordingly dissolved into the synthesis mixture before it was exposed to the higher temperature (100 °C) under hydrothermal aging process. By using this step of preparation, highly ordered structure of SBA-15 mesoporous silica was successfully obtained as clearly shown in Figure 32. In this case, the condensation and densification of silica species can be continued under hydrothermal treatment without the loss of SBA-15 mesostructure. Even though highly ordered mesostructure of SBA-15 silica was successfully obtained, the amount of cobalt loaded was very low. Consequently, the modification of sol-gel process was necessary to be continuously proceeded to particularly increase the amount of cobalt loading in silica structure.

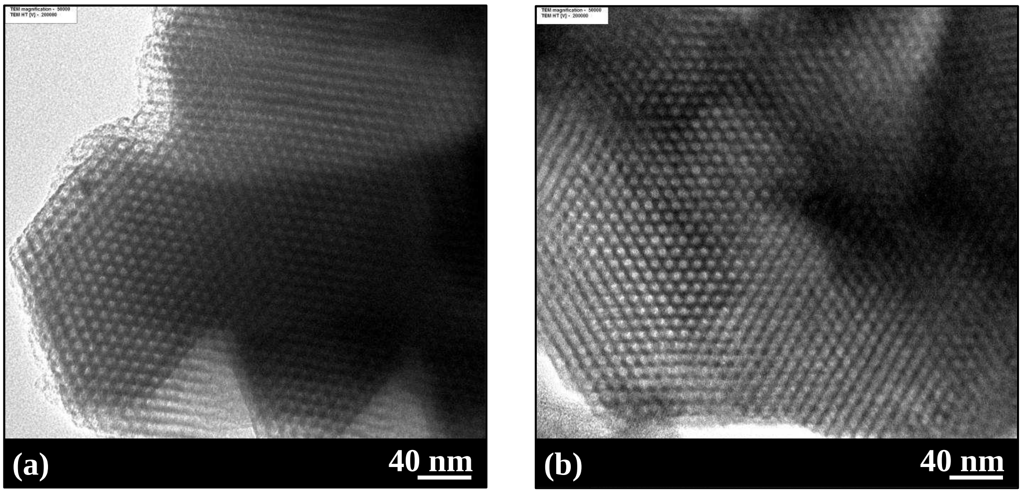

Figure 32 TEM images of the calcined cobalt-loaded sample prepared by adding cobalt nitrate solution into the synthesis mixture before the stage of hydrothermal aging process.

In order to increase the cobalt content while maintain the mesostructure of SBA-15 silica, the synthesis process was simply modified by applying the pH-adjusting approach. Cobalt species was expected to be incorporated in the framework of silica with high dispersion. According to the pH adjusting approach, pure SBA-15 gel solution silica was firstly prepared under low pH condition and after that the gel mixture was adjusted to higher pH value to enhance the degree of cobalt incorporation. A number of studies reported the synthesis of SBA-15 silica supported metal catalyst with high metal dispersion by using direct synthesis method (Wang *et al.*, 2005; Yang *et al.*, 2007; Lou *et al.*, 2008; Prashar *et al.*, 2008). It was shown that the pH control gave advantage over promoting the incorporation of metal atoms into the framework of SBA-15 silica (Tomiyama *et al.*, 2003; Lou *et al.*, 2007; Huang *et al.*, 2008).

In this study, after certain amount of cobalt nitrate solution was added into the solution obtained from hydrolysis-condensation reaction, the pH adjusting method involved the addition of an aqueous NaOH solution into the synthesis mixture was applied. The pH values of synthesis mixture were adjusted to pH 3, 6, 7.5 and 9. The addition of NaOH solution increased the amount of OH^- ions in the synthesis mixture and enhanced the formation of cobalt hydroxides which could easily precipitate in the framework of silica during the crystallization process (hydrothermal aging). The similar result was found by Tomiyama *et al.* (2003) and Takahashi *et al.* (2005). They reported the successful preparation of Ni/SiO_2 catalysts by increasing the pH of the synthesis solution. The uniform precipitating nickel hydroxide with high thermal stability was formed. As a result, the attempt to increase the amount of cobalt species incorporated in SBA-15 silica framework (based on 10 wt% in synthesis solution) was successfully done by simple adjusting the pH of synthesis mixture using aqueous NaOH solution without changing the structural order of the host SBA-15 silica.

2.2 Effect of pH on the Direct Synthesis of Co/SBA-15 Catalysts

The pH value of synthesis mixture was found to be the important parameter for preparing Co/SBA-15 catalysts by the direct synthesis method. The chemical compositions of various calcined Co/SBA-15 catalysts prepared by the direct synthesis method are presented in Table 2. It can be clearly seen that the incorporation degree of cobalt metal was increased with the increase of pH value of synthesis mixture. This phenomenon is related to the types of metallic species presented in the synthesis mixture at different pH values (Vinu *et al.,* 2005; Lou *et al.,* 2008). For instance, the DS0Co/SBA-15 catalyst, which prepared under highly acidic condition ($pH < 0$) without adjusting the pH value of synthesis mixture, had very low amount of Co species incorporated into SBA 15 porous structure. As the DS0Co/SBA-15 catalyst was synthesized under strong acidic condition, it was very difficult to prepare cobalt-loaded SBA-15 silica due to the high dissolution rate of the cobalt precursor. Cobalt species existing in the solution were in cationic form while the silica species were also positively charged (Shah *et al.,* 2007; Lou et al., 2008), and therefore the electrostatic repulsion between cobalt atoms and silica species limited the incorporation of cobalt species into silica framework. This result was in good agreement with previously published literatures (Bharat *et al.,* 2001; Li *et al.,* 2005; Bhoware *et al.,* 2006; Shah *et al.,* 2007) reported that highly acidic condition of the preparation of metal atoms loaded SBA-15 normally prohibited the incorporation of metal species from synthesis solution due to their high dissolution rate of metal precursors.

According to the pH-adjusting approach, before hydrothermal treatment stage, the obtained synthesis mixture from the hydrolysis-condensation reaction was added with certain amount of cobalt precursor. The NaOH solution was further added into the mixture in order to increase the pH value of synthesis mixture. It can be clearly seen from the results of cobalt loading (Table 2) that the increase of pH values (from pH 3 to pH 9) promoted the precipitation of cobalt hydroxide ($Co(OH)^{2+}$) species during the hydrothermal aging process. The deposition of cobalt species in silica framework (Co/SBA-15) was occurred by the precipitation of cobalt hydroxide in SBA-15 structure. This result was in agreement with previous works of Tas *et al.* (1992) and Hu *et al.* (1999). They prepared Ni/SiO_2 catalyst by the modified sol-gel process and found that the increase of pH value of the synthesis solution correspondingly enhanced the homogeneous precipitation of metal hydroxides in silica structure.

As shown in Table 2, when the pH values were increased from pH 3 to pH 9, the increases of the amount of Co ions incorporated into silica framework (based on 10 wt. % cobalt loading) were observed. According to the work done by Zhao *et al.* (1998), proceeding below pH 2 (isoelectric point of silica), the formation mechanism of mesostructured SBA-15 silica involved the electrostatic interactions between protonated silica (I^+) and protonated surfactant (H^+S^0) by means of inorganic anions (X^-). It was found that, with positively charged silica, the incorporation of metal species was inhibited due to the severely acidic condition. In this study, the pH values were increased above 2 and the charge of silica specie became negative. Thus, the deposition of cobalt hydroxyl ($Co(OH)^{2+}$) species in silica framework was promoted.

In the case of DS6Co/SBA-15 catalyst, it contained only 0.17 wt. % of cobalt loading within the product. This result implied that only few amount of cobalt species was introduced into SBA-15 framework at the media pH 6. At pH 7.5, most of cobalt species were incorporated into silica framework. The DS7.5Co/SBA-15 catalyst was composed of 9.88 wt. % of cobalt amount within the mesostructure, this amount was very close to the initial Co loading amount of synthesis mixture (as shown in Table 2). The dark grey color of calcined DS7.5Co/SBA-15 catalyst was remarkably observed as shown in Figure 33, comparing to DS3Co/SBA-15 and DS6Co/SBA-15 catalysts, the white color of SBA-15 silica were noticeably observed. The change in catalyst color is corresponding to the results of cobalt incorporation presented in Table 2. It was clearly seen that the increase of pH value could significantly promote the degree of metal incorporation into the silica mesostructure.

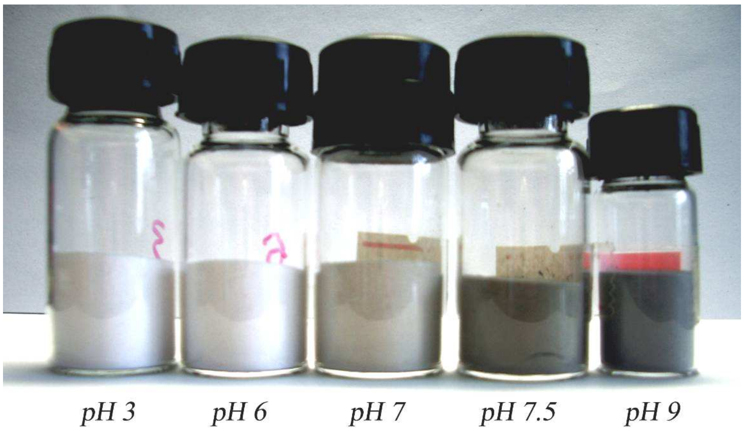

Figure 33 Photos of Co/SBA-15 catalysts prepared by direct synthesis method under various pH conditions (3, 6, 7, 7.5, and 9).

At pH 9, the amount of cobalt loading was slightly higher than that of the initial synthesis solution (14.29 wt. %). In all experiments, the same initial cobalt loading was set to 10 wt. % (based on 1 g of catalyst). The increase of cobalt wt. % for DS9Co/SBA-15 catalyst could be attributed to the removal of some amount of silica species during washing and filtration process. It was due to the high pH condition of synthesis solution which caused the dissolution of silica species during the hydrothermal aging process. The excess amount of NaOH in silica mixture led to higher pH of synthesis solution, which induced the dissolution of silica species (Tomiyama *et al.,* 2003). Indeed, the occurrence of dissolution-reprecipitation of silica was observed during the preparation Co/SBA-15 catalyst at high pH conditions and the precipitation of the silica species were simultaneously occurred with the deposition of the cobalt hydroxide species (Takahashi *et al.,* 2005). Therefore, the dissolved silica species existing in the high pH-value solution can be removed during the washing stage, resulting in the corresponding increase in wt. % of cobalt loading of the obtained DS9Co/SBA-15 catalyst.

2.3 Physical Properties of the Direct-synthesis Co/SBA-15 Catalysts

The DS3Co/SBA-15, DS6Co/SBA-15 and DS7.5Co/SBA-15 catalysts exhibited relatively high surface areas and pore volumes compared to the indirect-synthesis catalysts (Table 2). The specific surface areas were 553, 545, and 466 m^2/g when the pH conditions were adjusted to 3, 6, and 7.5, respectively. These properties confirmed that preparing Co/SBA-15 catalysts by using the direct-synthesis method could overcome the problem of pore blocking obtained from the indirect-synthesis method.

Moreover, the mean pore diameter of these catalysts was gradually increased from 6.55 to 7.80 cm^3/g as the pH values were increased (as shown in Table 2). As mentioned earlier, during the preparation Co/SBA-15 catalyst by the modified sol-gel method, the precipitation of cobalt species in silica network and the dissolution-reprecipitation of silica species were simultaneously taken place. The progress of this process was important to enlarge the pore size of silica (Takahashi *et al.,* 2005). With the increase of OH^- concentration, PEO (poly(oxyethylene)) chains became less efficient template for silica, and this effect was attributed to a weaker interaction between PEO chain and silica species caused by less hydrophilicity of PEO chains when increasing pH values. The decrease in strength of the PEO–silica interaction at higher pH values destabilized the corona of PEO-templated microporous silica which surrounded the micelles of the precursor mesophases, resulting in the increase of the size of the structural mesopores (Galarneau *et al.,* 2003).

Nonetheless, the negative characteristics of DS9Co/SBA-15 catalyst were clearly shown. The specific surface area (297 m^2/g) and pore size (3.8 nm) were sharply decreased among those of the direct-synthesis catalysts (Table 2). At strong basic condition (pH 9), the faster rate of dissolution-reprecipitation of silica species and cobalt hydroxide precipitation during hydrothermal aging process were observed and it had an effect on the change in the silica structure from a network to a particle-like structure (Takahashi *et al.*, 2005). The decrease in surface area and pore diameter of DS9Co/SBA-15 catalyst could also be described by the change of macroscopic morphology which highly depended on the pH condition of synthesis solution (Srinivasu *et al.*, 2008). More information was further discussed with TEM images.

For further understanding of pore structures of the direct-synthesis Co/SBA-15 catalysts, the N_2 adsorption-desorption isotherms of the corresponding Co/SBA-15 catalysts were investigated. As shown in Figure 34, the DS3Co/SBA-15, DS6Co/SBA-15 and DS7.5Co/SBA-15 catalysts exhibit type IV isotherm with a H1 capillary condensation steps, indicating the mesoporous structure of silica. The adsorption-desorption at P/P_0 ranging between 0.7 – 0.95 revealed the existence of Co/SBA-15 catalyst with large pore size.

Comparatively, DS6Co/SBA-15 catalyst had highly ordered mesostructure than that of DS7.5Co/SBA-15 catalyst as can be indicated by the increase in the steepness of DS6Co/SBA-15 isotherm at P/P_0 of 0.7-0.85 while the steep increase of DS7.5Co/SBA-15 isotherm was occurred at P/P_0 of 0.7-0.95 (Figure 34). It was clearly seen that the cobalt content due to pH adjustment directly affected the structural order of the obtained Co/SBA-15 catalyst. The DS6Co/SBA-15 catalyst containing only 0.17 % Co loading had high order of mesoporous structure, while the DS7.5Co/SBA-15 catalyst containing up to 9.88 % Co loading exhibited the relatively low structural order. This finding was similar to the previous research done by Srinivasu *et al.* (2008) since the amount of incorporated metal highly affected the morphology of supported SBA-15. With larger amount of cobalt species, the structural order was greatly decreased.

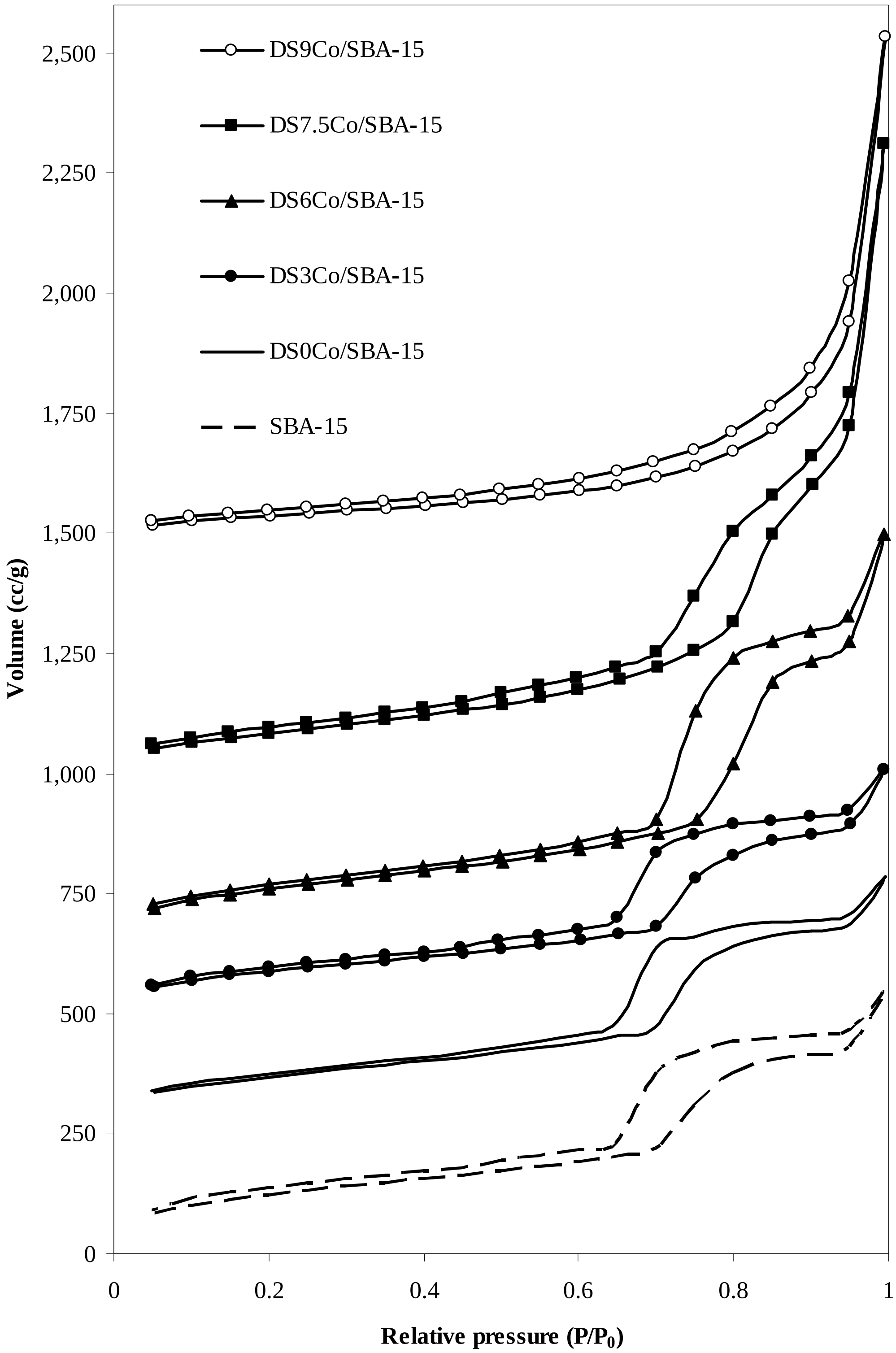

Figure 34 Nitrogen adsorption-desorption isotherms of SBA-15 silica and Co loaded SBA-15 catalysts prepared by the direct synthesis method at various pH values of synthesis mixture.

The N_2 adsorption-desorption isotherm of DS9Co/SBA-15 catalyst (Figure 34) is clearly evident that DS9Co/SBA-15 catalyst did not form as a typical mesoporous structure. It can be seen that the SBA-15 structure was not obtained under synthesis condition of pH 9. The large amount of OH^- could inhibit silica network formation of which would lead to disordered pore structure and lower the specific surface area (297 m^2/g) of catalyst (Jermy *et al.,* 2008).

Figure 35 shows the pore size distribution of the direct-synthesis Co/SBA-15 catalysts. The DS3Co/SBA-15, DS6Co/SBA-15 and DS7.5Co/SBA-15 catalysts clearly exhibited mesoporous structure with a relatively narrow pore size distribution. DS6Co/SBA-15 and DS7.5Co/SBA-15 catalysts have the mean pore size of 8 nm while DS3Co/SBA-15 catalysts exhibit the mean pore size of 6.5 nm. The increase in pore size of the Co/SBA-15 catalysts prepared under higher pH conditions (pH 6 and 7.5) is in agreement with the previous results obtained from nitrogen-adsorption analysis (as shown in Table 2); it was found that the mean pore size shifted to larger pore sizes. It can be clearly seen from Figure 35, DS0Co/SBA-15 and DS3Co/SBA-15 prepared under strong acidic condition have smaller pore diameters compared to DS6Co/SBA-15 and DS7.5Co/SBA-15 catalysts.

However, the peak intensity of DS7.5Co/SBA-15 catalyst was obviously decreased compared to the peak of DS6Co/SBA-15 catalyst, indicating less uniformity of DS7.5Co/SBA-15 mesostructure. For DS9Co/SBA-15 catalyst, its pore size distribution curve was greatly broad due to the less uniformity of hexagonal structure of Co-loaded silica catalyst when the synthesis condition was adjusted to pH 9. At pH 9, the larger pores of wide pore size distribution were obtained as clearly indicated by the broaden curve in Figure 35.

According to the results of chemical and physical properties of the direct-synthesis catalysts previously discussed from Table 2 and Figures 33, 34, and 35, it can be concluded that the pH condition of synthesis mixture not only had an effect on the degree of cobalt incorporation in silica framework but also directly influenced the morphology of the obtained catalysts.

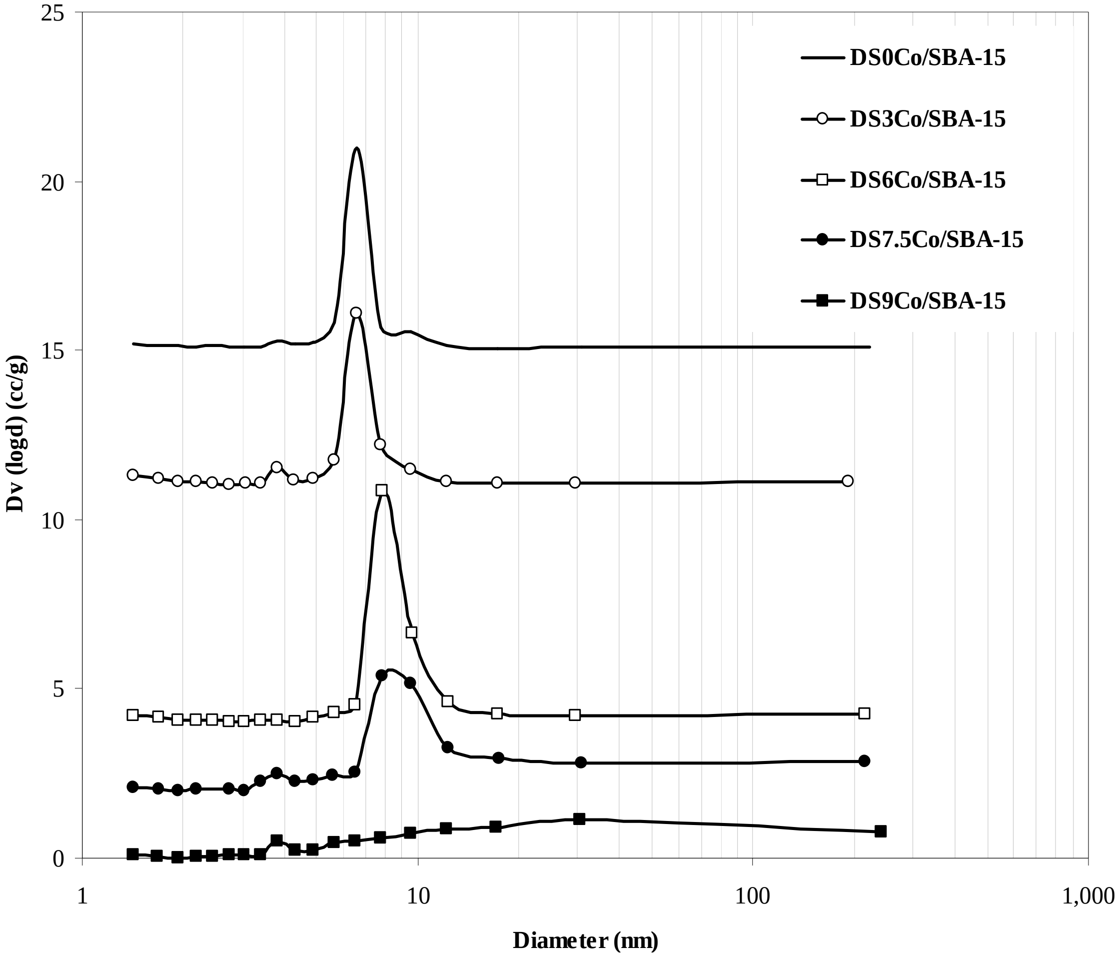

Figure 35 Pore size distribution for calcined Co/SBA-15 catalysts prepared by the direct synthesis method with various pH values of synthesis solution.

2.4 Morphologies of the Direct-synthesis Co/SBA-15 Catalysts

Figures 36, 37, 38, and 39 show TEM images of the calcined direct-synthesis Co/SBA15 catalysts prepared at pH 3, 6, 7.5, and 9, respectively. The DS3Co/SBA-15, DS6Co/SBA-15 and DS7.5Co/SBA-15 catalysts exhibited well-ordered hexagonal arrangement of SBA-15 mesoporous silica with homogeneous distribution of incorporated cobalt particles (as shown in Figures 36, 37, and 38).

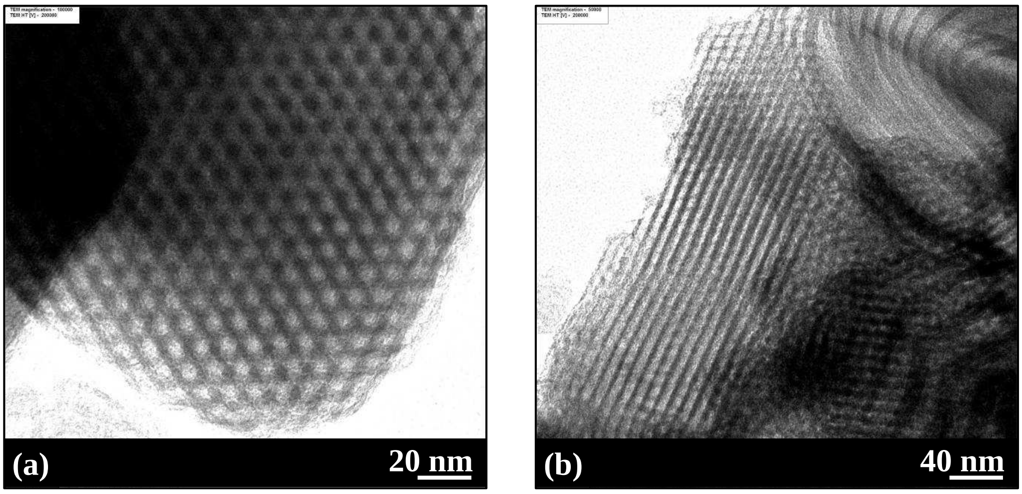

Figure 36 TEM images of calcined DS3Co/SBA-15 catalyst (a) in the direction of the pore axis and (b) in the direction perpendicular to the pore axis.

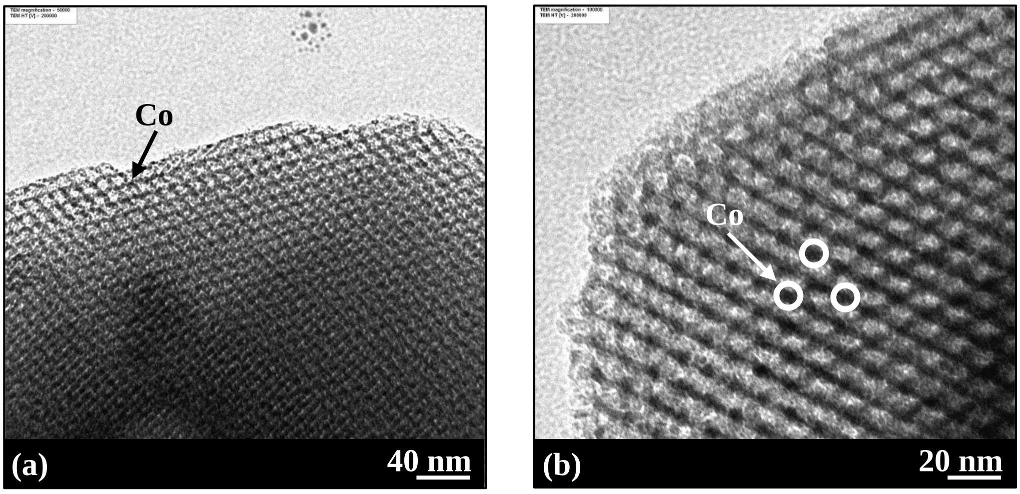

Figure 37 TEM images of calcined DS6Co/SBA-15 catalyst (a) in the direction of the pore axis and (b) at higher magnification.

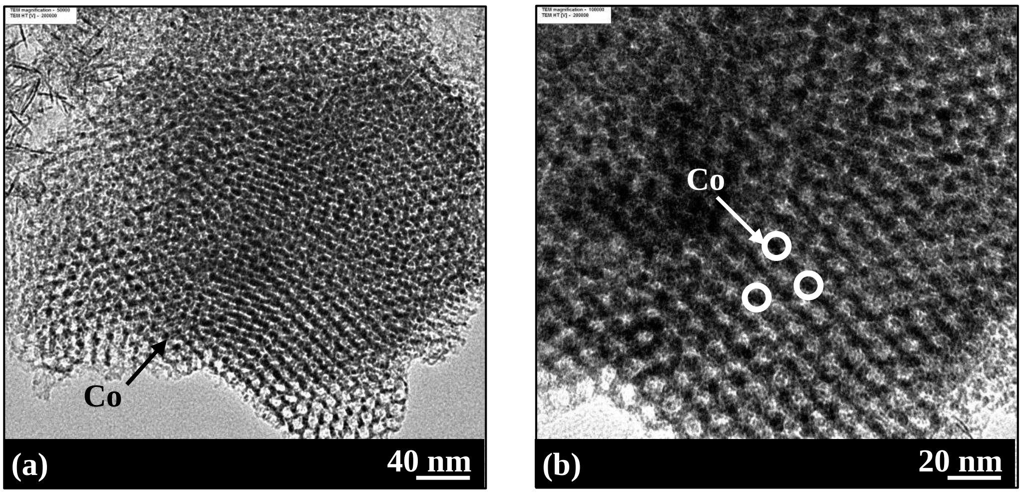

Figure 38 TEM images of calcined DS7.5Co/SBA-15 catalyst (a) in the direction of the pore axis and (b) at higher magnification.

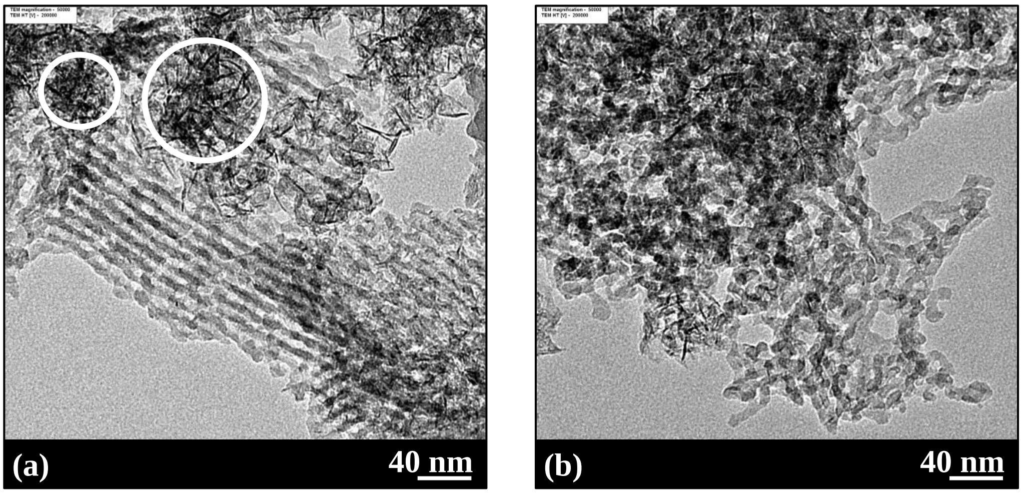

Figure 39 TEM images of calcined DS9Co/SBA-15 catalysts (a) in the direction perpendicular to the pore axis and (b) in the direction of the pore axis.

The morphologies of the direct-synthesis catalysts are significantly different from the indirect-synthesis catalysts (Figures 28 and 29). Well-distributed small particles of cobalt species in silica framework were clearly observed for the direct-synthesis catalysts, while the large size of cobalt aggregates on silica surface was observed in the indirect-synthesis catalysts (IMPCo/SBA-15 and SOVCo/SBA-

15). The differences in morphologies of Co/SBA-15 catalysts were directly attributed to the different preparation methods. As previously discussed, the characteristic structure of the direct-synthesis catalysts was considered to be formed through the concurrence of dissolution–reprecipitation of silica and the deposition of cobalt species into the silica framework (Tomiyama *et al.*, 2003). The increase of pH values promoted the precipitation of cobalt hydroxide species in the synthesis mixture during the hydrothermal aging process. Figures 37 and 38 clearly show the differences in the position of cobalt oxide species incorporated in silica framework. The cobalt species obtained from the direct-synthesis method were entrapped in silica wall with high metal dispersion, while those obtained from the indirect-synthesis method deposited on the surface of SBA-15 silica (as shown in Figures 28 and 29).

From the results, it was clearly indicated that the pH value of synthesis solution had an effect on the structural order of direct-synthesis catalysts. With the increase in an amount of incorporated cobalt species, the uniformity of SBA-15 mesostructure was decreased. It was clearly seen that DS6Co/SBA-15 catalyst with 0.17 wt. % cobalt loading (Figure 37) showed higher structure regularity than DS7.5Co/SBA-15 catalyst with 9.88 wt. % cobalt loading. Srinivasu *et al.* (2008) similarly reported that the incorporation of a small amount of metal in SBA-15 induced gentle curvatures in the rod-like structure and decreased the structural order of SBA-15 silica.

In the case of the synthesis of a pure SBA-15 silica, the formation of hexagonal phase through the surfactant-silica assembly bridged by anionic species through the $S^0H^+X^-I^+$ pathway (nonionic polymer surfactant (S^0), halide anions (X^-) and the protonated inorganic SiO_2 species (I^+)). The change in the morphology of the polymeric surfactant micelles was directly related to the spontaneous curvature of the polymeric surfactant layer (Regev, 1996). When the cobalt species were added, the adsorption and condensation of the silica species could be disturbed because of the difference in the size and the valency number of cobalt atoms. This process resulted in the increase of the spontaneous curvature and the reduction of long range mesoporous channels increased with the increasing amount of cobalt loading

(Srinivasu *et al.,* 2008). This finding is quite consistent to TEM results (Figures 37 and 38) which noticeably show the decrease in the order of hexagonal arrangement.

TEM images of DS9Co/SBA-15 catalyst (Figure 39) clearly show the formation of non-uniform amorphous phase of cobalt loaded silica catalyst at pH 9. The precipitation of cobalt species and the dissolution-reprecipitation of silica species were rapidly occurred and strongly affected the change in the silica structure from SBA-15 framework to a particle-like structure (Takahashi *et al.*, 2005). In this case, SBA-15 structure was not obtained, this can also be confirmed by the previous results of N_2 adsorption-desorption isotherm (Figure 34) and the broadening of pore size distribution curve (Figure 35). The size of cobalt particles incorporated in silica structure was larger than those obtained from DS6Co/SBA-15 and DS7.5Co/SBA-15 catalysts and the homogeneity of cobalt distribution was decreased. However, the distribution of incorporated cobalt particles in DS9Co/SBA-15 catalyst was still much better than those of the indirect-synthesis catalysts (Figures 28 and 29).

It can be considered that, by using pH-adjusting method, the direct-synthesis catalyst with highly distributed cobalt incorporated in SBA-15 framework was successfully obtained. At pH 7.5, the catalyst with high cobalt loading (approximately 10 wt. % cobalt loading) was effectively prepared while the uniformity of SBA-15 hexagonal structure was completely retained. The pH-adjusting method can overcome the formation of Co aggregates obtained from the indirect-synthesis method.

Investigation of Catalytic FTS Performance

The testing of FTS catalytic performance was carried out in order to study the influence of cobalt loading methods on the catalytic behavior of cobalt loaded catalysts. Each catalyst obtained from the previous synthesis stage was reduced before the activity test for 12 h at 400 °C for post-synthesis catalysts and at 650 °C for direct-synthesis catalysts. The catalytic FTS activities of different Co/SBA-15 catalysts were studied in a fixed-bed reactor at the H_2/CO molar ratio of 2, the total flow rate of 50 ml/min (NTP) and total pressure of 10 atm. The reaction temperature was fixed at 230 °C. Before the FTS reaction, reactant gases temperature was slowly increased from room temperature to 230 °C using the heating rate of 5 °C/min and this temperature rising program was applied throughout this study to avoid the deactivation of catalysts (Afonso *et al.,* 1997).

In this section, in order to study the influence of metal loading techniques on the catalyst performances and catalytic behaviors, the activity and selectivity over Co/SBA-15 catalysts prepared by post-synthesis and direct-synthesis methods were determined. The results of the FTS catalytic test over cobalt catalysts prepared by these two methods exhibited significant differences in catalytic behaviors as shown below.

1. Catalyst Activity

The results of syngas conversion and product distribution of Co/SBA-15 catalysts prepared from various metal loading techniques are presented in Table 3.

Table 3 CO conversion and product distribution of Co/SBA-15 catalysts prepared from various metal loading techniques

Catalysts*	CO conversion (%)	Product distribution (%)					
		CO_2	CH_4	C_2-C_4	C_5-C_9	C_{10}-C_{20}	C_{21+}
IMPCo/SBA-15	83.8	16.5	59.1	3.2	0.2	21.0	-
SOVCo/SBA-15	23.8	-	3.8	0.8	9.3	78.0	8.1
DS3Co/SBA-15	14.6	-	1.7	3.6	2.7	87.6	4.4
DS6Co/SBA-15	16.9	0.3	4.8	5.9	5.8	61.1	22.0
DS7.5Co/SBA-15	17.7	-	0.3	0.4	0.2	72.8	26.3
DS9Co/SBA-15	3.7	-	8.8	4.1	-	87.1	-

* Reaction conditions: P= 10 atm, T= 230 °C, H_2/CO= 2, flow rate= 50 ml/min (NTP)

As shown in Table 3, the Co/SBA-15 catalysts prepared via post-synthesis methods, especially IMPCo/SBA-15, was more active than Co/SBA-15 catalysts prepared via the direct-synthesis method (DSxCo/SBA-15). The IMPCo/SBA-15 catalyst exhibited the highest CO conversion (83.8 %) among all the catalysts. With the SOVCo/SBA-15 catalyst, significant reduction of CO conversion (23.8 %) was found when compared to that of the IMPCo/SBA-15 catalyst, however the higher CO conversion than that of the DSxCo/SBA-15 catalysts was still observed. Moreover, it was clearly found that even though the DSxCo/SBA-15 catalysts had less reactivity than IMPCo/SBA-15 and SOVCo/SBA-15 catalysts, their product selectivity towards heavy hydrocarbons (C_{5+}) were outstandingly increased. The differences in Co/SBA-15 catalyst performances and catalytic behaviors were explained as follows:

1.1 Post-synthesis Catalysts

The IMPCo/SBA-15 catalyst exhibited the highest activity (83.8 % CO conversion) in FTS reaction (as shown in Table 3). It could be due to the deposition of cobalt particles in IMPCo/SBA-15 mesostructure which located on the external surface of SBA-15 silica support. The deposition of cobalt active sites on the silica surface could strongly promote the accessibilities of CO and H_2 (Aguado *et al.*, 2008).

Indeed, the mechanism of FTS reaction was regarded as a surface-catalyzed polymerization process. The reaction of CO hydrogenation was taken place over the Co/SBA-15 catalyst surface. The mechanism began with the adsorption of CO and H_2 molecules on cobalt active sites (Equation 4) and the dissociation of H_2 (Equation 5) and CO (Equation 6) were further occurred. The hydrogenation of adsorbed C species was then performed, resulting in the CH_x monomers which were further polymerized to larger hydrocarbon products (Iglesia, 1997; Davis, 2001 and Burton, 2001). These mentioned mechanism was shown as follows:

$$CO + S_{Co} \longrightarrow CO\text{-}S_{Co} \qquad (4)$$

$$H_2 + S_{Co} \longrightarrow 2H\text{-}S_{Co} \qquad (5)$$

$$CO\text{-}S_{Co} + S_{Co} \longrightarrow C\text{-}S_{Co} + O\text{-}S_{Co} \qquad (6)$$

Where S_{Co} is cobalt active site.

$C\text{-}S_{Co}$ is adsorbed carbon on cobalt active site.

$O\text{-}S_{Co}$ is adsorbed oxygen on cobalt active site.

$H\text{-}S_{Co}$ is adsorbed hydrogen on cobalt active site.

$R\text{-}S_{Co}$ is adsorbed hydrocarbon products on cobalt active site.

The reaction between adsorbed carbon species and adsorbed hydrogen species were occurred and followed by the chain propagation as the following equations:

$$C\text{-}S_{Co} + H\text{-}S_{Co} \longrightarrow CH\text{-}S_{Co} \qquad (7)$$

$$CH\text{-}S_{Co} + CH\text{-}S_{Co} \longrightarrow R\text{-}S_{Co} \qquad (8)$$

Finally, the chain termination is occurred as shown in Equation 9:

$$R\text{-}S_{Co} \longrightarrow R + S_{Co} \qquad (9)$$

It is well-known that the FTS activity of supported cobalt catalyst strongly depends on the number of cobalt active sites after reduction and directly related to the reduction degree (Liu *et al.,* 2007). In addition, cobalt particle size is a key factor affecting the cobalt reducibility. According to TEM images of IMPCo/SBA-15 catalyst (Figure 28), it was clearly shown that cobalt species agglomerated to form large cobalt particles on the silica surface. The agglomeration of cobalt metal was attributed to the weak interaction between silica and cobalt precursor (Liu *et al.,* 2007). Therefore, IMPCo/SBA-15 catalyst with large cobalt particles had higher extent of cobalt reduction (Girardon *et al.,* 2007).

In general, for cobalt catalysts supported on silica, two-stage reduction was observed; Co_3O_4 was reduced to CoO and then to metallic Co. It could be ascribed to the successive reduction of Co_3O_4 to CoO at the step temperature around 300 °C and the subsequent reduction of CoO to metallic Co at around 550 °C (Steen *et al.,* 1996) as shown in Equations (10) and (11), respectively:

$$Co_3O_4 + H_2 \longrightarrow 3CoO + H_2O \qquad (10)$$

$$CoO + H_2 \longrightarrow Co + H_2O \qquad (11)$$

Furthermore, the FTS activity of cobalt supported catalyst was also related to the particular surface property of catalyst. Large cobalt particles provided large flat metallic surface, favoring bridge-type adsorbed CO (Zhang *et al.,* 2007). The large cobalt particles of IMPCo/SBA-15 catalyst were more easily to form the bridge-type CO during the FTS reaction compared to the small cobalt particles which promoted the formation of linear-type CO on active metals (Jalama *et al.,* 2007). Accordingly, IMPCo/SBA-15 catalyst with large cobalt particles greatly promoted the bridge-type CO formation than the linear-type CO of which preferably obtained from the smaller cobalt particles. The bridge-type CO had a weaker C–O bond and thus can be more easily dissociated to carbon and oxygen, which is one of the crucial processes in FTS reaction (Xiong *et al.,* 2008)

Considering the SOVCo/SBA-15 catalyst prepared via solvothermal technique, even though it was prepared by post-synthesis method, the result of CO conversion (23.8 %) was significant different from that of the IMPCo/SBA-15 catalyst (as shown in Table 3). From TEM images (Figure 29), it can be observed that SOVCo/SBA-15 catalyst exhibited the smaller sizes of cobalt particles with better cobalt distribution compared with IMPCo/SBA-15 catalyst. The smaller cobalt particles of SOVCo/SBA-15 catalyst promoted the stronger interaction between silica and cobalt species compared to IMPCo/SBA-15 catalyst (Kim *et al.,* 2005). These smaller cobalt particles of SOVCo/SBA-15 catalyst were also evident by the XRD patterns of the post-synthesis catalysts as shown in Appendix C. Similar fingerprint of XRD patterns was observed for calcined cobalt catalysts by both IMPCo/SBA-15 and SOVCo/SBA-15 catalysts. The diffraction peaks of 2θ at 31°, 37°, 45°, 59.5° and

65.5°, indicating the presence of Co_3O_4 (Panpranot *et al.*, 2005). The intensities of XRD peaks of SOVCo/SBA-15 catalyst were significantly decreased and the peaks were also broader compared to IMPCo/SBA-15 catalyst. This implied that the crystalline sizes of Co_3O_4 prepared from solvothermal technique were smaller than those prepared from impregnation method.

For solvothermal technique, tetrahydrofuran (THF) was used as an alternative solvent. Changing impregnating solvent from water to THF modified the surface polarity of SBA-15 porous silica. Roggenbuck *et al.*, 2008 reported that using THF instead of water increased the wettability of SBA-15 silica during the impregnation process according to a solvent of less polar than water. An enhancement of wettability of SBA-15 silica could be confirmed by the decrease in specific surface area of SOVCo/SBA-15 catalyst of ca. 53%, while a 48% reduction was observed when water was used as the impregnating solvent for IMPCo/SBA-15 catalyst (Table 1). It was clearly indicated that the polarity of impregnating solvent played an important role on the structure of impregnated catalyst. Furthermore, the difference in chemical property of impregnating solvents strongly affected the shapes and sizes of cobalt-loaded particles. As a result, it was found that using THF instead of water could change the vaporization rate of solvent, resulting in smaller particles size of the suspended cobalt species.

Consequently, the lower activity of SOVCo/SBA-15 catalyst was attributed to the smaller cobalt particles. The stronger interaction of cobalt species and the silica support resulted in the lower reducibility of cobalt metal resulted in the lower amount of Co^0 active sites (Girardon *et al.*, 2007).

1.2 Direct-synthesis Catalysts

It was clearly observed that the direct-synthesis catalysts (DSxCo/SBA-15) exhibited lower activity compared to those of post-synthesis catalyst. The CO conversion for DS3Co/SBA-15, DS6Co/SBA-15, DS7.5Co/SBA-15, and DS9Co/SBA-15 catalyst were 14.6 %, 16.9 %, 17.7 % and 3.7 %, respectively. The lower activity was attributed to the smaller sizes of cobalt particles which resulting in the decrease of the extent of reduction (Iglesia *et al.*, 1992). As observed from TEM images (Figures 36, 37 and 38), DSxCo/SBA-15 catalysts exhibited homogeneous distribution of incorporated smaller-size cobalt particles compared to those obtained from post-synthesis catalysts. The small cobalt particles with high dispersion strongly interacted with silica and were difficult to reduce. Some amount of incompletely reduced cobalt phases were inactive for CO hydrogenation and thus decreased the catalyst activity (Ernst *et al.,* 1999).

Comparatively, as observed from Table 3, IMPCo/SBA-15 catalyst was much more active (83.8 % CO conversion) than DS7.5Co/SBA-15 catalyst (17.7 % CO conversion) at similar cobalt loading amount (ca. 10 wt. %). Not only the cobalt particle size that effected on the reducibility of catalyst, but the FTS activity of Co-based catalysts also strongly depends on their structure. It was observed that the differences in the reduction behaviors between indirect and direct synthesis catalysts can be attributed to the different structure of catalysts. The different metal loading techniques significantly affected the cobalt structure.

In comparison, most of the cobalt oxides prepared from post-synthesis method were deposited as aggregates on silica surface, while those prepared from direct-synthesis method were entrapped in the silica framework (Tomiyama *et al.,* 2003). Cobalt particles in DSxCo/SBA-15 catalyst could partially remain in non-accessible positions inside the silica wall (Aguado *et al.,* 2008). Hence, the lower FTS activities would due to the encapsulation of cobalt active phase in the silica framework, resulting in a reduction of the active metal sites. It also implied that the potential benefit to the catalyst activity of a homogeneous cobalt distribution obtained through the direct-synthesis method was not significantly observed because of their poor reducibility.

Among the DSxCo/SBA-15 catalysts, DS7.5Co/SBA-15 catalyst exhibited the best performance, for which 17.7 % conversion of carbon monoxide was achieved. The increase in FTS activity of DS7.5Co/SBA-15 catalyst could be attributed to the higher amount of incorporated cobalt species which was seen as an advantage as it enhanced the catalytic activity.

Figure 40 shows the FTS activity of DSxCo/SBA-15 catalysts prepared under pH 3, 6, 7.5, and 9. The CO conversion gradually decreased and reached the steady state during the first 2 h. It was clearly observed that the FTS activities of DSxCo/SBA-15 catalysts were quite stable for the last 7 h. It could be due to the high dispersion of cobalt metal located in silica wall, which would have resistance to sintering of Co species during the reduction (Tomiyama *et al.*, 2003).

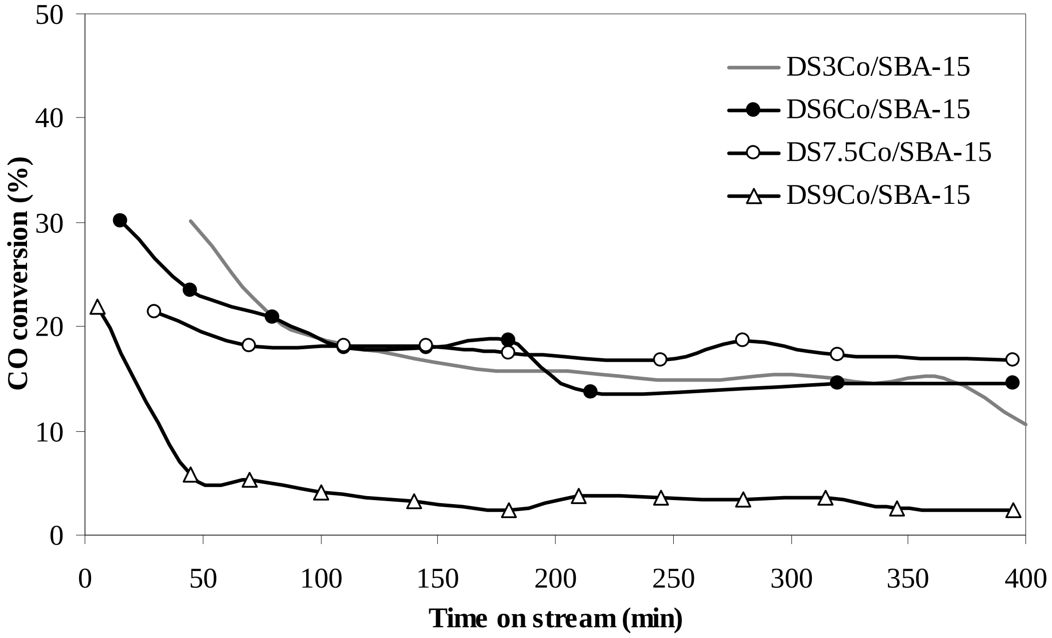

Figure 40 CO conversion toward FTS reaction over Co-supported catalysts prepared by direct synthesis method with various pH conditions.

As mentioned above, the stronger interaction between highly dispersed cobalt oxides and silica and the position of cobalt species in silica framework obtained from direct-synthesis catalysts decreased the degree of reduction. For post-synthesis catalyst, cobalt oxides located on the silica surface and they were easily reduced at low temperature (< 500 °C) (Mile *et al.*, 1998). However, in the case of DSxCo/SBA-15 catalyst, the reduction temperature used for post-synthesis catalysts

(400 ºC) was not suitably applied. The reduction temperature of direct-synthesis catalysts would be expected at higher temperature to obtain cobalt active sites. In this present work, the reduction temperature for direct-synthesis catalysts was changed to 650 °C to overcome the stronger cobalt-silica interaction.

Unfortunately, at higher reduction temperature, some amounts of cobalt silicate could also be formed during the reduction process (as shown in Equation 12). The formation of cobalt silicate can also suppress the reduction degree of supported cobalt (Soled *et al.*, 1995).

$$2CoO + SiO_2 \longrightarrow Co_2SiO_4 \qquad (12)$$

2. Product Selectivity

Significant differences can be observed in the FTS product distribution over Co/SBA-15 catalysts prepared by different metal loading techniques. The selectivities of Co/SBA-15 catalysts during the FT synthesis are strongly affected by their pore structures and the structural properties of metallic cobalts (Zhang *et al.*, 2007). The different catalytic behaviors for each Co/SBA-15 catalyst are reported as follows:

2.1 Post-synthesis Catalysts

Concerning the series of Co/SBA-15 catalysts prepared by post-synthesis methods, it can be seen that IMPCo/SBA-15 catalyst with ca. 10 wt. % Co loading presented a high selectivity towards light hydrocarbon products (62 %) and low selectivity towards heavy hydrocarbon products (C_5+) of approximately 21 % (as shown in Table 3). The selectivity towards methane over IMPCo/SBA-15 catalyst, which is undesired product, was significantly high (59 %).

The present investigation indicated that the product distribution was strongly affected by the particle size of cobalt species. Comparing to IMPCo/SBA-15 catalyst, the SOVCo/SBA-15 catalyst with the smaller size of cobalt particles clearly exhibited higher selectivity of long-chain hydrocarbons. The selectivity towards C_{10}+ product was increased from 21 % for IMPCo/SBA-15 catalyst to 86 % for SOVCo/SBA-15 catalyst. Figure 41 clearly shows that the hydrocarbon product distribution of SOVCo/SBA-15 catalyst was shifted towards the formation of heavy hydrocarbons, especially C_{10}+ hydrocarbons, compared with the IMPCo/SBA-15 catalyst. The SOVCo/SBA-15 catalyst with Better cobalt dispersion had influence on the FTS product selectivity. High dispersion of small cobalt particles increased the active metal surface area which promoted the chain growth of hydrocarbon chains during FTS reaction (Torabi *et al.*, 2004).

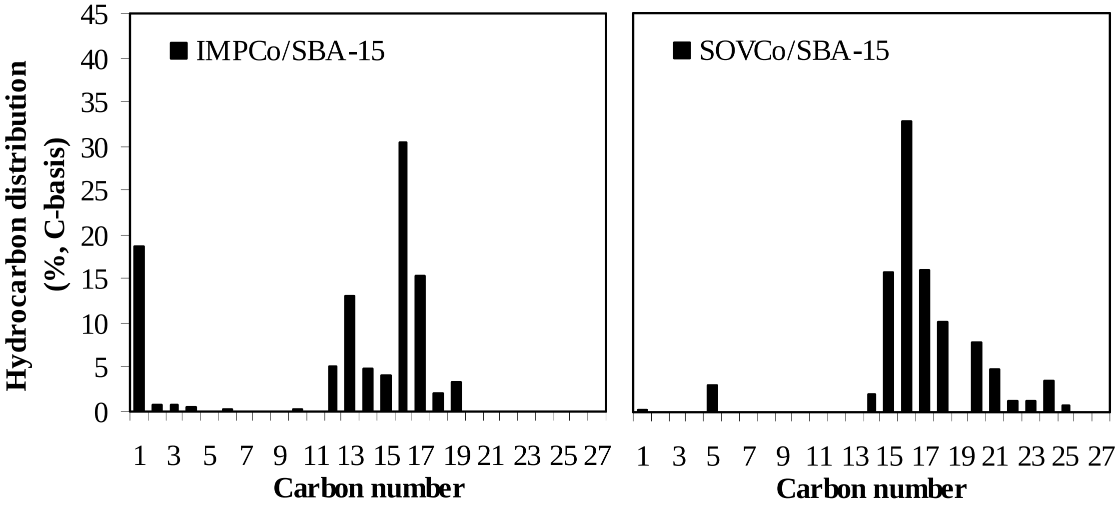

Figure 41 Hydrocarbon distributions (based on carbon atom) for IMPCo/SBA-15 and SOVCo/SBA-15 catalysts (T= 230 °C, P= 10 atm and $H_2/CO = 2$).

High methane selectivity over IMPCo/SBA-15 catalyst could be attributed to the surface property of cobalt catalyst. Large cobalt particles located on the silica support as mention earlier provided sites of weak CO adsorption in FTS. It was known that heavier hydrocarbon products were favored when CO and the intermediates are strongly adsorbed by metal sites (Ruel and Barthomolo, 1984; Khodakov *et al.,* 2002).

Additionally, the differences in the selectivity between each catalysts strongly depended on their pore structures. The pore blockage of cobalt clusters in IMPCo/SBA-15 catalyst decreased pore volume and pore diameter of catalyst (as previously discussed on the results of N_2-adsoprtion analysis). The decrease in pore size caused the hydrocarbons diffusion limit and condensation of heavy hydrocarbons in IMPCo/SBA-15 catalyst pores (Khodakov *et al.,* 2002). It can also be considered that the limitation of carbon monoxide diffusion in the pores of IMPCo/SBA-15 catalyst could increase H_2/CO ratio on the surface of catalyst, leading to chain termination and lower the chain growth probability. Thus light hydrocarbon products were produced (Kraum and Baerns, 1999) since the surface CH_x fragments were easily hydrogenated to terminate chain growth and thus increase the methane selectivity.

During the FTS, the higher H_2/CO surface ratio could also enhance the water-gas shift reaction as shown in Equation 13 (Ruel and Barthomolo, 1984).

$$CO + H_2O \longrightarrow CO_2 + H_2 \qquad (13)$$

The enhancement of water-gas shift reaction catalyzed by IMPCo/SBA-15 catalyst was evidenced by the emission of measurable amount of carbon dioxide (16.5 % selectivity) in the FTS catalytic result (as shown in Table 3). The CO_2 selectivity implied quite high activity for the competitive water gas shift reaction typically observed for Co-based FTS catalysts (Martinez *et al.,* 2003).

2.2 Direct-synthesis Catalysts

The hydrocarbon distributions were changed from each catalysts prepared by the direct synthesis and the unique selectivity was observed for the DSxCo/SBA-15 catalysts. The DSxCo/SBA-15 catalysts were less selective towards methanation, while their selectivity towards the C_{10}+ fraction was very high. The great amounts of long-chain hydrocarbon products, especially in diesel range hydrocarbons (C_{12}-C_{20}) were produced.

As observed in Table 3, the hydrocarbon selectivities of C_{10}+ hydrocarbons among the group of DSxCo/SBA-15 catalysts were very high. Increasing the cobalt contents by increasing pH values did not significantly affect the FTS product distribution since all the DSxCo/SBA-15 catalysts were selective to C_{10}+ products. Selectivity to heavy hydrocarbon products was noticeably high for the DS7.5Co/SBA-15 catalyst (99 % selective to C_{10}+). Comparing to IMPCo/SBA-15 catalyst, the very low selectivities to methane and CO_2 were clearly observed among all the DSxCo/SBA-15 catalysts.

Figure 42 shows the distribution of hydrocarbon products on a carbon basis of DSxCo/SBA-15 catalysts prepared under pH 3, 6, 7.5, and 9. The hydrocarbon product distributions of DSxCo/SBA-15 catalysts were obviously shifted towards the formation of heavy hydrocarbons, especially C_{10+} hydrocarbons, compared to the IMPCo/SBA-15 catalyst.

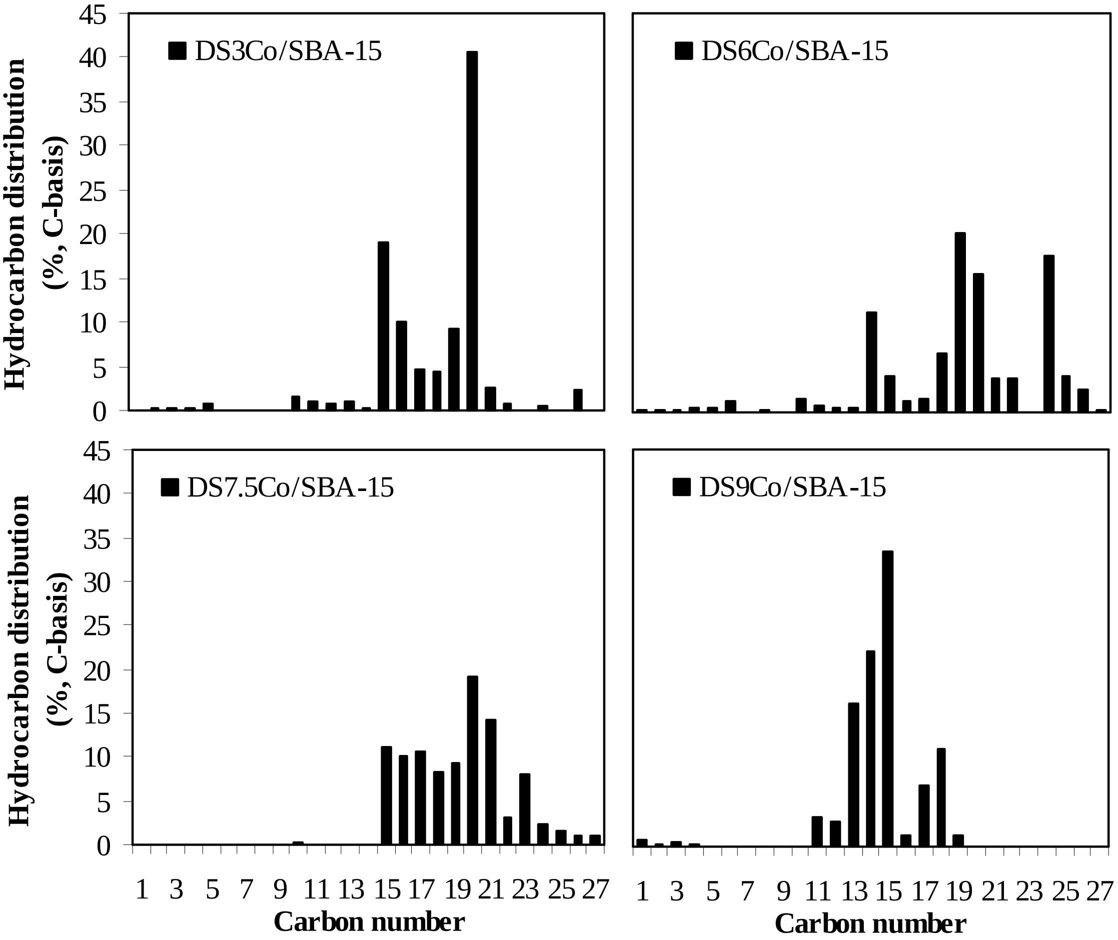

Figure 42 Hydrocarbon distributions (based on carbon atom) for DSxCo/SBA-15 catalysts prepared via direct synthesis using pH adjusting method (T= 230 °C, P= 10 atm and $H_2/CO = 2$).

It was clearly observed that the hydrocarbon product distributions of DSxCo/SBA-15 catalysts were strongly influenced by high dispersion of cobalt species in silica framework. A homogeneous distribution of cobalt species in silica framework promoted high dispersion of cobalt active sites which exhibited as large area of active metal in DSxCo/SBA-15 catalysts. High dispersion of metal active sites significantly increased the catalytic polymerization ability in the FTS reaction, resulting in higher selectivity to long-chain hydrocarbons (Iglesia *et al.*, 1992).

Considering the pore structure of DSxCo/SBA-15 catalysts, the pore blocking from cobalt aggregates were hardly observed. Therefore, the larger pore size of catalyst, compared to IMPCo/SBA-15, could overcome mass transfer limitation of reactant and hydrocarbon products (Khodakov *et al.*, 2001; Tsubaki *et al.*, 2001; Ohtsuka *et al.*, 2004). As a result, the DSxCo/SBA-15 catalyst with relatively larger pore size enhanced the diffusion of syngas and hydrocarbon products in mesoporous channels, and thus long-chain hydrocarbons were produced (Lapszewicz *et al.*, 1993).

It can be concluded that a simple modification of sol-gel process using pH adjusting approach could be potentially applied to prepare the FTS catalyst with high metal dispersion. The undesired methane product, normally occurred over cobalt catalysts prepared by the conventional impregnation method, was distinguishly reduced while the long-chain hydrocarbon products, particularly the diesel-range, were remarkably promoted over the DS7.5Co/SBA-15 catalyst. The selectivity of diesel products was relatively increased from 20.8 % for IMPCo/SBA-15 catalyst to 72.6 % over DS7.5Co/SBA-15 catalyst (as shown in Figure 43).

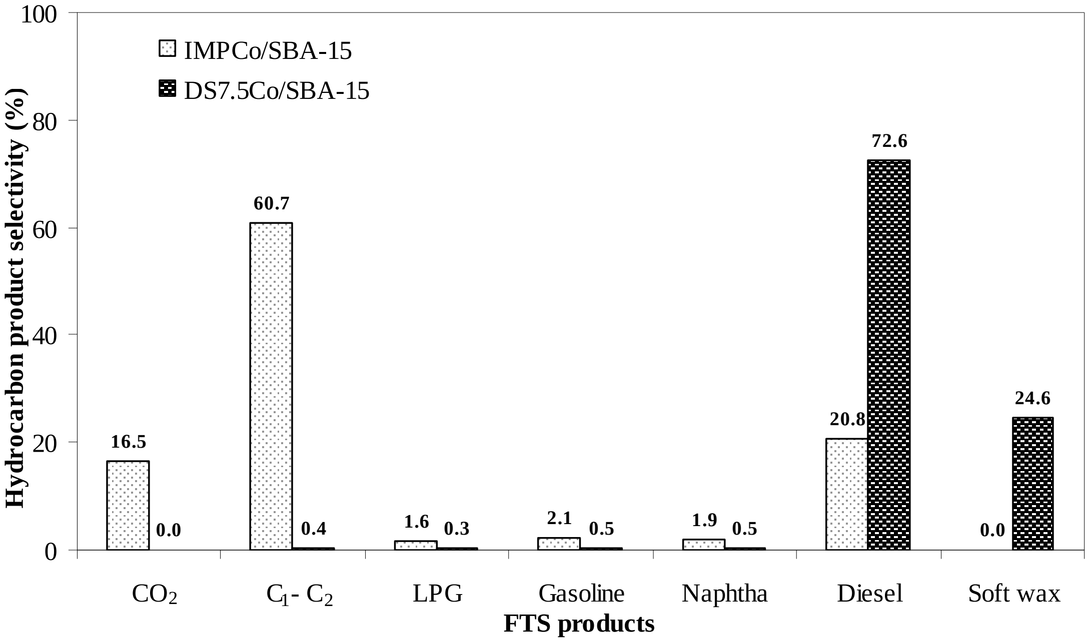

Figure 43 Variation of FTS products including CO_2, fuel gas (C_1-C_2), LPG (C_3-C_4), gasoline (C_5-C_{12}), naphtha (C_8-C_{12}), diesel (C_{12}-C_{20}) and soft wax (C_{21}-C_{25}) over ca. 10 wt. % cobalt loaded SBA-15 catalysts prepared by direct (IMPCo/SBA-15) and indirect (DS7.5Co/SBA-15) synthesis methods.

CONCLUSION

The Co/SBA-15 catalysts were prepared by the post-synthesis method and the direct synthesis method using cobalt nitrate as a cobalt precursor. The physical characteristics and catalytic properties for the Fischer-Tropsch synthesis (FTS) reaction were investigated as a function of metal loading techniques. The results can be concluded as follows:

1. It was found that IMPCo/SBA-15 catalyst was much more active (83.8 % CO conversion) than DS7.5Co/SBA-15 catalyst (17.7 % CO conversion) at similar cobalt loading amount (ca. 10 wt. %). The lower FTS activity of the direct-synthesis catalyst was attributed to the encapsulation of cobalt active phase in the silica framework, resulting in a reduction degree of the active metal sites, while most of the cobalt particles prepared from post-synthesis method were deposited on the silica surface.

2. The FTS product selectivity towards methane over IMPCo/SBA-15 catalyst was very high (59 %) while the selectivity towards heavy hydrocarbon products (C_{10+}) was relatively low (21 %) compared to DS7.5Co/SBA-15 catalyst (99 %).

3. A simple modification of sol-gel process by pH-adjusting approach was applied and Co/SBA-15 catalyst with highly distributed cobalt species within the SBA-15 mesostructure was successfully prepared.

4. At pH 7.5, the highly-ordered SBA-15 hexagonal structure with high cobalt loading (approximately 10 wt. % cobalt loading) was effectively prepared.

5. The pH-adjusting method can overcome the formation of cobalt aggregates obtained from the indirect-synthesis method. High dispersion of cobalt active phase over direct-synthesis catalyst significantly promoted the production of long-chain hydrocarbons, especially diesel-range products (76 %), and greatly decreased the methanation.

LITERATURE CITED

Afonso, J.C., D. A.G. Aranda, M. Schmal and R. Frety. 1997. Regeneration of a Pt/Al_2O_3 catalyst: influence of heating rate, temperature and time of regeneration. **Fuel Processing Technology** 50: 35-48.

Aguado, J., G. Calleja, A. Carrero and J. Moreno. 2008. One-step synthesis of chromium and aluminium containingSBA-15 materials: New phillips catalysts for ethylene polymerization. **Chemical Engineering Journal** 137: 443–452.

Alexandridis, P., P. Holmqvist and B. Lindman. 1997. Poly(ethylene oxide)-containing amphiphilic block copolymers in ternary mixtures with water and organic solvent: effect of copolymer and solvent type on phase behavior and structure. **Colloids and Surfaces A: Physicochemical and Engineering Aspects** 129: 3-21.

Anonymous. 2008. **BP Statistical Review of World Energy June 2008.** BP Global. Available source: http://www.bp.com/liveassets/bp_internet/globalbp/globalbp_uk_english/reports_and_publications/statistical_energy_review_2008.htm, December 8, 2008.

Baes, C.F. and R.E. Mesmer. 1976. **The Hydrolysis of Cations**. John Wiley, New York.

Bechara, R., D. Balloy and D. Vanhove. 2001. Catalytic properties of Co/Al_2O_3 system for hydrocarbon synthesis. **Applied Catalysis A: General** 207: 343-353.

Beck, J.S., J.C. Vartuli, W.J. Roth, M.E. Leonowicz, C.T. Kresge, K. D. Schmitt, C. T-W. Chu, D. H. Olson, E.W. Sheppard, S.B. McCullen, J.B. Higgins and J.L. Schlenkert. 1992. A new family of mesoporous molecular sieves prepared with liquid crystal templates. **Journal of the American Chemical Society** 114: 10834-10843.

Bessell S. 1993. Support effects in cobalt-based fischer-tropsch catalysis. **Applied Catalysis A: General** 96: 253-268.

Bharat L., N.J. Olanrewaju and S. Komarneni. 2001. Direct synthesis of titanium-substituted mesoporous SBA-15 molecular sieve under microwave-hydrothermal conditions. **Chemistry of Materials** 13: 552-557.

Bhoware, S.S. and A.P. Singh. 2006. Characterization and catalytic activity of cobalt containing MCM-41 prepared by direct hydrothermal, grafting and immobilization methods. **Journal of Molecular Catalysis A: Chemical** 266: 118-130.

Bian, G., N. Fujishita, T. Mochizuki, W. Ning, M. Yamada. 2003. Investigations on the structural changes of two Co/SiO_2 catalysts by performing Fischer–Tropsch synthesis. **Applied Catalysis A** 252: 251-260

Bourikas, K., C. Kordulis, J. Vakros and A. Lycourghiotis. 2004. Adsorption of cobalt species on the interface, which is developed between aqueous solution and metal oxides used for the preparation of supported catalysts: a critical review. **Advances in Colloid and Interface Science** 110: 97-120.

Brady, R.C. and R. Pettit. 1980. Reactions of diazomethane on transition-metal surfaces and their relationship to the mechanism of the Fischer-Tropsch reaction. **Journal of the American Chemical Society** 102: 6181-6182.

Calleja, G., J. Aguado, A. Carrero and J. Moreno. 2007. Preparation, characterization and testing of Cr/AlSBA-15 ethylene polymerization catalysts. **Applied Catalysis A: General** 316: 22-31.

Chanenchuk, C.A., I.C. Yates and C.N. Satterfield. 1991. The Fischer-Tropsch synthesis with a mechanical mixture of a cobalt catalyst and a copper-based water gas shift catalyst. **Energy and Fuels** 5: 847-855.

Chareonpanich, M., T. Namto, P. Kongkachuichay and J. Limtrakul. 2004. Synthesis of ZSM-5 zeolite from lignite fly ash and rice husk ash. **Fuel Processing Technology** 85: 1623-1634.

_____, A. Nanta-ngern and J. Limtrakul. 2007. Short-period synthesis of ordered mesoporous silica SBA-15 using ultrasonic technique. **Materials Letters** 61: 5153–5156.

Chen, S.Y., L.Y. Jang and S. Cheng. 2004. Synthesis of Zr-incorporated SBA-15 mesoporous materials in a self-generated acidic environment. **Chemistry of Materials** 16: 4147-4180.

Cheng M., Z. Wang, K. Sakurai, F. Kumata, T. Saito, T. Komatsu and T. Yashima. 1999. Creation of acid sites on SBA-15 mesoporous silica by alumination. **Chemistry Letters** 2: 131-132.

Coma, A. 1997. From microporous to mesoporous molecular sieve materials and their use in catalysis. **Chemical Reviews** 97: 2373-2379.

Coulter, K. E. and A. G. Sault. 1995. Effects of activation on the surface properties of silica-supported cobalt catalysts**. Journal of Catalysis** 154: 56-64.

Davis, B.H. 2001. Fischer-Tropsch synthesis: current mechanism and futuristic needs. **Fuel Processing Technology** 71:157-166.

Davis, B.H. 2005. Fischer–Tropsch synthesis: Overview of reactor development and future potentialities. **Topics in Catalysis** 32: 143-168.

Dimitrova P.G. and D.R. Mehandjiev. 1994. Active Surface of γ-Al2O3-Supported Co_3O_4. **Journal of Catalysis** 145: 356-363.

Dry, M.E. 1990. The fischer-tropsch process - commercial aspects. **Catalysis Today** 6: 183-206.

______, 1996. Practical and theoretical aspects of the catalytic Fischer-Tropsch process. **Applied Catalysis A: General** 138 (2): 319-344.

______, and A.P. Steynberg. 2004. Chapter 5 Commercial FT process applications. **Studies in Surface Science and Catalysis** 152: 406- 481.

Dunn B.C., G.C. Turpin, P. Cole, M.C. Webster, Z. Ma, R.J. Pugmire, R.D. Earnst and E.M. Eyring. 2004. Cobalt and ruthenium Fischer-Tropsch catalysts supported on silica aerogel. **Preprint Papers - American Chemical Society, Division of Petroleum Chemistry** 49: 431-434.

______, D.J. Covington, P. Cole, R.J. Pugmire, H.L.C. Meuzelaar, R.D. Earnst, E.C. Heider and E.M. Eyring. 2004. Silica xerogel supported cobalt metal Fischer-Tropsch catalysts for syngas to diesel range fuel conversion. **Energy and Fuels** 18: 1519-1521.

Earnst, B., A. Bensaddik, L. Hilaire, P. Chaumette, A. Kiennemann. 1998. Study on a coabalt silica catalyst during reduction and Fischer-Tropsch reaction: In situ EXAFS compared to XPS and XRD. **Catalysis Today** 39: 329-341.

Ernst, B., S. Libs, P. Chaumette and A. Kiennemann. 1999. Preparation and characterization of Fischer–Tropsch active Co/SiO_2 catalysts. **Applied Catalysis A: General** 186: 145–168.

Girardon, J.S., A.S. Lermontov, L. Gengembre, P.A. Chernavskii, A.G. Constanta and A.Y. Khodakov. 2005. Effect of cobalt precursor and pretreatment conditions on the structure and catalytic performance of cobalt silica-supported Fischer–Tropsch catalysts. **Journal of Catalysis** 230: 339-352.

Grieken, R.V., J.M. Escola, J. Moreno and R. Rodriguez. 2006. Liquid phase oligomerization of 1-hexene over different mesoporous aluminosilicates (Al-MTS, Al-MCM-41 and Al-SBA-15) and micrometer/nanometer HZSM-5 zeolites. **Applied Catalysis A: General** 305: 176-188.

Guari, Y., C. Thieuleux, A. Mehdi, C. Reye, R.J.P. Corriu, S. Gomez-Gallardo, K. Philippot, B. Chaudret and R. Dutartre. 2001. In-situ formation of gold nanoparticles within functionalized ordered mesoporous silica via an organometallic chimie douce approach. **Chemical Communications** 1374-1375.

Hosseini, S.A., A. Taeb, F. Feyzi and F. Yaripour. 2004. Fischer-Tropsch synthesis over Ru promoted Co/γ-Al_2O_3 catalysts in a CSTR. **Catalysis Communications** 5: 137-143.

Hu, M.Z., R.D. Hunt, E.A. Payzant and C.R. Hubbard. 1999. Nanocrystallization and phase transformation in monodispersed ultrafine zirconia particles from various homogeneous precipitation methods. **Journal of the American Ceramic Society** 82: 2313-2320.

Huang, Z., F. Cui, H. Kang, J. Chen, X. Zhang and C. Xia. 2008. Highly dispersed silica-supported copper nanoparticles prepared by precipitation-gel method: a simple but efficient and stable catalyst for glycerol hydrogenolysis. **Chemistry of Materials** 20: 5090-5099.

Iglesia, E., S. L. Soled and R. A. Fiato. 1992. Fischer-Tropsch synthesis on cobalt and ruthenium: Metal dispersion and support effects on reaction rate and selectivity. **Journal of Catalysis** 137: 212-224.

Iglesia, E. 1997. Design, synthesis, and use of cobalt-based Fischer-Tropsch synthesis catalysts. **Applied Catalysis A: General** 161: 59-78.

Inagaki, S., Y. Fukushima and K. Kuroda. 1993. Synthesis of highly ordered mesoporous materials from a layered polysilicate. **Journal of the Chemical Society, Chemical Communications** 1993: 680-682.

Jacobs, G., T. K. Das, Y.Zhang, J. Li, G. Racoillet and B. H. Davis. 2002. Fischer–Tropsch synthesis: support, loading, and promoter effects on the reducibility of cobalt catalysts. **Applied Catalysis A: General** 233: 263 -281.

Jalama, K., N.J. Coville, D. Hildebrandt, D. Glasser and L.L. Jewell. 2007. Fischer–Tropsch synthesis over Co/TiO_2: Effect of ethanol addition. **Fuel**s 86: 73-80

Jana, S.K., T. Kugita and S. Namba. 2003. Bisphenol F synthesis over mesoporous aluminosilicate MCM-41 molecular sieves. **Catalysis Letters** 90: 143-147.

Jermy, B.R., D.R. Cho, K.V. Bineesh, S.Y. Kim and D.W. Park. 2008. Direct synthesis of vanadium incorporated three-dimensional KIT-6: A systematic study in the oxidation of cyclohexane. **Microporous and Mesoporous Materials** 115: 281-292.

Khodakov, A.Y., J. Lynch, D. Bazin, B. Rebours, N. Zanier, B. Moisson and P. Chaumette. 1997. Reducibility of Cobalt Species in Silica-Supported Fischer–Tropsch Catalysts. **Journal of Catalysis** 168: 16-25.

Khodakov, A.Y., A. Griboval-Constant, R. Bechara and F. Vilain. 2001. Pore-size control of cobalt dispersion and reducibility in mesoporous silicas. **Journal of Physical Chemistry B** 105: 9805-9811

______, A. Griboval-Constant, R. Bechara and V.L. Zholobenko. 2002. Pore size effects in Fischer-Tropsch synthesis over cobalt-supported mesoporous silicas. **Journal of Catalysis** 206: 230-241.

______, R. Bechara and A. Griboval-Constant. 2003. Fischer-Tropsch synthesis over silica supported cobalt catalysts: mesoporous structure versus cobalt surface density. **Applied Catalysis A: General** 254: 273-288.

______, V. L., Zholobenko, R. Bechara and D. Durand. 2005. Impact of aqueous impregnation on the long-range ordering and mesoporous structure of cobalt containing MCM-41 and SBA-15 materials. **Microporous and Mesoporous Materials** 79: 29-39.

Knottenbelt, C. 2002. Mossgas "gas-to-liquid" diesel fuels—an environmentally friendly option. **Catalysis Today** 71: 437–445.

Konya, Z., V.F. Puntes, I. Kiricsi, J. Zhu, P. Alivisatos and G.A. Somorjai. 2002. Novel Two-Step Synthesis of Controlled Size and Shape Platinum nanoparticles Encapsulated in Mesoporous Silica. **Catalysis Letters** 81: 137-140.

Kraum, M. and M. Baerns. 1999. Fischer-Tropsch synthesis: The influence of various cobalt compounds applied in the preparation of supported cobalt catalysts on their performance. **Applied Catalysis A: General** 186: 189-200.

Kresge, C.T., M.E. Leonowicz, W.J. Roth, J.C. Varturi and J.S. Beck 1993. Ordered mesoporous molecular sieves synthesized by a liquid-crystal template mechanism. **Solid State Nuclear Magnetic Resonance** 2: 253-259.

Kresge, C.T., M. E. Leonowicz, W. J. Roth, J. C. Vartuli and J. S. Beck. 1992. Ordered mesoporous molecular sieves synthesized by a liquid-crystal template mechanism. **Nature** 359: 710 – 712.

Kustrowski, P., L. Chmielarz, R. Dziembaj, P. Cool and E.F. Vansant. 2005. Modification of MCM-48-, SBA-15-, MCF-, and MSU-type mesoporous silicas with transition metal oxides using the molecular designed dispersion method. **Journal of Physic Chemistry B** 109: 11552-11558.

Lapszewicz, J.A., H.J. Loeh, and J.R. Chipperfield 1993. The effect of catalyst porosity on methane selectivity in the Fischer–Tropsch reaction. **Journal of the Chemical Society, Chemical Communications** 11: 913 – 914.

Li, Y., Z. Feng, Y. Lian, K. Sun, L. Zhang, G. Jia, Q. Yang and C. Li. 2005. Direct synthesis of highly ordered Fe-SBA-15 mesoporous materials under weak acidic conditions. **Microporous and Mesoporous Materials** 84: 41–49.

Lira, E., C.M. Lopez, F. Oropeza, M. Bartolini, J. Alvarez, M. Goldwasser, F.L Linares, J.F. Lamonier and M.J.P. Zurita. 2008. HMS mesoporous silica as cobalt support for the Fischer-Tropsch synthesis: Pretreatment, cobalt loading and particle size effects. **Journal of Molecular Catalysis A: Chemical** 281: 146-153.

Lou, Z., R. Wang, H. Sun, Y. Chen and Y. Yang. 2008. Direct synthesis of highly ordered Co-SBA-15 mesoporous materials by the pH-adjusting approach. **Microporous and Mesoporous Materials** 110: 347-354.

Luo, M. and B.H. Davis. 2003. Fischer–Tropsch synthesis: activation of low-alpha potassium promoted iron catalysts. **Fuel Processing Technology** 83 (1-3): 49-65.

Luan, Z., E.M. Maes, V. Heide, A.W. Paul, D. Zhao, R.S. Czernuszewicz and K. Larry. 1999. Incorporation of Titanium into Mesoporous Silica Molecular Sieve SBA-15. **Chemistry of Materials** 11: 3680-3686.

Martínez, A., C. Lopez, F. Marquez and I. Diaz. 2003. Fischer–Tropsch synthesis of hydrocarbons over mesoporous Co/SBA-15 catalysts: the influence of metal loading, cobalt precursor, and promoters. **Journal of Catalysis** 220: 486–499.

Mile, B., D. Stirling, M.A. Zammitt, A. Lovell and M. Webb. 1990. TPR studies of the effects of preparation conditions on supported nickel catalysts. **Journal of Molecular Catalysis 62**: 179-198.

Min, B.K., A.K. Santra and D.W. Goodman. 2003. Understanding silica-supported metal catalyst: Pd/silica as a case study. **Catalysis Today** 85: 113-124.

Ming, H. and B.G. Baker. 1995. Characterization of cobalt Fischer-Tropsch catalysts Of Unpromoted cobalt-silica gel catalysts. **Applied Catalysis A: General**, 123: 23-36.

Mirji, S.A., S.B. Halligudi, N. Mathew, N.E. Jacob, K.R. Patil and A.B. Gaikwad. 2007. Adsorption of methanol on mesoporous SBA-15. **Material Letters** 61: 88-92.

Mochizuki, T., T. Hara, N. Koizumi and M.Yamada. 2006. Surface structure and Fischer–Tropsch synthesis activity of highly active Co/SiO_2 catalysts prepared from the impregnating solution modified with some chelating agents. **Applied Catalysis A: General** 317: 97–104.

Mu, Z., J.J. Li, Z.P. Hao and S.Z. Qiao. 2008. Direct synthesis of lanthanide-containing SBA-15 under weak acidic conditions and its catalytic study. **Microporous and Mesoporous Materials** 113: 72-80.

Murugavel, R. and H.W. Roesky. 1997. Titanosilicate: neue entwicklungen in der synthese und bei der anwendung als oxidationskatalysatoren. **Angewandte Chemie** 109: 491-494.

Nanta-Ngern, A. 2005. **The Synthesis of SBA-15 Mesoporous Silica from Rice Husk Ash.** M.S. Thesis, Kasetsart University.

Ohtsuka, Y., Y. Takahashi, M. Nogushi, T. Arai, S. Takasaki, N. Tsubouchi and Y. Wang. 2004. Novel utilization of mesoporous molecular sieves as supports of cobalt catalysts in Fischer-Tropsh synthesis. **Catalysis Today** 89: 419-429.

Panpranot, J., S. Kaewgun and P. Praserthdam. 2005. Metal-support interaction in mesoporous silica supported cobalt Fischer-Tropsch catalysts. **Reaction Kinetics and Catalysis Letters** 85: 299-304.

Prashar, A.K., R.P. Hodgkins, R. Kumar and R.N. Devi. 2008. *In situ* synthesis of Pt nanoparticles in SBA-15 by encapsulating in modified template micelles: sized restricted growth within the mesochannels. **Journal of Materials Chemistry** 18: 1765 – 1770.

Ponec, V., W.M.A. Sachtler and J.M. Kool. 1979. The role of carbon in methanation by cobalt and ruthenium. **Journal of Catalysis** 56: 284-286.

Reubroycharoen, P., T. Vitidsant, Y. Lui, G. Yang and N. Tsubaki. 2007. Highly active Fischer-Tropsch synthesis Co/SiO2 catalysts prepared from microwave irradiation. **Catalysis Communication** 8: 375-378.

Reuel, R.C. and C.H. Bartholomew. 1984. The stoichiometries of H_2 and CO adsorptions on cobalt: Effects of support and preparation. **Journal of Catalysis** 85: 63-77.

Regev, O. 1996. Nucleation events during the synthesis of mesoporous materials using liquid crystalline templating. **Langmuir** 12: 4940-4944.

Roggenbuck, J., T. Waitz and M. Tiemann. 2008. Synthesis of mesoporous metal oxides by structure replication: Strategies of impregnating porous matrices with metal salts. **Microporous and Mesoporous Materials** 113: 575–582.

Ryoo, R. and C.H. Ko. 2000. Block-Copolymer-Templated Ordered Mesoporous Silica: Array of Uniform Mesopores or Mesopore-Micropore Network. **Journal of Physical Chemistry B** 104: 11465-11471

Saib, A.M., M. Claeys and E.V. Steen. 2002. Silica supported cobalt Fischer-Tropsch catalysts: effect of pore diameter of support. **Catalysis Today** 71: 395-402.

Selvaraj, M., A. Pandurangan, K.S. Seshadri, P.K. Sinha and K.B. Lal. 2002. Synthesis, characterization and catalytic application of MCM-41 mesoporous molecular sieves containing Zn and Al. **Applied Catalysis A: General** 242: 347-364.

_____ and S. Kawi. 2008. Direct synthesis and catalytic performance of ultralarge pore GaSBA-15 mesoporous molecular sieves with high gallium content. **Catalysis Today** 131: 82-89.

Shah, P., A.V. Ramaswamy, K. Lazar and V. Ramaswamy. 2007. Direct hydrothermal synthesis of mesoporous Sn-SBA-15 materials under weak acidic conditions. **Microporous and Mesoporous Materials** 100: 210-226.

Soled, S.L., J. E. Baumgartner, S.C. Reyes, E. Iglesia. 1995. Synthetic design of cobalt Fischer-Tropsch synthesis catalysts**. Materials Research Society Symposium Proceedings** 368: 113-115.

Soled, S.L., E. Iglesia, R.A. Fiato, J.E. Baumgartner, H. Vroman, M. Sabato. 2003. Control of metal dispersion and structure by changes in the solid-state chemistry of supported cobalt Fischer-Tropsch catalysts. **Topics in Catalysis** 26: 101-109.

Srinivasu, P., C. Anand, S. Alam, K. Ariga, S.B. Halligudi, V.V. Balasubramanian and A. Vinu. 2008. Direct synthesis and the morphological control of highly ordered two-dimentional P6mm mesoporous nionium silicates with high niobium content. **The Journal of Physical Chemistry C** 112: 10130-10140.

Steen, E.V., G.S. Sewell, R.A. Makhothe, C. Micklethwaite, H. Manstein, M. Lange and C.T. O'Connor. 1996. TPR Study on the Preparation of Impregnated Co/SiO_2 Catalysts. **Journal of Catalysis** 162: 220-229.

Sumiya, S., Y. Oumi, T. Uozumi and T.Sano. 2001. Characterization of Al/SBA-15 prepared by post-synthesis alumination with trimethylaluminium. **Journal of Materials Chemistry** 11: 1111-1115.

Sun, S., N. Tsubaki and K. Fujimoto. 2000. The reaction performances and characterization of Fischer-Tropsch synthesis Co/SiO_2 catalysts prepared from mixed cobalt salts. **Applied Catalysis A: General** 202: 121-131.

Takahashi R., K. Nakanishi, N. Soga. 2005. Insight on structural change in sol-gel-derived silica gel with aging under basic conditions for mesopore control. **Journal of Sol-Gel Science and Technology** 33: 159-167.

Takahashi, R., S. Sato, T. Sodesawa and S. Tomiyama. 2005. CO_2-reforming of methane over Ni/SiO_2 catalyst prepared by homogeneous precipitation in sol-gel derived silica gel. **Applied Catalysis A: General** 286: 142-147.

Takeshita, T. and K. Yamaji. 2008. Important roles of Fischer-Tropsch synfuels in the global energy future. **Energy Policy** 36: 2773– 2784.

Tas, A.C. 1999. Preparation of lead zirconate titanate (Pb(Zr0.52Ti0.48)O3) by homogeneous precipitation and calcination. **Journal of the American Ceramic Society** 82: 1582-1584.

Tomiyama, S., R. Takahashi and S. Sato. 2003. Preparation of Ni/SiO_2 catalyst with high thermal stability for CO_2-reforming of CH_4. **Applied Catalysis A: General** 241: 349-361.

Torabi, F., A. Karimi, A. Tavasoli. 2004. Enhancement of FTS activity and selectivity by introducing CO during catalyst reducttion. **Petroleum & Coal** 46: 81-87.

Tsubaki, N., S. Sun and K. Fujimoto. 2001. Different functions of the noble metals added to cobalt catalysts for Fischer-Tropsch synthesis. **Journal of Catalysis** 199: 236-246.

Tuel, A., V. Gramlich, Ch. Baerlocher. 2004. Synthesis and crystal structure of a new layered aluminophosphate $[Al_3P_4O_{16}][C_6N_3H_{17}][H_3O]$. **Journal of Solid State Chemistry** 177: 2484-2493.

Tauster, S.J., S.C. Fung, R.T.K. Baker and J.A. Horsley. 1981. Strong interactions in supported-metal catalysts. **Science** 211: 1121 – 1125.

Van Der Laan, G.P. and A. A. C. M. Beenackers. 1999. Kinetics and Selectivity of the Fischer-Tropsch Synthesis: A Literature Review. **Catalysis Reviews** 41: 255– 318.

Vannice, M.A. 1977. The catalytic synthesis of hydrocarbons from H_2/CO mixtures over the Group VIII metals V. The catalytic behavior of silica-supported metals. **Journal of Catalysis** 50: 228-236.

Vinu, A., V. Murugesan and M. Hartmann. 2003. Pore size engineering and mechanical stability of the cubic mesoporous molecular sieve SBA-15. **Chemistry of Materials** 15: 1385-1393.

Vinu, A., D.P. Sawant, K. Ariga, K.Z. Hossain, S.B. Halligudi, M. Hartmann and M. Nonura. 2005. Direct synthesis of well-ordered and unusually reactive Fe-SBA-15 mesoporous molecular sieves. **Chemistry of Materials** 17: 5339-5345.

Wan, H., B. Wu, C. Zhang, H. Xiang and Y. Li. 2008. Promotional effects of Cu and K on precipitated iron-based catalysts for Fischer–Tropsch synthesis. **Journal of Molecular Catalysis A: Chemical** 283: 33–42.

Wang, L., A. Kong, B. Chen, H. Ding, Y. Shan and M. He. 2005. Direct synthesis, characterization of Cu-SBA-15 and its high catalytic activity in hydroxylation of Phenol by H2O2. **Journal of Molecular Catalysis A: Chemical** 230: 143-150.

Wojciechowski, B.W. and J. Abbot. 1988. The effect of temperature on the product distribution and kinetics of reactions of n-hexadecane on HY zeolite. **Journal of Catalysis** 109(2): 274-283.

Wu, S., Y. Han, Y.C. Zou, J.W. Song, L. Zhao, Y. Di, S.Z Liu and F.S. Xiao. 2004. Synthesis of heteroatom substituted SBA-15 by the “pH-Adjusting” method. **Chemistry of Materials** 16: 486-492.

Xiong, H., Y. Zhang, K. Liew and Jinlin Li. 2008. Fischer–Tropsch synthesis: The role of pore size for Co/SBA-15 catalysts. **Journal of Molecular Catalysis A: Chemical** 295: 68-76.

Yang, G., J. He, Y. Yoshiharu, Y. Tan, Y. Han and N. Tsubaki. 2007. Preparation, characterization and reaction performance of H-ZSM-5/cobalt/silica capsule catalysts with different sizes for direct synthesis of isoparaffins. **Applied Catalysis A: General** 329: 99-105.

Yang, Y., Y. Liu, G. Yang, S. Sun and N. Tsubaki. 2007. Effect of impregnation solvent on Co/SiO2 catalyst for Fischer-Tropsch synthesis: A highly active and stable catalyst with bimodal sized cobalt particles. **Applied Catalysis A: General** 321: 79-85.

Zennaro, R., M. Tagliabue and C.H. Bartholomew. 2000. Kinetics of Fischer-Tropsch synthesis on titania-supported cobalt. **Catalysis Today** 58: 309-319.

Zhao, D., J. Feng, Q. Huo, N. Melosh, G.H. Fredrickson, B.F. Chmelka and G.D. Stucky. 1998. Triblock copolymer syntheses of mesoporous silica with periodic 50 to 300 angstrom pores. **Science** 279: 548-552.

______, Q. Huo, J. Feng, B.F. Chmelka, and G.D. Stucky. 1998. Nonionic Triblock and Star Diblock Copolymer and Oligomeric Surfactant Syntheses of Highly Ordered, Hydrothermally Stable, Mesoporous Silica Structures. **Journal of the American Chemical Society** 120: 6024-6032.

Zhang, C.H., Y. Yang, B.T. Teng, T.Z. Li, H.Y. Zheng, H.W. Xiang and Y.W. Li. 2006. Study of an iron-manganese Fischer–Tropsch synthesis catalyst promoted with copper. **Journal of Catalysis** 237: 405-415.

Zhang, W.H., J. Lu, B. Han, M. Li, J. Xiu, P. Ying and C. Li. 2002. Direct synthesis and characterization of titanium-substituted mesoporous molecular sieve SBA-15. **Chemistry of Materials** 14: 3413-3421.

Zhang, Y., Y. Liu, G. Yang, S. Sun and N. Tsubaki. 2007. Effect of impregnation solvent on Co/SiO$_2$ catalyst for Fischer-Tropsh synthesis: A highly active and stable catalyst with bimodal sized cobalt particles. **Applied Catalysis A: General** 321: 79-85.

Zholobenko, V.L., A. Evans, D. Plant and S.M. Holmes 2001. Acid sites in mesoporous materials: a DRIFTS study. **Microporous and Mesoporous Materials** 44-45: 793-799.

______, V.L, A.Y. Khodakov, M. Impéror-Clerc, D. Durand and I. Grillo. 2008. Initial stages of SBA-15 synthesis: An overview. **Advances in Colloid and Interface Science** 142: 67-74.

APPENDICES

Appendix A

Qualitative and Quantitative Results from Gas Chromatography

Quantitative and Qualitative Results from Gas Chromatography

Gas chromatography was performed in a specially designed instrument. The major instrumental components consisted of a flowing mobile phase, an injector port, a separation column containing the stationary phase, a detector, and a data recording system as shown in Appendix Figure A1. Certain amount of gaseous mixture, 0.5 mL in this research, was injected into gas chromatograph at the injector port and was volatilized in a hot injection chamber before it was transported to the head of the chromatic column. Then, a flow of inert carrier gas (as a mobile phase) swept the injected mixture through a heated column which contained the stationary phase. The gaseous sample moved along the packing column whereas its component gas moved with different flow rates and thus separated into pure component. Before each component exited the instrument, it passed through a detector. The detector sent an electronic signal to the recorder and the analyzed results were printed out.

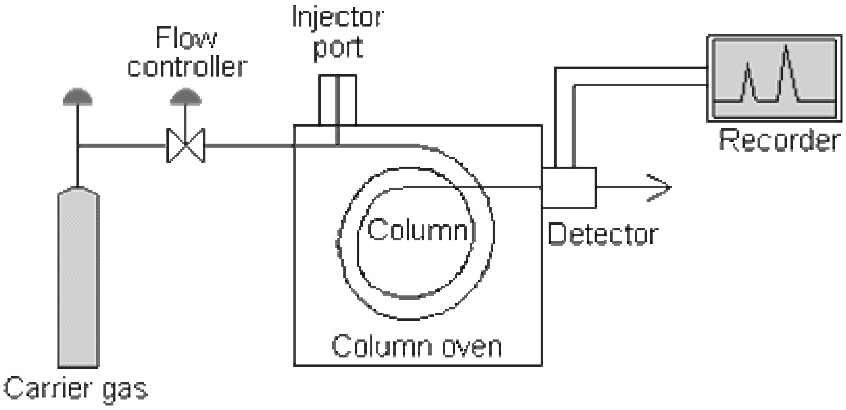

Appendix Figure A1 Schematic diagram of gas chromatograph.

In this work, the quantitative and qualitative data of product composition was obtained from 2 types of gas chromatography including TCD-GC and FID-GC as mention in the experimental chapter. Before analysis, the condition of operation was set and kept on running for about an hour to stabilize the based line. Certain volume of sample mixture (0.5 mL in this case) was injected into the injection port by gas syringe. After the mixture of sample gas was analyzed, the qualitative and quantitative data were interpreted from the peak area obtained from the recorder. The component of injected gas mixture can be identified by using the value of retention time data compared with the retention time received from injected standard gas. The chromatogram of standard gases and liquids used in this research were shown as following figures:

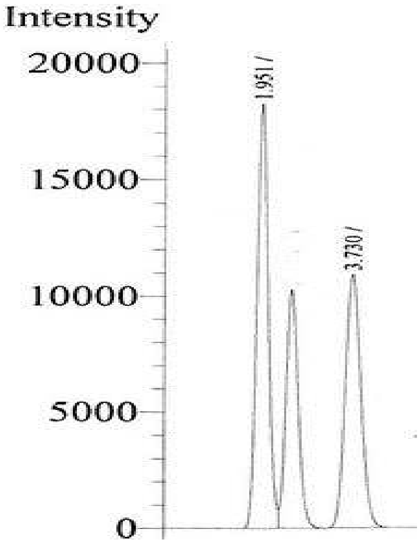

Appendix Figure A2 Chromatogram of standard gases for CO and CO_2.

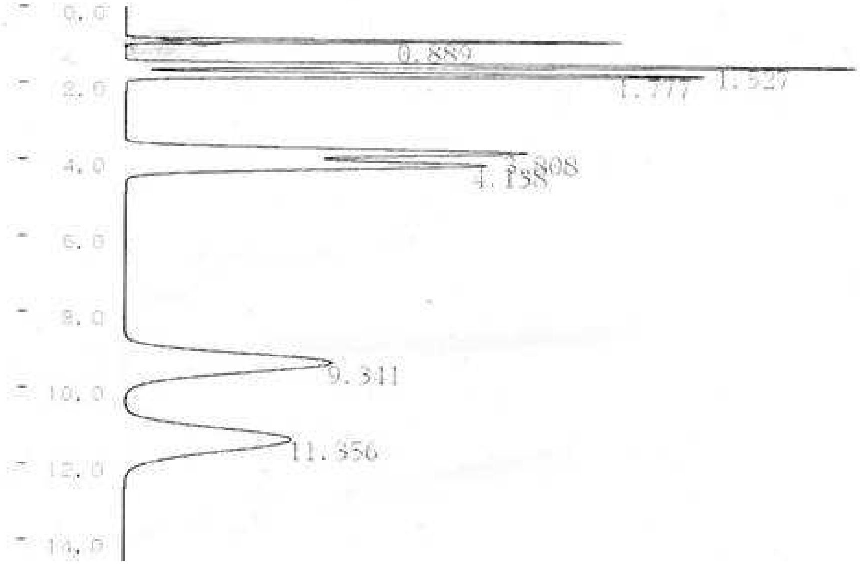

Appendix Figure A3 Chromatogram of standard gases for C_1-C_4 hydrocarbons.

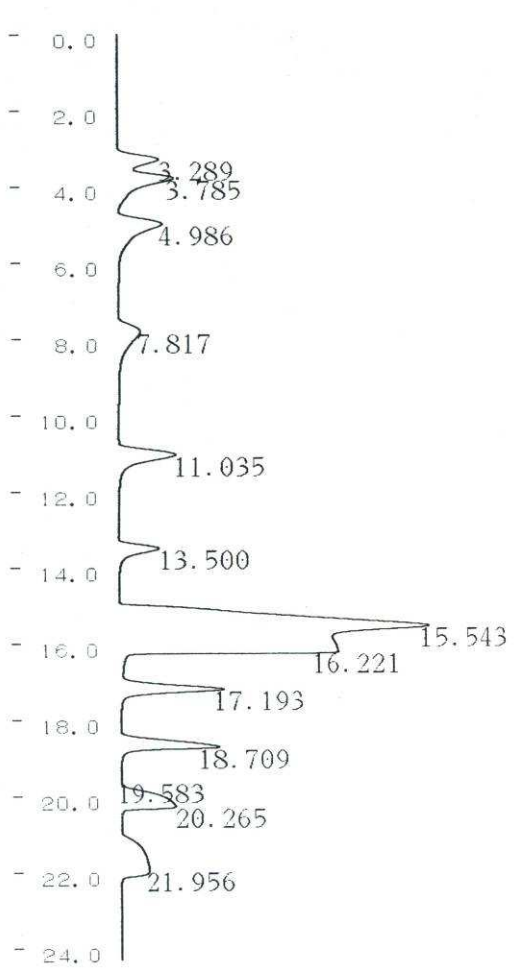

Appendix Figure A4 Chromatogram of standard liquids for C_5-C_{15} hydrocarbons.

The quantitative analysis of gas and liquid samples were obtained from the calibration curves where the correlation between the amount of injected gas or liquid sample (mole) and the peak area of gas chromatograms were proposed. The correlation between these parameters (mole and area) was analyzed by a linear regression equation. All the calibration curves for each single standard gas and liquid used in this research were shown in Appendix Table A1.

Appendix Table A Equation of calibration curves for standard gas and liquid

Substance	Equation	R^2
CO	mol = $4.46\text{x } 10^{-11}$ x area	0.999
CO_2	mol = $4.38\ 10^{-11}$ x area	0.999
CH_4	mol = $2.0\text{x } 10^{-14}$ x area	0.999
C_2H_4	mol = $7.0\text{x } 10^{-15}$ x area	0.996
C_2H_6	mol = $8.0\text{x } 10^{-15}$ x area	0.998
C_3H_6	mol = $6.0\text{x } 10^{-15}$ x area	0.999
C_3H_8	mol = $6.0\text{x } 10^{-15}$ x area	0.998
C_4H_{10}	mol = $2.0\text{x } 10^{-7}$ x area	0.999
C_5H_{12}	mol = $3.05 \text{ x } 10^{-13}$ x area	0.997
C_6H_{14}	mol = $1.39 \text{ x } 10^{-13}$ x area	0.997
C_7H_{16}	mol = $1.39 \text{ x } 10^{-13}$ x area	0.997
C_8H_{18}	mol = $1.97 \text{ x } 10^{-13}$ x area	0.997
C_9H_{20}	mol = $1.13 \text{ x } 10^{-13}$ x area	0.997
$C_{10}H_{22}$	mol = $1.97 \text{ x } 10^{-13}$ x area	0.988
$C_{11}H_{24}$	mol = $7.36 \text{ x } 10^{-14}$ x area	0.995
$C_{12}H_{26}$	mol = $6.85 \text{ x } 10^{-14}$ x area	0.996
$C_{13}H_{28}$	mol = $6.67 \text{ x } 10^{-14}$ x area	0.997
$C_{14}H_{30}$	mol = $6.15 \text{ x } 10^{-14}$ x area	0.992
$C_{15}H_{32}$	mol = $6.25 \text{ x } 10^{-14}$ x area	0.993

The calculation for the amount of each component in a standard-gas mixture can be calculated as follows:

$$\text{Amount of component}_i \text{ (mol)} = \frac{V_i \text{ x } T}{100 \text{ x } 22{,}400} \qquad \text{(A1)}$$

where V_i = % volume of component_i (cm^3/cm^3)

T = volume of standard gases mixture (mL)

The calculation for the amount of each component in a standard liquids mixture that can be calculated as follows:

$$\text{Amount of component}_i\text{ (mol)} = \frac{V_i \text{ x } T \text{ x } D \text{ x } P \text{ x } 10^{-3}}{MW} \qquad \text{(A2)}$$

where V = % volume of component$_i$ (cm^3/cm^3)

T = volume of liquid mixture (μL)

D = density (g/cm^3)

P = purity (%)

MW = molecular weight (g/mol)

Appendix B

Conversion and Selectivity Results

Conversion and Selectivity Results

The calculation for the conversion of carbon monoxide to hydrocarbon products in Fischer-Tropsch synthesis (FTS) reaction are shown as follows:

Percent of CO conversion:

$$\text{CO conversion (\%)} = (CO_{in} - CO_{out})/CO_{in} \times 100$$

Percent of effluent composition for FTS products:

$$\text{Effluent composition of product}_i\ (\%) = \frac{\text{moles of product}_i \times 100}{\sum \text{moles of FTS products}}$$

Percent of hydrocarbon selectivity for hydrocarbon products:

$$\text{Selectivity of hydrocarbon}_i\ (\%) = \frac{\text{moles of hydrocarbon}_i \times 100}{(\sum \text{moles of hydrocarbon products}) \times n}$$

where CO_{in} is a mole number of inlet carbon monoxide

CO_{out} is a mole number of outlet carbon monoxide

n is a number of carbon atoms in hydrocarbon_i

The examples of calculation for the CO conversion and hydrocarbon selectivity can be shown as following tables:

Appendix Table B1 Calculation of CO conversion and selectivity of hydrocarbons over 10IMPCo/SBA-15 catalyst

Description	Calculation
FTS reaction at T = 230 °C, P = 10 atm	
Inlet: CO amount (PV = nRT)	0.000006489 mol
Outlet: Peak areas of CO, CO_2	21772, 85024
CO amount (4.46x 10^{-11} x area)	9.71908×10-7 mol
CO_2 amount (4.38 10^{-11} x area)	3.7283×10^{-6} mol
CO conversion	85.73 %
Peak areas of CH_4, C_2H_6, C_3H_8, C_4H_{10}	6696023, 415510, 409523, 358906
CH_4 amount (2.0x 10^{-14} x area)	1.3395×10^{-7} mol
C_2H_6 amount (8.0x 10^{-15} x area)	3.52408×10^{-9} mol
C_3H_8 amount (6.0x 10^{-15} x area)	2.65714×10^{-9} mol
C_4H_{10} amount (2.0x 10^{-7} x area)	9.47813×10^{-10} mol
C_6H_{14} amount	4.89141×10^{-10} mol
$C_{10}H_{22}$ amount	3.46195×10^{-10} mol
$C_{11}H_{24}$ amount	1.02451×10^{-10} mol
$C_{12}H_{26}$ amount	3.88064×10^{-9} mol
$C_{13}H_{28}$ amount	9.17209×10^{-9} mol
$C_{14}H_{30}$ amount	3.22953×10^{-9} mol
$C_{15}H_{32}$ amount	2.53954×10^{-9} mol
Total hydrocarbons amount	2.27×10^{-7} mol
C_1 hydrocarbon selectivity	14.6 %
C_2 hydrocarbon selectivity	0.8 %
C_3 hydrocarbon selectivity	0.9 %
C_4 hydrocarbon selectivity	0.4 %

Appendix C

X-ray Diffraction of Co/SBA-15 Catalysts

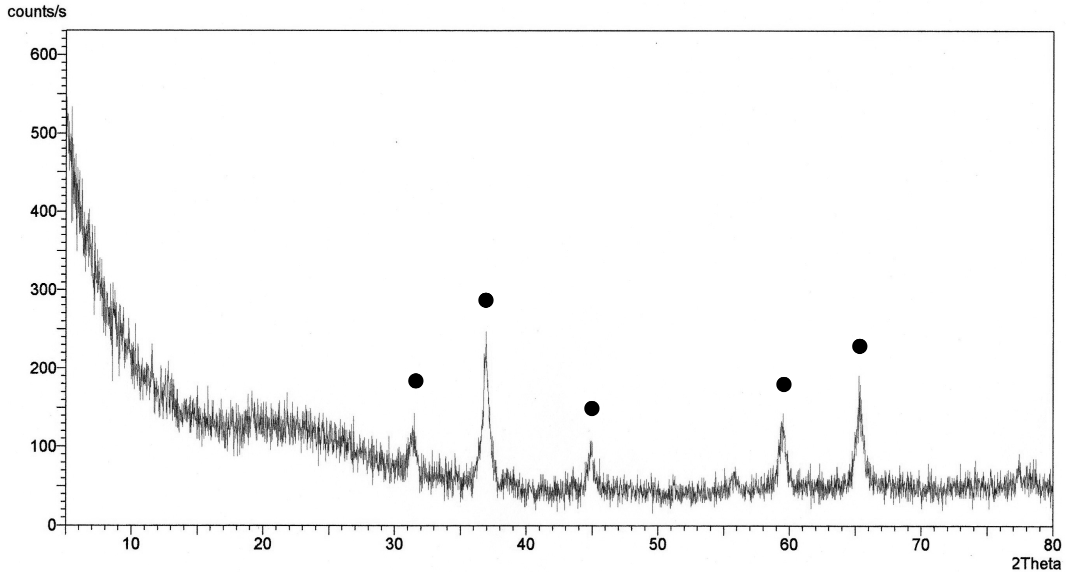

Appendix Figure C1 X-ray diffraction of IMPCo/SBA-15 catalyst; ● : Co_3O_4 phase.

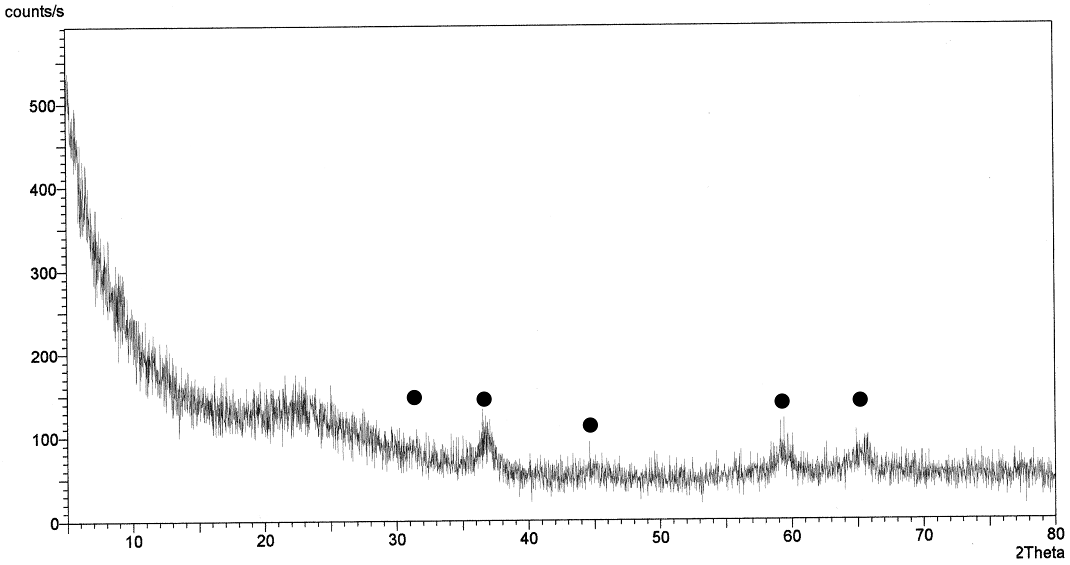

Appendix Figure C2 X-ray diffraction of SOVCo/SBA-15 catalyst; ● : Co_3O_4 phase.

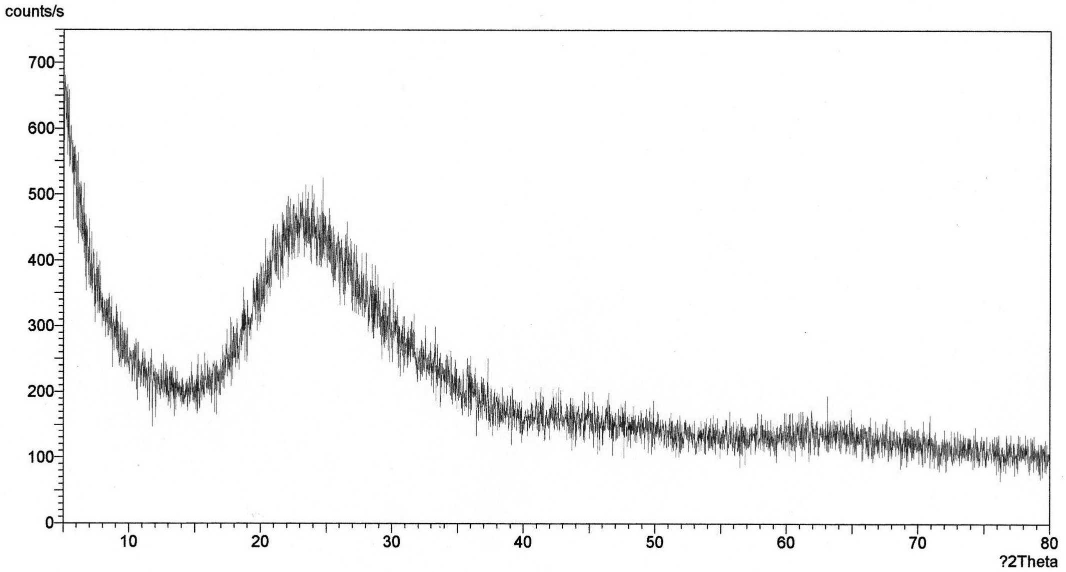

Appendix Figure C3 X-ray diffraction of DS3Co/SBA-15 catalyst.

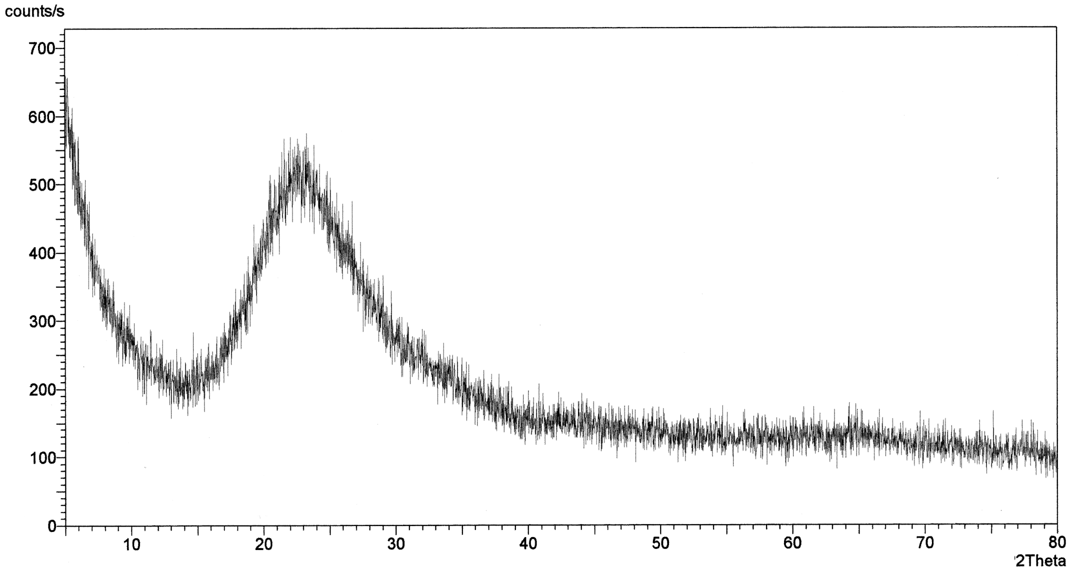

Appendix Figure C4 X-ray diffraction of DS6Co/SBA-15 catalyst.

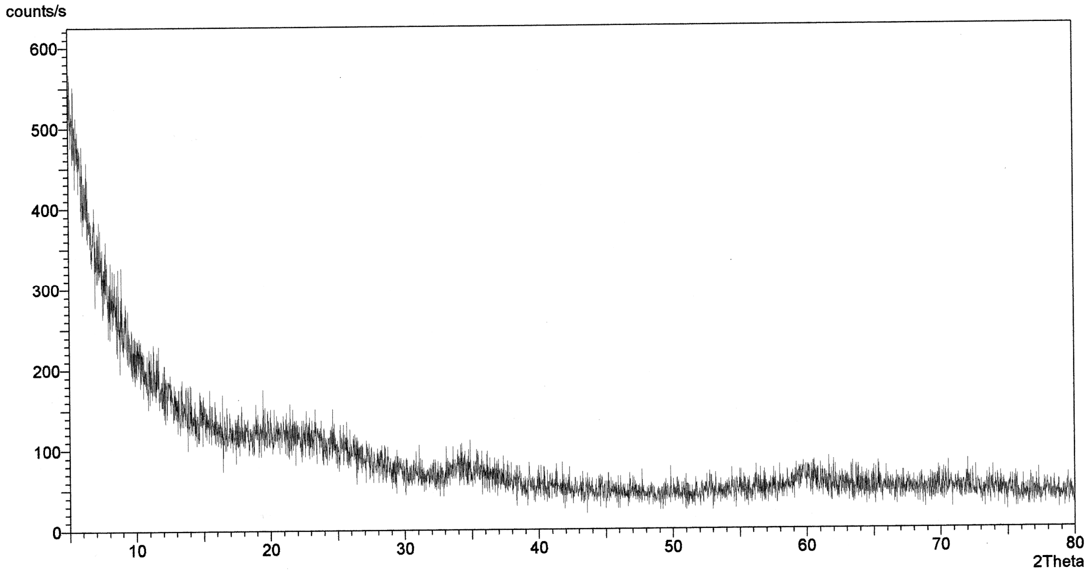

Appendix Figure C5 X-ray diffraction of DS7.5Co/SBA-15 catalyst.

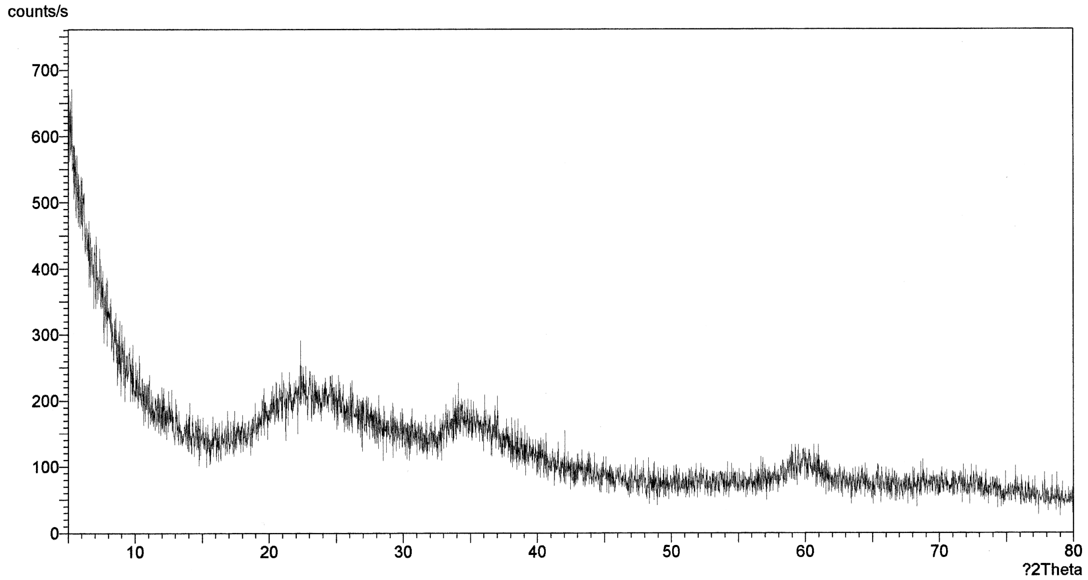

Appendix Figure C6 X-ray diffraction of DS9Co/SBA-15 catalyst.

Appendix D

Inductively coupled plasma atomic emission spectroscopy (ICP-AES)

Basic overview of ICP-AES

Inductively coupled plasma atomic emission spectroscopy (ICP-AES), also referred to as inductively coupled plasma optical emission spectrometry (ICP-OES), is an analytical technique used for the detection of trace metals. It is a type of emission spectroscopy that uses the inductively coupled plasma to produce excited atoms and ions that emit electromagnetic radiation at wavelengths characteristic of a particular element. The intensity of this emission is indicative of the concentration of the element within the sample. The image of ICP process is shown in Appendix Figure D1.

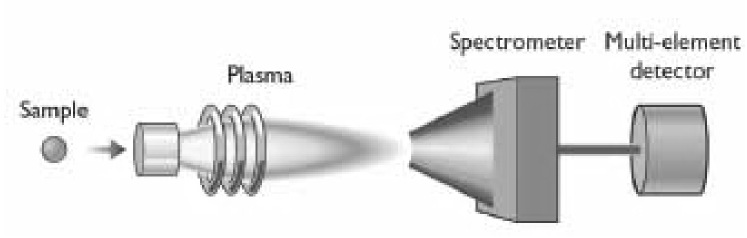

Appendix Figure D1 The schematic photo of ICP process.

1. Mechanism

The ICP-AES is composed of two parts, the ICP and the optical spectrometer. The ICP torch consists of 3 concentric quartz glass tubes that is water cooled and a coil of the radio frequency (RF) generator which surrounds part of this torch. Argon gas is typically used to create the plasma. When the torch is turned on, an intense magnetic field from the RF generator is turned on. The argon gas flowing through is ignited with a Tesla unit (typically a copper strip on the outside of the tube). The argon gas is ionized in this field and flows in a particular rotationally symmetrical pattern towards the magnetic field of the RF coil. A stable, high temperature plasma of about 7000K is then generated as the result of the inelastic collisions created between the neutral argon atoms and the charged particles.

A peristaltic pump delivers an aqueous or organic sample into a nebulizer where it is atomized and introduced directly inside the plasma flame. The sample immediately collides with the electrons and other charged ions in the plasma and is broken down into charged ions. The various molecules break up into their respective atoms which then lose electrons and recombine repeatedly in the plasma, giving off the characteristic wavelengths of the elements involved. A shear gas, typically nitrogen or dry compressed air is used to 'cut' the plasma flame at a specific spot. 1 or 2 transfer lenses are then used to focus the emitted light on a diffraction grating where it is separated into its component radiation in the optical spectrometer. The light intensity is then measured with a photomultiplier tube at the specific wavelength for each element line involved**.** The intensity of each line is then compared to previous measured intensities of known concentrations of the element and its concentration is then computed by extrapolation along the calibration line.

2. Advantages and Disadvantages

Advantages of using an ICP include its ability to identify and quantify all elements with the exception of Argon; since many wavelengths of varied sensitivity are available for determination of any one element, the ICP is suitable for all concentrations from ultratrace levels to major components; detection limits are generally low for most elements with a typical range of 1 - 100 g / L. Probably the largest advantage of employing an ICP when performing quantitative analysis is the fact that multielemental analysis can be accomplished, and quite rapidly. A complete multielement analysis can be undertaken in a period as short as 30 seconds, consuming only 0.5 ml of sample solution. Although in theory, all elements except Argon can be determined using and ICP, certain unstable elements require special facilities for handling the radioactive fume of the plasma. Also, an ICP has difficulty handling halogens--special optics for the transmission of the very short wavelengths become necessary.

CIRRICULUM VITAE

NAME : Ms. Sinee Kraokaw

BIRTH DATE : November 14, 1983

BIRTH PLACE : Bangkok, Thailand

EDUCATION :

YEAR	INSTITUTE	DEGREE
2006	Kasetsart Univ.	B.Eng. (Chemical)
2009	Kasetsart Univ.	M.Eng.(Chemical)

SCHOLARSHIP : Teacher Assistant Scholarship from ADB Program of Department of Chemical Engineering, Kasetsart University 2007-2008